UNIVERSITÀ DEGLI STUDI DI NAPOLI
FEDERICO II

PhD School in Industrial Engineering
INTERNATIONAL PHD SCHOOL IN NOVEL TECHNOLOGIES FOR MATERIALS, SENSORS AND IMAGING

27^{th} Cycle

Resonant states in structured dielectric loss-free media: study and characterization

CANDIDATE: Silvia Romano
TUTOR: Dr. Vito Mocella

ACADEMIC YEAR 2014-2015

La più inutile delle giornate è quella in cui non si è riso.

N. De Chamfort

Contents

Introduction

The local enhancement of electric field in photonic structures can be very useful to manipulate light and boost non-linear phenomena. In particular high field enhancement factors can be generated in metallic nanoentities, such as metallic nanostructures [1], nanoparticles [2] or nanoantennas [3], by exploiting *Surface Plasmon Polaritons*, which propagate at metal/dielectric interface. This phenomenon is extremely appealing for a wide range of applications such as optical detection [4, 5], single-molecule sensing [2, 6], energy conversion [7]. Over the past two decades, devices based on *Surface Plasmon Resonances* have been developed for label-free chemical and biological sensing, [1, 8–13] allowing the study of the interactions between a biomolecule and its specific target with very high sensitivity and low detection limits. In particular sensors based on surface plasmon resonances employ several different methods for the optical excitation of surface plasmons, including total internal reflection [14] and diffraction on periodic metallic gratings [15, 16]. Another useful application of plasmon resonances in optical biosensing is represented by Surface Enhanced Raman Spectroscopy (SERS) [17–19], where local plasmon states are excited by the incident light nearby to metallic nano-particles, allowing the enhancement of the Raman signal coming from investigated analytes [18, 19]. The field amplification takes place in *metallic nanostructures*, where the enhancement factor is about $10^4 - 10^6$ and in *metallic nanoparticles* where the degree of confinement is strongly dependent on particle size, shape, composition, and relative arrangement. Alternatively a large electromagnetic field can be produced and confined in the gap region of *metallic nanoantennas* in which two metallic structures are separated by a small gap [20, 21]. In this case the enhancement factor depends on the structure shapes and on their interdistance.

However, despite their remarkable performances, the achievable resolution in resonance angle shift and the sensitivity of the surface plasmon resonance technique is limited by resonance width, which, in turn, depends on the large optical absorption induced by metallic layer [22]. In addition, the local heating associated to such losses leads to high dissipations in the fluid medium carrying the analyte, causing

unwanted vortices in the carrier flow and eventually damaging the biological material [23].
Nevertheless, plasmonic metallic materials are not the only way to achieve optical field enhancement. The field enhancement in a structured dielectric surface is a relatively unexplored area that has gained increasing attention in the last years. [24–27]. Therefore, it would be of great interest the possibility of managing surface electromagnetic states, mimicking surface plasmon resonances in terms of spatial localization, high field intensity and dispersion characteristics, while avoiding heat dissipation due to metallic substrates [28].
In this thesis the possibility to excite high Q-factor resonances connected to high field enhancement factors in loss-free media, such as photonic crystal slabs, will be reported.
The thesis is organized in two main blocks, a theoretical introduction about the photonic crystal properties and the experimental results collected in this three years. The most part of the work was performed in the Institute for Microelectronics and Microsystems Laboratories (IMM - CNR) in Naples under the supervision of Dr. Vito Mocella. A section was carried out in California, at the Molecular Foundry - Lawrence Berkeley National Laboratory under the supervision of Dr. Stefano Cabrini.
In **Chapter 1** the basic theory about the light propagation in a photonic crystal, the band structure and the origin of the band gap are examined. In **Chapter 2** we begin to deal with the issue of the localized states and surface modes in a photonic crystal. In the last section we go to the core of this thesis topic: resonance states in photonic crystals.
Last three chapters are about the experimental results.
In **Chapter 3** the new phenomenon of *Plasmon-like resonances* in a silicon photonic crystal with a negative refractive index is analyzed. In particular, the negative behaviour in a certain frequency range can involve the existence of surface states at the interface between a photonic crystal and a dielectric medium with properties similar to the plasmonic ones. The similarity between this phenomenon and plasmon resonances in metallic structure is underlined and experimental evidences about the phenomenon are reported.
Besides this modes, the same photonic crystal sample can support also *Guided Mode Resonances*, peaks due to the coupling of infrared radiation with the crystal modes. These resonances appear in the reflection or transmission spectrum and can be connected with the light propagation in a negative refractive photonic crystal. In **Chapter 4** for the first time negative refraction is experimentally detected out-of-plane by monitoring the backward propagation of such resonances through the slab. In addition to the experimental data, a new theoretical approach is pre-

sented to analyze the reflection spectrum features.
Lastly, **Chapter 5** is about the coupling of *Bound States in Continuum* in photonic crystal membranes. In particular we demonstrate and prove experimentally the existence of this special type of resonances in the visible transmission spectrum of a very thin two-dimensional photonic crystal slab. For this purpose, we design and fabricate a square lattice array of holes in two different material with high refractive index, *titania* and *silicon nitride*. To this end, we compare two different fabrication approach, *Nanoimprint Lithography* and *Electron Beam Lithography*. The final samples are, then, characterized by performing angular resolved spectral analysis. High Q-factor resonances connected with a simulated huge field enhancement of about 10^6 are experimentally determined setting the foundation for immediate applications in several fields.

1

Photonic Crystals: an overview

The analogy between electromagnetic wave propagation in multidimensionally periodic structures and electron-wave propagation in real crystals has proven to be a fruitful one. Initial efforts were motivated by the prospect of a photonic band gap, a frequency band in three-dimensional dielectric structures in which electromagnetic waves are forbidden irrespective of the propagation direction in space. Today many new ideas and applications are being pursued in two and three dimensions and in metallic, dielectric, and acoustic structures.

E. Yablonovitch—Photonic band-gap structures, J. Opt. Soc. Am. B, Vol. 10, No. 2, 1993

1.1 Introduction to photonic crystals

Photonic crystals have been described for the first time by E. Yablonovitch [29] and S. John [30] nearly simultaneously in 1987. During the last 25 years the developments in the fabrication techniques and in the numerical simulations allowed the photonic crystal access in different applications. Photonic crystals exhibit several properties that are very appealing for photonic integrated circuits, mainly strong confinement and dispersion. The confinement can be exploited for compact channel waveguides, sharp bends and high isolation between adjacent channels (i.e. low crosstalk), whereas the dispersive properties lend themselves

for wavelength separation (e.g. *superprism effect*) and pulse shape modification (*e.g. pulse compression*). Photonic crystals therefore allow not only traditional applications, such as designing dichroic mirrors, interference filters, or dispersion compensators, but also quantum mechanical manipulation or the targeting of directional characteristics by emitters introduced in such crystals.
Photonic crystals are artificial materials consisting of a periodic repetition of a module, the *lattice*, with the periodicity of the order of the electromagnetic wave. In this way the refractive index is periodically modulated in one, two or three dimensions (Figure 1.1). The perfect order of the structure causes interference phenomena that deeply influence the electromagnetic wave propagation. In particular, if the difference between the refractive index of the materials which form the photonic crystal is large enough, a band gap arise in the band structure. These band gaps are no more than frequency range where light propagation is forbidden. Therefore the resulting dispersion exhibits a band structure analogous to the electronic band structure in a solid and the theoretical approach is very similar if the periodic lattice in a photonic crystal is considered equivalent to the crystalline atomic potential in a semiconductor.

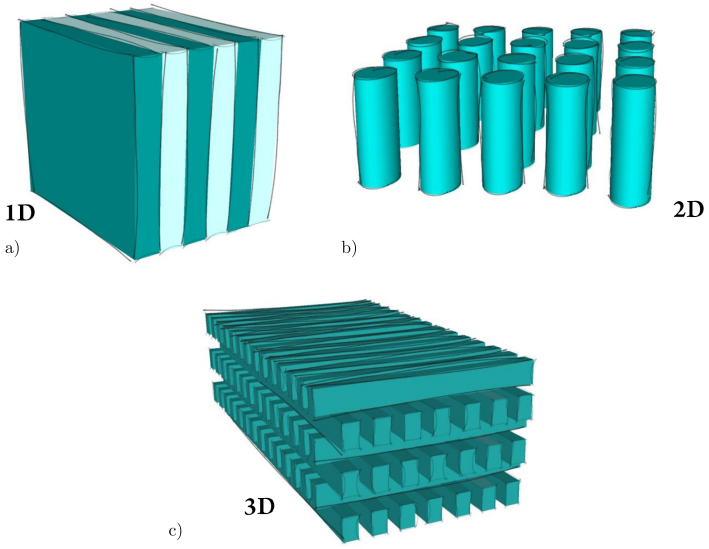

Figure 1.1: Sketch of a photonic crystal structures; the refractive index is periodically modulated in a) one, b) two or c) three dimensions.

Similarly to a semiconductor, the introduction of a defect in the regular arrangement of a photonic crystal produces an allowed mode, with a certain frequency, into the band gap. Therefore, for every kind of defect it is possible to have

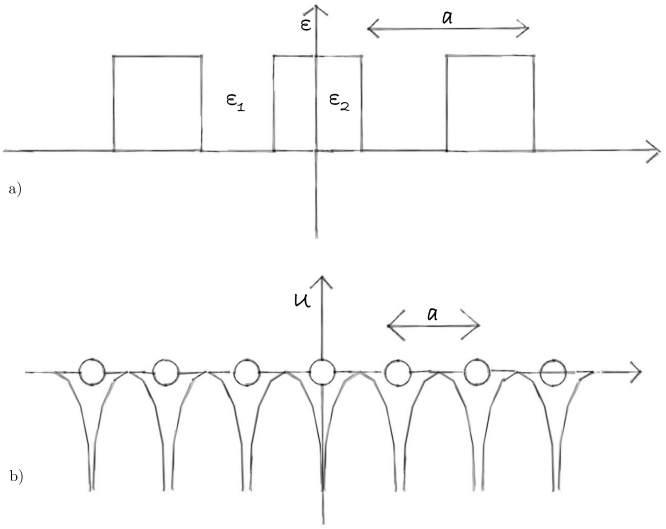

Figure 1.2: a) Modulation of the dielectric constant versus b) periodic potential in a crystal. Photonic crystal dispersion exhibits a band structure analogous to the electronic band structure in a solid and the theoretical approach can be similar.

different types of devices. For example, a point defect can create a resonant cavity or a line defect can create a waveguide (Figure 1.3, for details, see Chapter 2). In this way the functional characteristics are inherent properties of the photonic crystal. If in a solid crystal the electron in a periodic potential is described by the *Schroedinger equation* leading to an *eigenvalue equation*, also in the photonic crystals case an *eigenstate problem* describes the propagation of light in the material. In order to understand and describe it, the theory of band structure calculation based on *Maxwell's equation* has been shown.

1.2 Band structure and theoretical approach

As previously said, the optical analogy of a crystalline material, like a semiconductor, is a photonic crystal where the electronic bandgap for the electrons is replaced by the photonic bandgap for the radiation (Figure 1.4). The required condition to have it is that the periodicity of the refractive index is of the order of the wavelength propagating through the structure. In order to well understand the physical basis of the electromagnetic wave propagation in photonic crystals, *Maxwell's equations* have to be quoted. They relate, through differential equations, the dependence of electric and magnetic field by time and space:

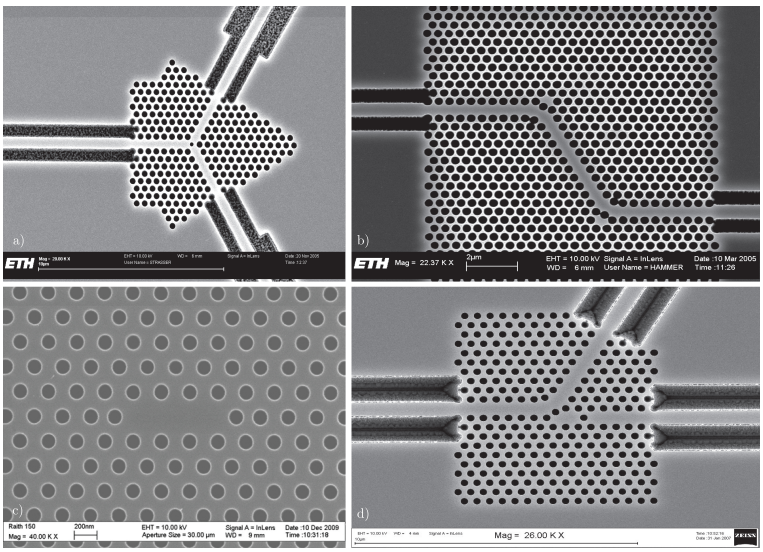

Figure 1.3: SEM images of a) a photonic-crystal based power splitter, b) an optimized photonic-crystal based double 60° bend, c) a photonic crystal cavity and d) an integrated photonic crystal add-drop-coupler in InP (from ETH Zurich and University of Sheffield).

$$\nabla \cdot \varepsilon \mathbf{E}(\mathbf{r}, t) = \rho(\mathbf{r}, t) \tag{1.1}$$

$$\nabla \cdot \mu \mathbf{H}(\mathbf{r}, t) = 0 \tag{1.2}$$

$$\nabla \cdot \mathbf{E}(\mathbf{r}, t) = -\mu \frac{\partial \mathbf{H}(\mathbf{r}, t)}{\partial t} \tag{1.3}$$

$$\nabla \cdot \mathbf{H}(\mathbf{r}, t) = \mathbf{J}(\mathbf{r}, t) + \varepsilon \frac{\partial \mathbf{E}(\mathbf{r}, t)}{\partial t} \tag{1.4}$$

where μ and ε are, respectively, the permeability and the permittivity of the material. In the case of a photonic crystal, these equations can be simplified by doing some considerations. First, the material is isotropic, and its losses are negligible. Also free charges can be neglected, so $\rho = 0$ and $\mathbf{J} = 0$, and only dielectric media with $\mu_r = 1$ are considered. Finally, photonic crystals are non homogeneus media and thus the dielectric constant depends on the position, so $\varepsilon = \varepsilon_0 \varepsilon_r(\mathbf{r})$. Therefore Maxwell's equations become:

$$\nabla \cdot \varepsilon_0 \varepsilon_r(\mathbf{r}) \mathbf{E}(\mathbf{r}, t) = 0 \tag{1.5}$$

$$\nabla \cdot \mu_0 \mathbf{H}(\mathbf{r}, t) = 0 \tag{1.6}$$

$$\nabla \cdot \mathbf{E}(\mathbf{r}, t) = -\mu_0 \frac{\partial \mathbf{H}(\mathbf{r}, t)}{\partial t} \tag{1.7}$$

$$\nabla \cdot \mathbf{H}(\mathbf{r}, t) = \varepsilon_0 \varepsilon_r(\mathbf{r}) \frac{\partial \mathbf{E}(\mathbf{r}, t)}{\partial t} \tag{1.8}$$

Generally these equations are very complicated to solve but, since Maxwell's equations are linear, it is possible to separate the time dependence from the spatial one by considering the fields expansion in harmonic modes, i.e. harmonic functions of time t for a given angular frequency ω. By using this approach, i.e. the *plane-wave expansion method*, the electric and magnetic field can be written as:

$$\mathbf{E}(\mathbf{r}, t) = \mathbf{E}(\mathbf{r}) e^{i\omega t} \tag{1.9}$$

$$\mathbf{H}(\mathbf{r}, t) = \mathbf{H}(\mathbf{r}) e^{i\omega t} \tag{1.10}$$

where the real parts are the amplitudes of the electric and magnetic fields and the exponential part describes the time dependence of the fields. After some algebraic transformations, we can obtain an eigenvalue problem entireley in $\mathbf{H}(\mathbf{r})$, known as the *master equation*:

$$\nabla \times \left(\frac{1}{\varepsilon(\mathbf{r})} \nabla \times \mathbf{H}(\mathbf{r}) \right) = \left(\frac{\omega}{c} \right)^2 \mathbf{H}(\mathbf{r}) \tag{1.11}$$

If we define the Hermitian operator:

$$\widehat{\Theta} \mathbf{H}(\mathbf{r}) = \nabla \times \left(\frac{1}{\varepsilon(\mathbf{r})} \nabla \times \mathbf{H}(\mathbf{r}) \right) \tag{1.12}$$

the 1.11 can be read as a traditional *eigenvalue problem*:

$$\widehat{\Theta} \mathbf{H}(\mathbf{r}) = \left(\frac{\omega}{c} \right)^2 \mathbf{H}(\mathbf{r}) \tag{1.13}$$

This equation governs the propagation of monochromatic light of frequency ω in a dielectric material described by $\varepsilon_r(\mathbf{r})$. By solving the 1.13, we can found the eigenstates $\mathbf{H}(\mathbf{r})$ with eigenvalues ω^2/c and then electric field will be determined. Since $\widehat{\Theta}$ is a linear operator, any linear combination of solutions is still a solution.

Moreover the periodicity of the photonic crystal structure involves that no fundamental constant depends on the spatial lenght of the crystal, so when the vector $\mathbf{r}$ is scaled by a factor $s = \frac{\mathbf{r}'}{\mathbf{r}}$, it is still possible to solve the eigenvalue equation for $\mathbf{H}\left(\frac{\mathbf{r}'}{s}\right)$ and the frequency $\omega\left(\frac{\mathbf{r}'}{s}\right)$. The new mode profile and its frequency can be found by rescaling the old mode profile.
Another consequence of the crystal periodicity is that a photonic crystal has discrete translational symmetry, that is, it is invariant under translation of distances multiple of some steps. The basic step lenght is the lattice constant a and the basic step vectors are the primitive lattice vectors, $\mathbf{a}_1 = a\widehat{\mathbf{x}}$, $\mathbf{a}_2 = a\widehat{\mathbf{y}}$ and $\mathbf{a}_3 = a\widehat{\mathbf{z}}$. Because of this simmetry, also the dielectric permittivity is invariant under translation of an integer multiple l of $\mathbf{a}$, $\varepsilon(\mathbf{r}) = \varepsilon(\mathbf{r} \pm l\mathbf{a})$. This translational discrete simmetry allows the definition of a primitive cell, that is the smallest volume element of the crystal, defined by the primitive lattice vectors $\mathbf{a}_i$. Also in the reciprocal space, the primitive reciprocal lattice vectors $\mathbf{b}_1, \mathbf{b}_2$ and $\mathbf{b}_3$ span a reciprocal lattice and they are defined so that $\mathbf{a}_i \cdot \mathbf{b}_j = 2\pi\delta_{ij}$.
Because of the periodicity of the dielectric constant, **Bloch-Floquet theorem** [31] for a periodic eigenproblems can be applied. It states that the solutions to the 1.11 can be chosen as:

$$\mathbf{H}(\mathbf{r}) = e^{i(\mathbf{k}\cdot\mathbf{r})}\mathbf{u}_{\mathbf{k}}(\mathbf{r}) \tag{1.14}$$

where $\mathbf{u}_{\mathbf{k}}(\mathbf{r})$ is a function with the same periodicity of the photonic crystal lattice and $\mathbf{k} = k_1\mathbf{b}_1 + k_2\mathbf{b}_2 + k_3\mathbf{b}_3$ is the Bloch wave vector. Thus the *master equation* become:

$$(\nabla + i\mathbf{k}) \times \frac{1}{\varepsilon_r(\mathbf{r})} (\nabla + i\mathbf{k}) \times \mathbf{u}_{n,\mathbf{k}}(\mathbf{r}) = \left(\frac{\omega_n(\mathbf{k})}{c}\right)^2 \mathbf{u}_{n,\mathbf{k}}(\mathbf{r}) \tag{1.15}$$

The 1.15 is a different Hermitian eigenproblem over the primitive cell of the lattice at each Bloch wavevector $\mathbf{k}$. This primitive cell is a finite domain if the structure is periodic in all directions, leading to discrete eigenvalues $\omega_n(\mathbf{k})$ labelled by the index $n = 1, 2, \ldots$. These eigenvalues are continuous functions of $\mathbf{k}$ and form the discrete bands in a dispersion diagram. Another fundamental property is that the eigensolutions are periodic functions of $\mathbf{k}$, thus the solution at $\mathbf{k}$ is the same at $\mathbf{k} + m\mathbf{b}$. In this way we can consider only the eigensolutions for $\mathbf{k}$ lying in the **first Brillouin zone**, the set of inequivalent wavevectors closest to the origin $\mathbf{k} = 0$, defined by

$$\left[-\pi/a, \pi/a\right]$$

This region can further become the **irreducible Brillouin zone** (see Figure 1.4), if considering the additional symmetries owned by the photonic crystal. This zone

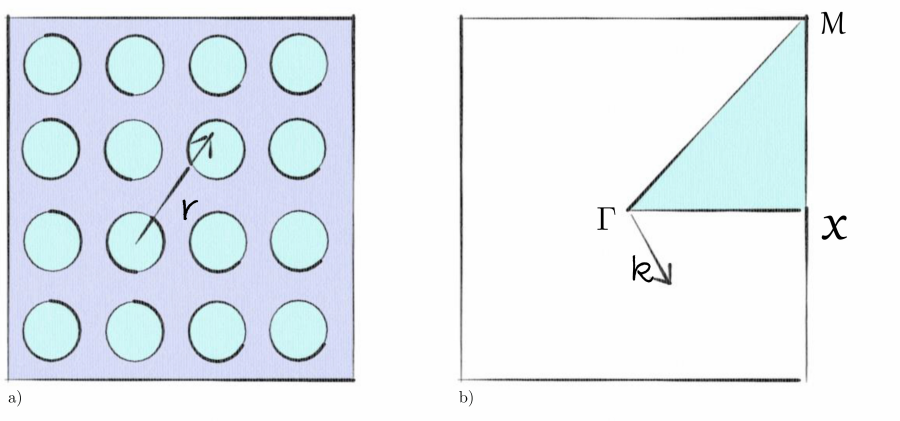

Figure 1.4: Sketch of a) a photonic crystal consisting of a square lattice of holes. An arbitrary vector r is shown and b) the relative Brillouin zone, centered at the origin Γ. An arbitrary wave vector **k** is shown. The irreducible zone is the light blue triangular wedge. The special points at the center, corner, and face are conventionally known as Γ, M and χ.

is a convex polyhedron and is different for every crystalline structures.

1.3 The origin of the photonic band gap

One of the most important feature of a photonic crystal is the possibility to have a complete **photonic band gap**. A photonic band gap is a range of frequency in which the propagation of radiation is forbidden because there are no propagating solutions of Maxwell's equations for any **k**. In this case the band gap is complete and it is surrounded by propagating states above and below it. In order to explain the origin of this gap, let us consider a one-dimensional system with a constant dielectric permittivity $\varepsilon = 1$ which has planewave eigensolutions $\omega(\mathbf{k}) = c\mathbf{k}$. In this trivial case the modes lie along the light line and, in the Brillouin zone, the light line folds back into the region after reaching the edges (Figure 1.5).

In particular the mode corrisponding to $k = -\pi/a$ and the mode corrisponding to $k = \pi/a$ are equivalent, i.e. the system has a degeneracy. The planewave solutions with electric fields $E(x) \sim e^{\pm i\pi x/a}$ can be write as a combination of $A(x) = cos(\pi x/a)$ and $B(x) = sin(\pi x/a)$ both at $\omega = c\pi/a$. Now let us consider a slightly perturbated dielectric permittivity, for example a sinusoidal function $\varepsilon = 1 + \Delta \cdot cos(2\pi x/a)$. In this case the degeneracy between $A(x)$ and $B(x)$ is broken. From the study of electromagnetic variational theorem [31], it follows that the smallest eigenvalue ω_0^2/c^2, and thus the lowest-frequency mode, corresponds to the field pattern that minimizes the functional, named *Rayleigh quotient*:

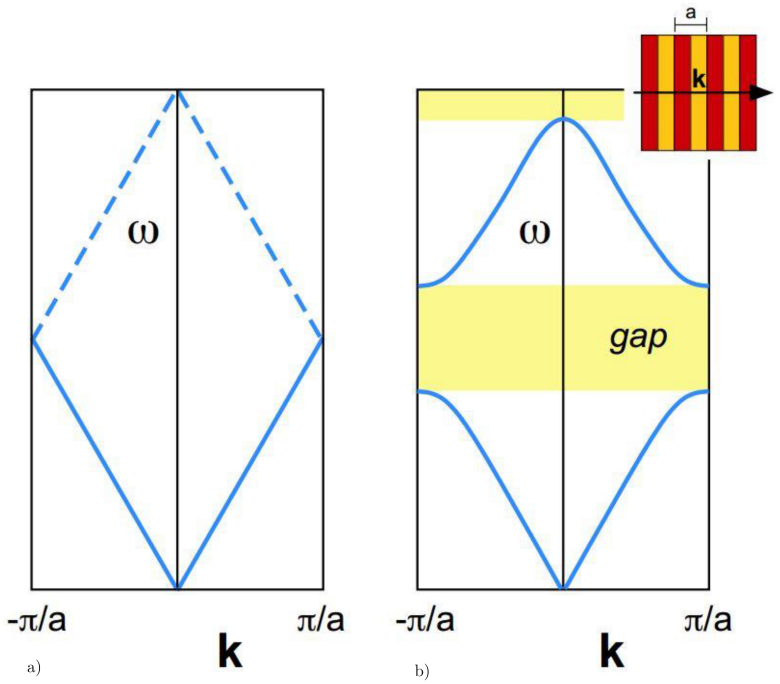

Figure 1.5: a) Dispersion relation (band diagram), frequency ω versus wavenumber k, of a uniform one-dimensional medium. The dashed lines show the "folding" effect of applying Bloch's theorem with lattice constant a. b) Schematic effect on the bands of a physical periodic dielectric variation (inset), where a gap has been opened by splitting the degeneracy at the Brillouin-zone boundaries (as well as a higher-order gap at k = 0). *From: Introduction to Photonic Crystals: Bloch's Theorem, Band Diagrams, and Gaps (But No Defects), Steven G. Johnson and J. D. Joannopoulos, MIT*

$$U_f(\mathbf{H}) \triangleq \frac{(\mathbf{H}, \widehat{\Theta}\mathbf{H})}{(\mathbf{H}, \mathbf{H})} \tag{1.16}$$

It can be demonstrated [31] that the way to minimize it is to concentrate the field in regions of high dielectric constant ε, with the constrain to be orthogonal to the lower frequency modes. Thus, if $\Delta > 0$, the field $A(x)$ is more concentrated in the higher-ε regions than B(x), and so lies at a lower frequency. This opposite shifting of the bands creates a band gap (Figure 1.5).
By generalizing in 3D, the eigenvalues minimize the *variational problem*:

$$\omega^2_{n,\mathbf{k}} = \min_{\mathbf{E}_{n,\mathbf{k}}} \frac{\int \left|(\nabla + i\mathbf{k}) \times \mathbf{E}_{n,\mathbf{k}}\right|^2}{\int \varepsilon \left|\mathbf{E}_{n,\mathbf{k}}\right|^2} c^2 \tag{1.17}$$

in terms of the periodic electric field envelope $\mathbf{E}_{n,\mathbf{k}}$. The $n > 1$ bands have to satisfied the constraint to be orthogonal to the lower bands:

$$\int \mathbf{H}^*_{m,\mathbf{k}} \cdot \mathbf{H}_{n,\mathbf{k}} = \int \varepsilon \mathbf{E}^*_{m,\mathbf{k}} \cdot \mathbf{E}_{n,\mathbf{k}} = 0$$

Thus, for each $\mathbf{k}$, there will be a gap between the lower "dielectric" bands concentrated in the high dielectric and the upper bands that are less concentrated in the high dielectric. Often, in 2D and 3D photonic crystals, the low- ε regions are air regions and it can be convenient to name *air band* the band above the photonic gap and *dielectric band* that below the gap. In this way the dielectric/air bands are analogous to the valence/conduction bands in a semiconductor.
Unfortunately, in order to have a complete band gap in two or three dimensions, the situation is more complicated and it is necessary to add other constraints. First, the band gaps in every one-dimensional direction have to overlap in frequency and thus the gaps has to be enough large, which implies a minimum ε contrast. Second, the vectorial electrical field has to satisfied the vectorial boundary conditions and this can be obtained for crystals with high-ε regions connected by narrow veins. It is easy to imagine that these are hard hurdles and therefore for 3D crystals complete photonic band gaps are rare.

1.4 Beam propagation in a photonic crystal: unusual phenomena

The equi-frequency curves

A photonic crystal consists of a periodic repeat of a module realized by different media. In the long wavelenght region, the crystal can be approximated as a homogeneous material by using mathematics homogenization techniques based on analyzing limiting values. But in order to understand the propagation of a beam through a photonic crystal as well as the refraction or reflection processes this homogenization method can be not enough. For this purpose **equi-frequency curves** of the photonic band structure can be a good approach.
Let us consider a two-dimensional photonic crystals sketched in fig.1.1b. The equi-frequency profiles are obtained by horizontally cutting the dispersion surfaces. Such curves define the permitted phase wavevectors inside the photonic crystal at one frequency ω. The group velocity is defined by the normal to the equi-frequency surface $\omega(\mathbf{k}) = \omega_0$ at point (k_x, k_y) and is given by:

$$\mathbf{v}_g = \nabla_k \omega(\mathbf{k}) \tag{1.18}$$

In the dispersion diagram, the group velocity vector versus is defined as the slope of the band. If the slope is negative, the vector goes inwards the isofrequency curve, if it is positive it goes outwards. Before moving on to the case for photonic crystal, first we examine a simpler case, the light propagation in a dielectric material. The photonic band $\omega = ck/n$ can be represented by a circle in the $k-$space. A light incident from air with refractive index n_1 to a dielectric material n_2 can be described by the Snell's law

$$n_1 sin\theta_1 = n_2 sin\theta_2 \tag{1.19}$$

with θ_1 and θ_2 incidence and refraction angles and can be graphically represented as in Figure 1.6left. The refracted wave can be found by drawing a line perpendicular to the interface until the intersection with the material equi-frequency curve.

Another example is the light propagation through a grating with period d, pictured in Figure 1.6right. For the grating periodicity, equifrequency curves are repeated along the periodic axis. The vector $\mathbf{v}_a$ corrisponds to the transmitted wave and starts from the intersection with the circle centered in the origin. The vector $\mathbf{v}_b$ is a diffracted wave and starts from the circle centred at the reciprocal lattice point. In this way we have graphically represented the formula for a diffraction grating:

$$m\lambda = dsin\theta \tag{1.20}$$

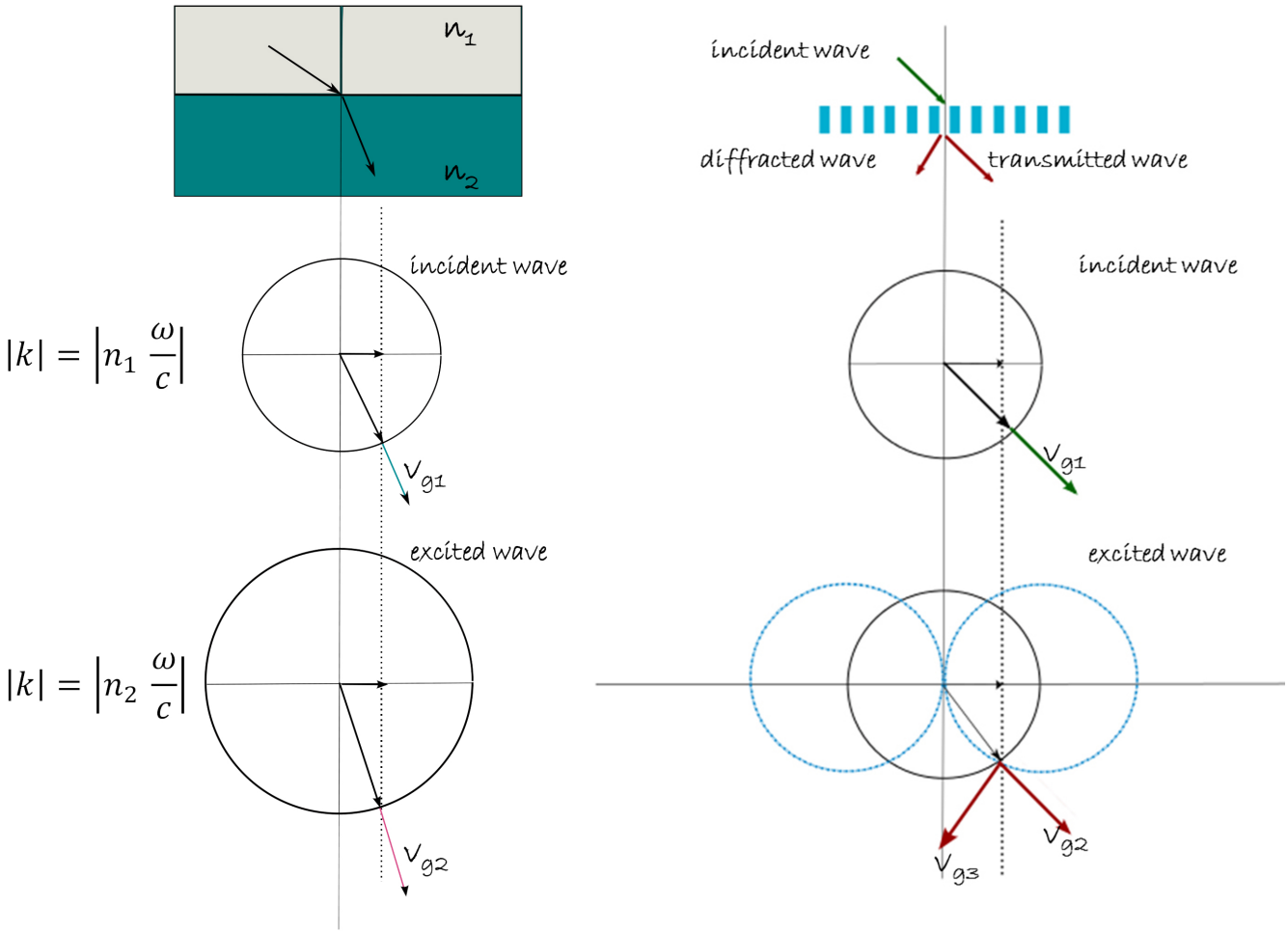

Figure 1.6: Wave vector diagram of conventional refraction (left) and of a diffraction grating (right). v_{g_i} denote the group velocity vectors corresponding to the incident and refracted, diffracted or transmitted wave vector.

With this approach some unusual phenomena occurring in photonic crystals can be easier to understand. Photonic crystals are artificial materials and it is possible to design and fabricate them with a certain structure in order to achieve unusual properties. Some of the most important, such as the negative refractive refraction, the imaging and the autocollimation will be now outlined.

Negative refractive index

The beam propagation in a photonic crystal is determined by its spatial dispersion. One of the phenomenon related to spatial dispersion is the *refraction* occurring when a light beam is incident on the surface of a material. In a conventional material, the phenomenon is governed by the Snell's law: the light beam is refracted at the boundary surface and propagates in the direction determined by Snell's law (see eq. 1.19). The refracted angle and the refractive index are always both positive. Nevertheless it was discovered [32] that a photonic crystal can be designed in order to have negative refractive index in a certain frequency range.

Let us consider the equi-frequency circle for an isotropic material, with $|k| = |n\omega/c|$. We assume that the energy flux has to be parallel to k and one of the wavevectors should be excluded when the energy flux conservation at the boundary is considered. The beam propagation direction is determined by the relation between the energy flux direction and the wavevector. In a conventional material, these are parallel and coincident and the group velocity vector at the selected k is outward normal to the equi-frequency circle. However, if the group velocity vector and the wavevector happen to be anti-parallel, this leads to negative refraction. In this case the group velocity goes in inward to the equi-frequency circle (see Figure 1.8). So, the velocity group plays a key role in this phenomenon because negative refraction happens when velocity sign is inverted. Let us come back to the photonic crystals. In order to have negative refractive behaviour and negative velocity group, strongly modulated 2D or 3D photonic crystals are necessary because the strength of the periodic modulation plays an important role [32].

Infact, when the index modulation becomes stronger, the equi-frequency curves undergo an heavy modification. In Figure 1.7 the equi-frequency surface of GaAs (n = 3.6) 2D air-hole hexagonal photonic crystals, obtained from a cross-section of the band structure at a fixed frequency, are shown. When the frequency is far from the band edge, the equi-frequency curves are similar to that for weakly modulated structure but, approaching the band edges, the equi-frequency curves become circular [32]. The effect of this is that the equi-frequency curve of a strongly modulated photonic crystal resembles that for isotropic homogeneous materials (Figure 1.6). Thus, the beam propagation through this kind of photonic crystal

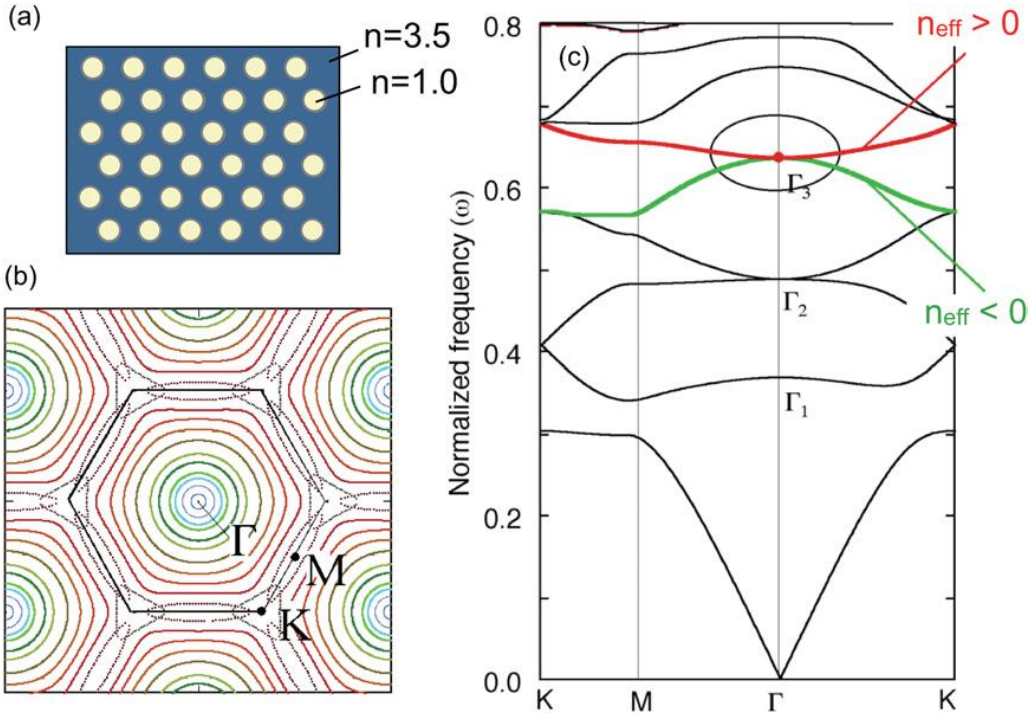

Figure 1.7: Numerical calculation of negative-index strongly modulated photonic crystals from *Manipulating light with strongly modulated photonic crystals, M. Notomi*. (a) 2D hexagonal air-hole photonic crystal. (b) Calculated EFS at various frequencies in the vicinity of the Γ_3 point. As ω approaches the mode edge, the EFS shape becomes rounded. (c) Photonic band structure of modes with electric field perpendicular to the 2D plane

can be described by Snell's law and the photonic crystal behaves like an isotropic medium with an *effective refractive index*. The orientation of the energy flux is determined by the band dispersion, which can be negative. In particular the circular equi-frequency arises from a band with a negative slope, hence, photonic crystals in this frequency range behave like an isotropic material with a constant negative refractive index.

Perfect imaging and autocollimation

As just stated, a photonic crystal can be opportunely designed and fabricated in order to behave like a negative refractive material in a certain frequency range. This property can involve some unusual and interesting phenomena in the *imaging* field. Let us consider a medium with a constant refractive index. In the paraxial approximation, all ray emitted from a positive index material and then propagating in the negative medium will be focused in a single point (figura). Thus a structure composed by a positive and a negative material behaves as a flat lens. For a conventional lens, the spatial coordinates for an object and an image are expressed as $(x, y, z) \rightarrow (-x(f/z), -y(f/z), -f^2/z)$ where f is the focal lenght. The image formation is then affected by the position of the object and of the focus point so it is not possible perfect 3D imaging. On the contrary, for a negative refractive material $(x, y, z) \rightarrow (x, y, zn_1/n_2)$, i.e. it is indipendent from the focal lenght or the focus point. In particular if $n_1 = -n_2$, the formula becomes the same of a mirror, but, while a mirror produces a virtual image in the half-space opposite the object space, a negative refracting medium can behave like a *perfect lens* producing a *real image*.

Another impressive application of the negative refractive index is the possibility to collimate a light beam travelling through a particular heterostructure based on negatively refracting photonic crystal [33]. Let us consider a structure consisting of alternating layers, air and photonic crystal, with positive $n = 1$ and negative $n = -1$ refractive index. A full photonic bandgap appears whenever an exactly zero-average refractive index occurs and the radiation cannot propagate inside the structure. Thus, in order to allow the light transmission, a slight imbalance between the alternating layers is required. In this way the structure becomes a quasi-zero-average-index (QZAI) heterostructure. The beam is now propagating and is refocused in every stripe due to the alternating positive and negative refractive index. The result is a strong macroscopic self-collimation effect over the entire length of the metamaterial (see figure 1.9).

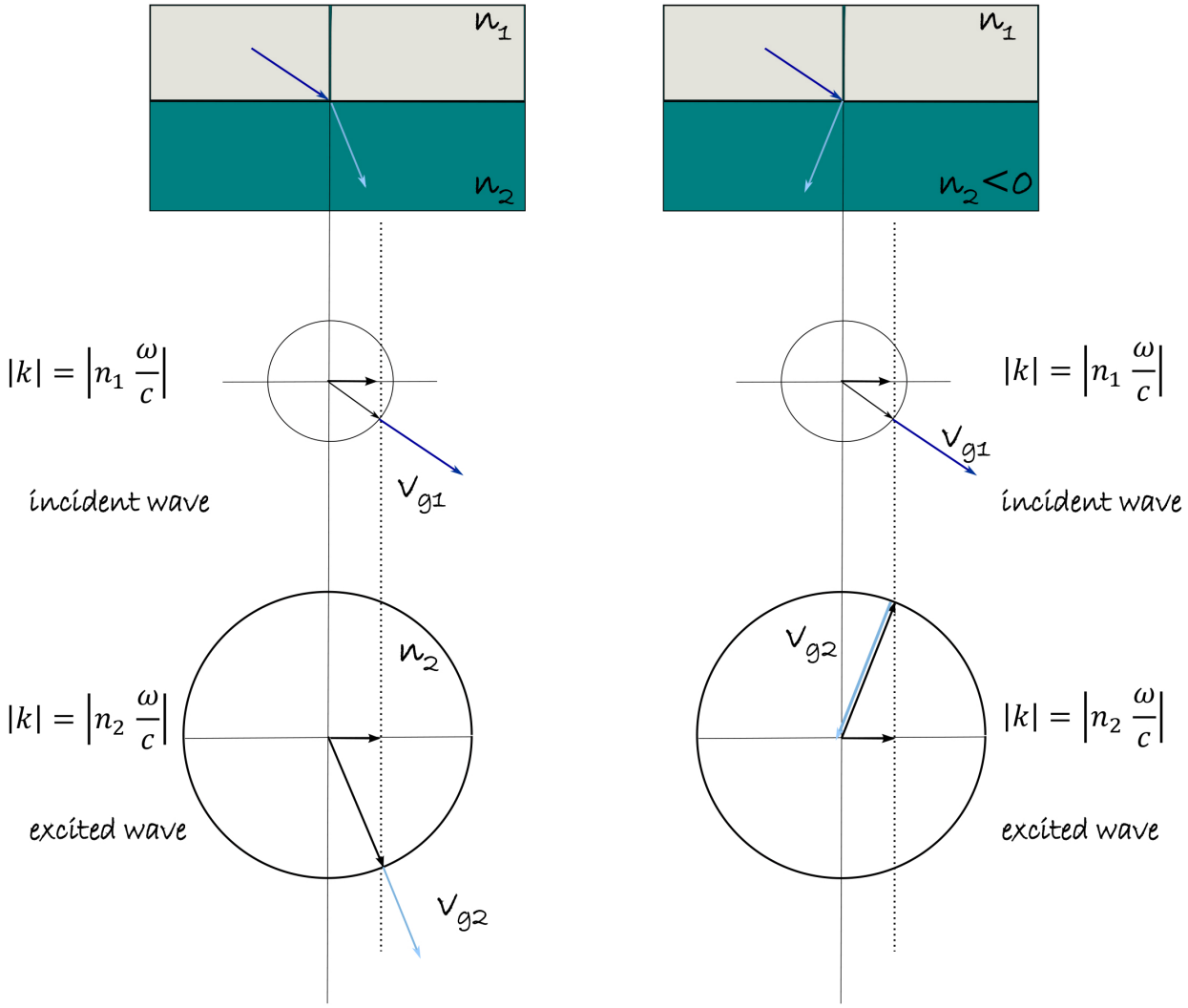

Figure 1.8: Comparison between conventional refraction (left) and negative refraction (right).

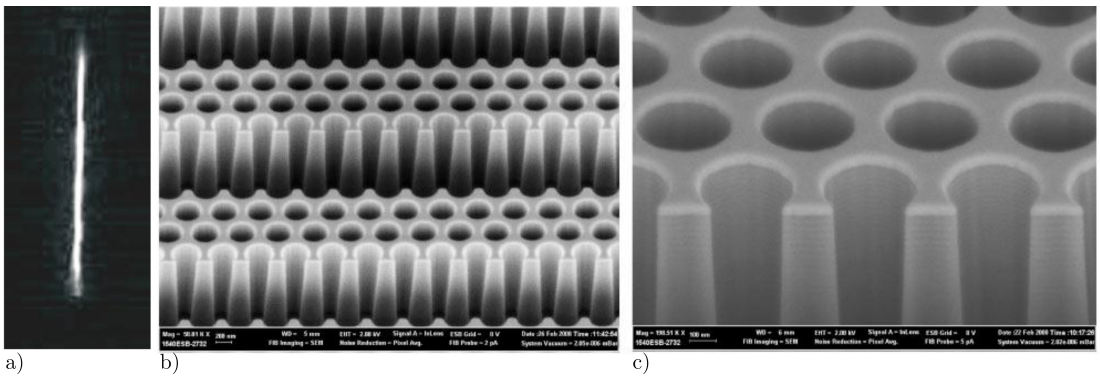

a) b) c)

Figure 1.9: a) The experimental images of the collimated beam travelling through the structure. SEM images of the nanofabricated device.(a) Alternating of space and photonic crystal material, with different termination on each photonic crystal structure. (b) Magnified image.

1.5 Photonic crystals slabs

One of the great advantages of photonic crystals is the possibility to manipulate electromagnetic radiation in all spatial directions and for this purpose 3D photonic crystals could be very suitable. However 3D photonic crystals are technologically challenging structures and the difficulty is to integrate the fabrication process to already existing production processes. A very good compromise taking into account the structure simplicity and light manipulation in all different spatial directions are photonic crystal slabs in two dimensions. These structures consist of alternating hole-slab or rode-slab of high-index material arranged in a lattice thin slabs of high-index material. The height of the slab is negligible compared to the other lenghts but its finite dimension introduces new characteristics. Under some conditions a total internal reflection happens at the interface between the slab and the lower-index materials lying above and below it and in this way three-dimensional light confinement in two-dimensional photonic crystal is obtained. This *index guiding* is due to the fact that the periodicity in 2D implies that the Bloch wavevector $\mathbf{k}_{//}$ is a conserved quantity. In particular the slab has the periodicity only in two direction, for example x and y, so $\mathrm{k}_{//}=\sqrt{k_x^2+k_y^2}$ and can be interesting to plot ω versus it, obtaining the *projected band structures*. To construct a band diagram projected onto the k_x direction, for example, one fixes the value of k_x and then plots on the same graph the states with all otherwise allowed k_y values. If the slab is surrounded by air, the eigensolutions of the bulk air and that are not confined into the slab are $\omega= \mathrm{c}\sqrt{\left|k_{//}\right|^2+k_\perp^2}$. For a given value of $\mathbf{k}_{//}$, there will be modes with every possible frequency, thus the spectrum of states

is continuous for all frequencies above the **light line** $\omega = ck_{//}$ forming the *light cone*. The presence of the slab introduces new electromagnetic solutions below the light cone.

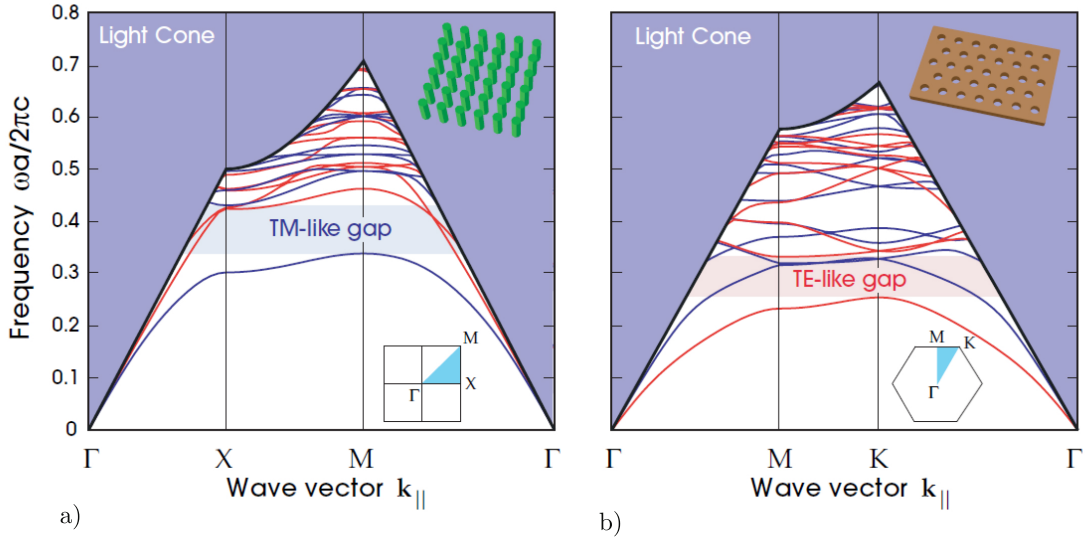

Figure 1.10: Band diagrams for photonic crystal slabs suspended in air (inset): the rod slab (left) and the hole slab (right). The blue shaded area is the light cone, all of the extended modes propagating in air. Below it are the guided bands localized to the slab: blue/red bands indicate TM/TE-like modes, respectively (odd/even with respect to the z=0 mirror plane). The rod/hole slabs have gaps in the TM/TE-like modes, which are shaded light blue/red respectively. From *Joannopulos, Photonic crystals: Molding the Flow of Light, s.nd edition.*

These modes have lower frequencies because of the higher dielectric constant of the slab (Figure 1.10) and must be localized in the vicinity of the slab decaying exponentially away from it. These modes are called **index-guiding modes** and they form a set of discrete bands. In two-dimensional structures there is a fundamental distiction between the TM and TE polarizations. In the first case, the magnetic field **H** is parallel to the holes or cylinders axes, in the second case the electric field **E** is parallel to them. Each of them has different dispersion relations and different stop bands, so it is possible to have an *incomplete* band gap. However for this special case of a thin structure, we can continue to consider two different modes that are mostly polarized. In particular, since the photonic crystal slab is invariant under reflections [31] respect to the z axis, we can keep on distinguish two kinds of modes, the *TE-like* and the *TM-like*, corresponding to even and odd modes. In Figure 1.10 we can see the different band gaps for *TE-like* and

TM-like modes; in particular, the rod slab favors a TM-like gap while the hole slab favors the TE-like gap. However the gaps in photonic crystal slabs are incomplete and they refer only to guided modes and not the light cone. In addition to this, under certain conditions, it is also possible to localize electromagnetic modes at the photonic crystal surface, exciting *surface modes* or to let interact the external radiation with the modes allowed into the photonic crystal slab, via the guided mode resonances. But we will talk about it into the next chapter.

2

Electric field localization in photonic crystals

A defect, or mistake in the periodicity, could lead to localized photonic states in the gap, whose shapes and properties would be dictated by the nature of the defect. A point defect could act like a microcavity, a line defect like a waveguide, and a planar defect like a perfect mirror. This ability to manipulate a photon provides us with a new dimension in our ability to mould or control the properties of light. Therein lies the exciting potential of photonic crystals.

J.D. Jannopoulos, P. Villenevue, S. Fan—Photonic crystals: putting a new twist on light, Nature, vol. 386, 1997

Introduction

Photonic crystals are periodic artificial materials and so it is possible to confer them unusual properties by opportunely designing and fabricating the structure. In this chapter some examples of phenomena connected to the localized states formation will be presented. In the first paragraph the possibility to confine and guide the radiation propagating in a photonic crystal will be explained while in the second one surface modes as consequence of the finite dimension of a photonic crystal will

be shown. In last paragraph we start to get to the heart of the thesis. Three kind of resonance phenomena will be presented: **Plasmon-like resonances, Guided Mode resonances** and **Bound State in Continuum**. Each of them represents a slice of my experimental work expanded during my PhD formation and thus they will be examined in depth in next chapters.

2.1 Localized states and defects in photonic crystals

In the first chapter the strong similarity between semiconductors and photonic crystals and the possibility to have a photonic band gap analogous to the electronic band gap in a solid crystal have been underlined. As it happens in semiconductors, also in this case the introduction of defects by a local distortion of the periodicity leads to the creation of states with frequencies within the band gap. These states form modes that are laterally confined into the photonic crystal and thus a defect can be used to attempt to trap or localize the light. The properties of these localized modes depend on the kind of defect: a line defect can generate a **waveguide**, a point defect can generate a **cavity**. For the sake of conciseness, let us consider the simple case of a photonic crystal slab.

Waveguides

By using a linear defect, a light beam can be guided from a point to another of a photonic crystal slab. In particular, since the frequencies allowed are inside the band gap, the radiation is confined into the *waveguide* and is forced to move along it even if the waveguide has tight corners. The fields decay exponentially at the boundary of the defect. In order to understand the guiding mechanism, the simple case of a square lattice of dielectric rods is considered.

The projected band corresponding to TM modes along the direction of propagations are reported in figure 2.2. The blue region represents the states that can propagate through the crystal. The yellow region is the band gap and the red line is the band of states which can travel freely within the waveguide channel. Since the band is inside the prohibited band gap, the modes are forbidden to escape into the crystal. Moreover, the only loss channel can be reflection back out of the waveguide entrance whereas no losses are during the propagation so the light can be guided efficiently through the crystal. By removing one row of rods (or holes), a single-mode waveguide is realized otherwise by removing multiple rows a multimode waveguide results. Figure 2.3 shows the electric-field pattern associated

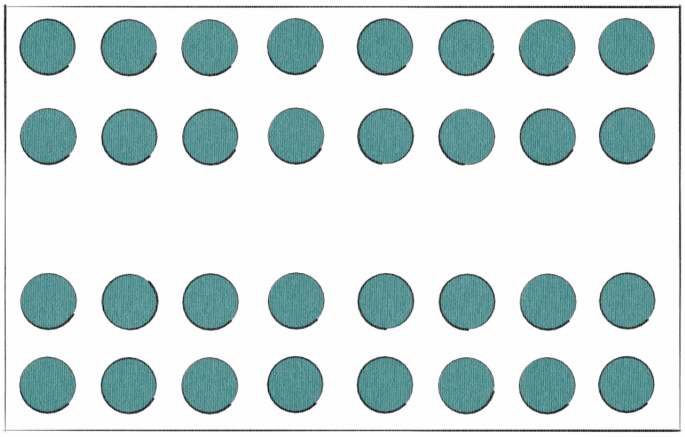

Figure 2.1: Sketch of a waveguide in a photonic crystal slab. By removing one line of rods, the light is forced to propagate from a slab side to the other one.

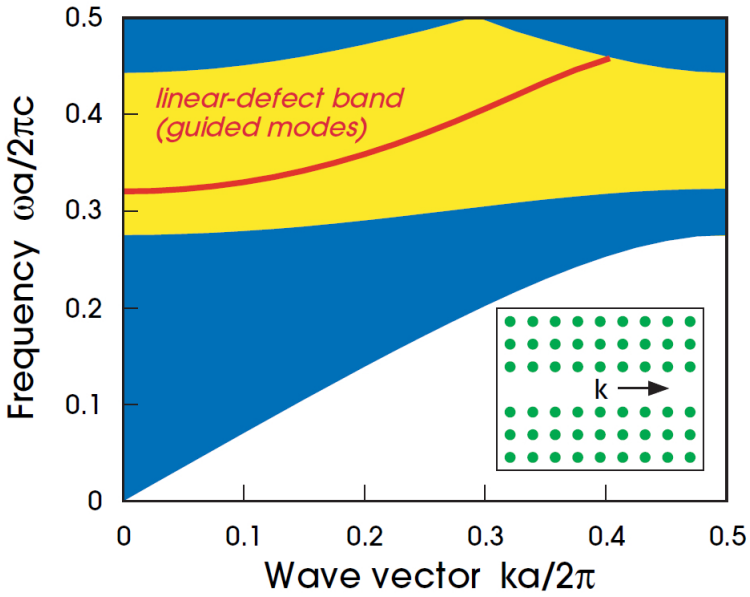

Figure 2.2: The projected band structure of the line defect formed by removing a row (or column) of rods from square lattice plotted versus the wave vector component k along the defect. The extended modes in the crystal become continuum regions (blue), whereas inside the band gap (yellow) a defect band (red) is introduced corresponding to a localized state. *From: Introduction to Photonic Crystals: Bloch's Theorem, Band Diagrams, and Gaps (But No Defects), Steven G. Johnson and J. D. Joannopoulos, MIT.*

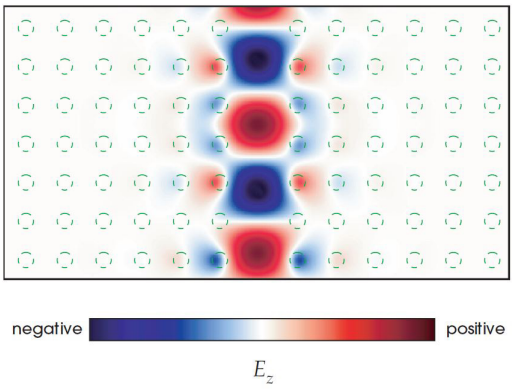

Figure 2.3: Electric-field (E_z) pattern associated with a linear defect formed by removing a column of rods, shown as dashed green outlines, in a slab. The resulting field is a waveguide mode propagating along the defect. *From: Introduction to Photonic Crystals: Bloch's Theorem, Band Diagrams, and Gaps (But No Defects), Steven G. Johnson and J. D. Joannopoulos, MIT.*

with a linear defect formed by removing a column of rods from an perfect square lattice of rods in air. The resulting field is a waveguide mode propagating along the defect.

Cavities

The simplest kind of photonic crystal *cavity* can be formed by introducing a point defect into the perfectly periodic photonic crystal slab. A point defect involves a modification of a single hole inside the crystal. The hole can be changed in size, dielectric properties or even be omitted (see fig. 2.4).

As a result of the defect, the translational symmetry of the photonic crystal is broken. For appropriate defects in dimensions and in position, localized modes with frequencies inside the photonic band gap can arise. Since for the unperturbed photonic crystal no propagating modes exist inside the bandgap, energy stored inside a localized mode cannot be transported through the slab. Thus localized modes with frequency inside the bandgap are laterally confined. Propagating waves exhibit a field profile infinitely extending along the direction of propagation. The spatial distribution of the electric field and its wave vector distribution are linked by the Fourier transform. A propagating mode with an infinite field distribution along one direction leads to precise definition of the wave number. A spatially localized mode, in contrast, has a continuous k-vector spectrum which is proportional to the Fourier transform of the mode electric field. A part of this continuous k-vector spectrum is necessarily inside the light cone and therefore is not confined by the total internal reflection of the slab anymore. This part of the k-vector spec-

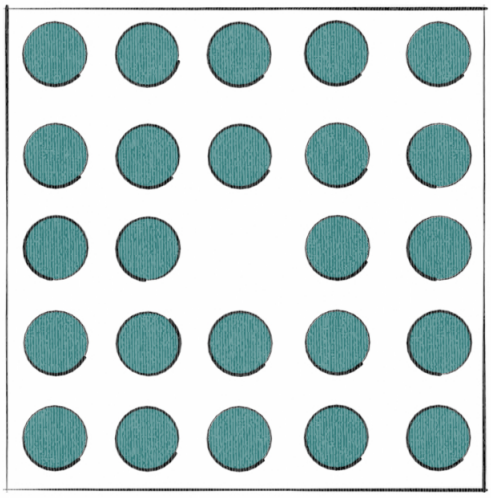

Figure 2.4: Sketch of a photonic crystal point defect cavity created by removing a single hole from a photonic crystal slab.

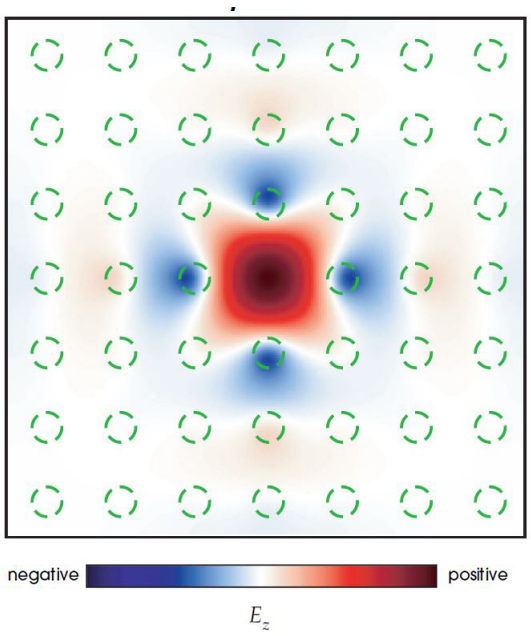

Figure 2.5: Electric-field (E_z) patterns of states localized by completely removing a rod in a square lattice. The rods are shown as dashed green outlines. *From: Introduction to Photonic Crystals: Bloch's Theorem, Band Diagrams, and Gaps (But No Defects), Steven G. Johnson and J. D. Joannopoulos, MIT.*

trum can leave the cavity vertically [34]. Point defect cavities can have very small mode volumes. This property is interesting for integrated lasers where small mode volumes can reduce the pump threshold [35]. On the other hand, a small mode volume implies a strong lateral confinement of the mode and thus wide spectrum of wave vectors. In such a strongly confined structure, a considerable part of the k-vector spectrum is inside the light cone and thus is leaky. This is the reason why the Q-factors achieved with point defect cavities are moderate compared to larger cavity concepts. In most applications this type of cavity is coupled vertically simply by shining light on top. In-line coupling concepts exist but are only rarely used because the coupling waveguide distorts the symmetry of the point defect cavity and thus splits the resonances. Figure 2.5 shows the electric-field patterns of states localized around a defect in a square lattice of rods in air, formed by completely removing a rod, which has a single lobe in the defect and high symmetry.

2.2 Surface modes in truncated photonic crystal

Up this point we did not care about the finite dimensions of the photonic crystal but we refered to a slab of infinite extent. However real crystals are inevitably bounded and this involves some important effects such as the presence of **surface modes**. When a surface mode is excited, the field is localized at the interface between the photonic crystal and the environment and decays exponentially away from the surface. In the presence of a bandgap,it decays within the photonic crystal and within the environment (e.g. air) because it is index-guided. An important parameter for the characterization of a surface mode is the *termination* of the surface which specifies where the photonic crystal is truncated. For example the slab can end after a row of holes or after a row of holes cut in half. Another important parameter is the *inclination* of the surface which specifies the angles between the surface normal and the crystal axes. In order to study this phenomenon, consider two slabs of rods arranged in a square lattice, one ending with a row of columns and the other ending with columns cut in half in the x direction. Moreover we choose planes of constant x for the surface inclination. In this way in z and in y directions, the structure has a continuous translational simmetry whereas in the x direction the truncation of the periodic crystal has broken the translational simmetry and thus k_x is no more conserved. Figure 2.6a shows the projected band structure of the square lattice truncated with a row of rods. The TM band structure has a photonic band gap between the first and the second band. The different regions correspond to the modes propagating separately in air and within the photonic crystal and are labelled with two letters, the first one refers to the air region, the second one to the

photonic crystal region. The letters E and D indicate Extended or Decaying so the union between regions EE and ED corresponds to free light modes into the surface Brillouin zone. The union between EE and DE represents the projected band structure of the photonic crystal. In the region EE the light is transmitted, in the region DE is internally reflected and in the region ED in externally reflected. So, in this case, no surface states are allowed.

Consider, now, the slab ending with a row of rods cut in half (see fig. 2.6b). In addition to the already seen modes, in this case another type of mode appears, the DD, which decays exponentially away from the surface in both directions (DD). The modes in the DD region are below the light line of the air modes, and are also within the band gap of the crystal. The fields therefore decay exponentially in both directions and light is imprisoned at the surface of the crystal. Only when a mode is evanescent on both sides of the interface, a surface wave can exist. It can be demonstrated that every periodic material has surface modes for some choice of termination [31].

2.3 Resonance states in photonic crystals

Up to now, the possibility to localize field in a photonic crystal by creating a defect in the lattice or by truncating the structure are presented. In addition to this, photonic crystal slabs can also interact with external radiations in complex and interesting ways by the excitation of resonance phenomena. In particular, in this thesis I will analyze three different resonance phenomena. The first two, *Plasmon-like surface states* and *Guided Mode resonances*, occurring on the same photonic crystal slab with a negative refractive index in the infrared range. The third one occurs in the visible range when resonances are excited in a very thin photonic crystal membranes and it is connected with the *Bound States in Continuum* phenomenon. All these optical phenomena make photonic crystals an appealing alternative to plasmon metallic substrates and so the presented results open new solutions in light manipulation and trapping at the nanoscale especially for sensing applications and Raman interrogation of single molecules.

2.3.1 Surface states in negative refractive index photonic crystal

Negative refractive index represents an important property of photonic crystal metamaterials and is experimentally verified in a large number of unusual electromagnetic phenomena. As already stated in chapter 1, the group velocity plays an im-

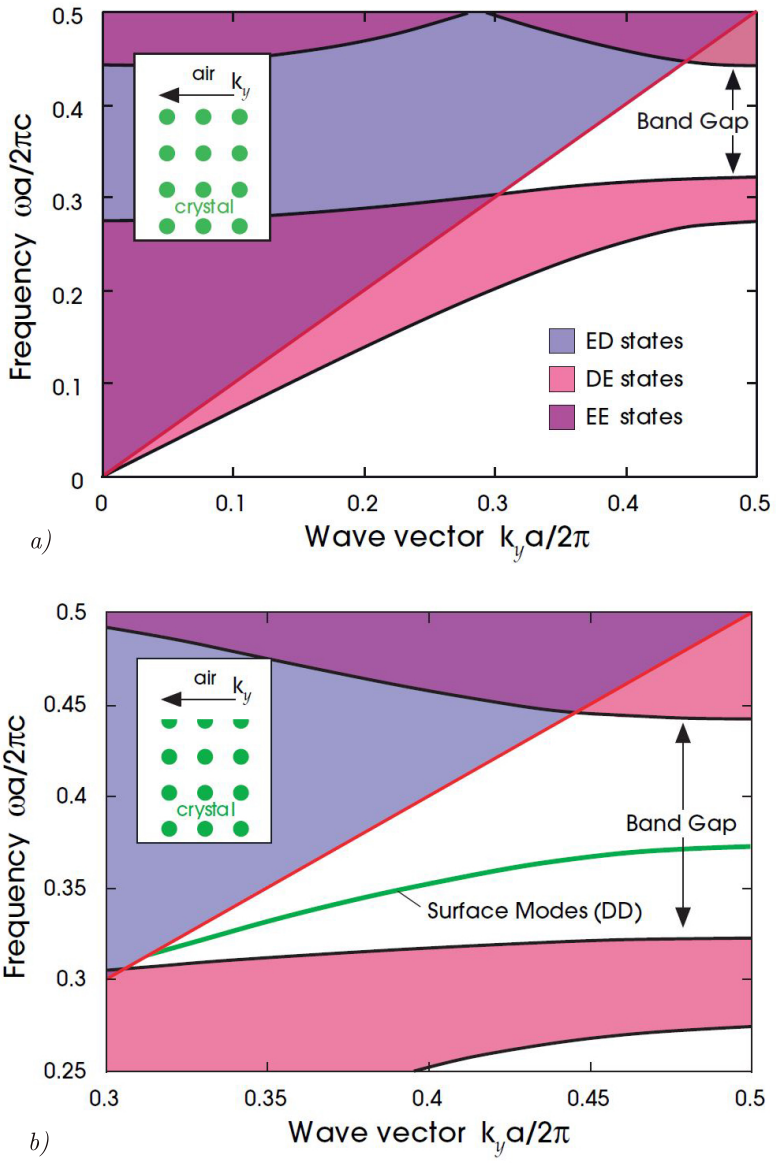

Figure 2.6: The projected band structure of the constant-x surface of the square lattice of rods in air. The shading denotes regions in which light is transmitted (purple EE states), internally reflected (red DE states), and externally reflected (blue ED states). a) The crystal is terminated after a row of rods; this termination has no surface states. b) The slab is truncated at half rods. The line in the gap corresponds to a surface band in which light is exponentially localized to the surface (green, DD).

portant role in this phenomenon. In particular the scalar product $\mathbf{v_g} \cdot \mathbf{k}$ is negative, so $\mathbf{v}_g = {}^{\partial\omega}/_{\partial\mathbf{k}}$ is directed inwards, pointing to the origin of the first Brillouin zone. For example, if we consider a negative photonic crystal slab consisting of holes in silicon, for light that is polarized perpendicular to the surface of the photonic slab (i.e., transverse magnetic with the electric field along the direction of the circular holes), the equifrequency surface exhibits a circular shape (figure 2.7) corresponding to an isotropic medium with an effective index of refraction $n_{eff} = -1$. As in the classical derivation of an optical surface wave, the permittivity satisfies the following condition at the interface between two media 1 and 2 [36]:

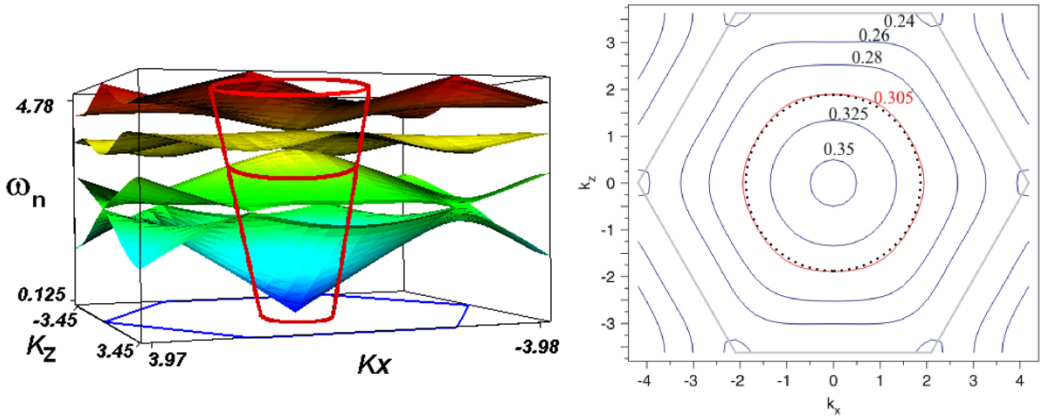

Figure 2.7: a) Band structure of dispersion relation of photonic crystal in the full 2D reciprocal space (k_x, k_z) versus the normalized frequency ω_n. The red cone shows the dispersion relation of air. b) The Equi Frequency Surfaces of photonic crystal. The red circle is the in-plane air dispersion curve for $\omega_n = 0.305$ (colour on line).

$$\frac{k_z^1}{\epsilon_1} = -\frac{k_z^2}{\epsilon_2} \tag{2.1}$$

where $k_z^{1,2}$ is the wavevector in the direction normal to the interface and $\epsilon_{1,2}$ is the permittivity in medium 1 and 2 respectively; the field decays away from the interface if $k_z^{1,2}$ is a positive real number [37]. In the case of a simple metal, the Drude model brings to an effective permittivity given by $\epsilon = \epsilon_0 - \omega_p^2/(\omega^2 - i\gamma\omega)$, therefore assuming negative values in a range of frequencies. The free electron plasma is the physical origin of the Drude model, where electrons oscillate around their equilibrium position at a characteristic plasma frequency ω_p, γ takes into account the damping and ϵ_0 is the permittivity far from the resonance frequency. Non-metal materials, on the other side, are often well described by a harmonic oscillator model

that adds a restoration force to the Drude model, summarized by the Lorentz formula:

$$\epsilon = \epsilon_{0e} + \frac{\omega_p^2}{\omega_0^2 - \omega^2 - i\gamma\omega} \tag{2.2}$$

According to equation 2.2, the permittivity of non-metals can be negative at certain frequency ranges (see Fig.2.8). Thus non-metal materials described by this dielectric permittivity support surface waves with properties similar to SPs in metals [37], with the difference that, usually, the permittivity reaches negative values in the mid-infrared spectral region, whereas metals often do it in the visible or near infrared range.
In a photonic crystal, spatial dispersion can not be neglected because adds a dependence of ϵ by the wavevector k. Nevertheless, we recently demonstrated that equation (2) also holds for photonic crystals, well describing their behaviour in the frequency range where the effective refractive index is negative [38]. In this case, the main advantage of photonic crystals with respect to bulk materials is represented by the possibility of choosing the frequency range of negative permittivity, for instance in the visible or near infrared, by means of an appropriate design of the photonic crystal structure. Experimental evidences about the presence of **Plasmon-like surface states** on a photonic crystal slab will be shown into the chapter 3.

2.3.2 Guided mode resonances

In 1902 Wood observed the presence of narrow bright and dark bands in the reflectivity spectrum of an optical grating. These bands were dependent on the polarization of the incident light and, since they could not be explained by grating theory, they were classified as anomalies [39]. This effect was theorized for the first time by Rayleigh [40] and then by A. Hessel and A. A. Oliner in 1965 who demonstrated that anomalies in the reflection from gratings could be connected to the excitation of surface waves on metallic grating structures [41]. Similar resonant anomalies, named **Guided Mode Resonances**, appear in many materials with a periodic patterning applied to a surface supporting excitations, such as plasmon polariton resonances or sharp spectral features in shallow grating waveguide structures [42] and in photonic crystal structures. In particular reflection and transmission of an incident wave on a photonic crystal slab can exhibit sharp resonances in the spectrum when radiation is coupled with modes of the structure (see fig. 2.9) [43–45].

Guided-mode resonances are now well studied in photonic crystal literature and can provide an efficient way to channel light from within the slab to the exter-

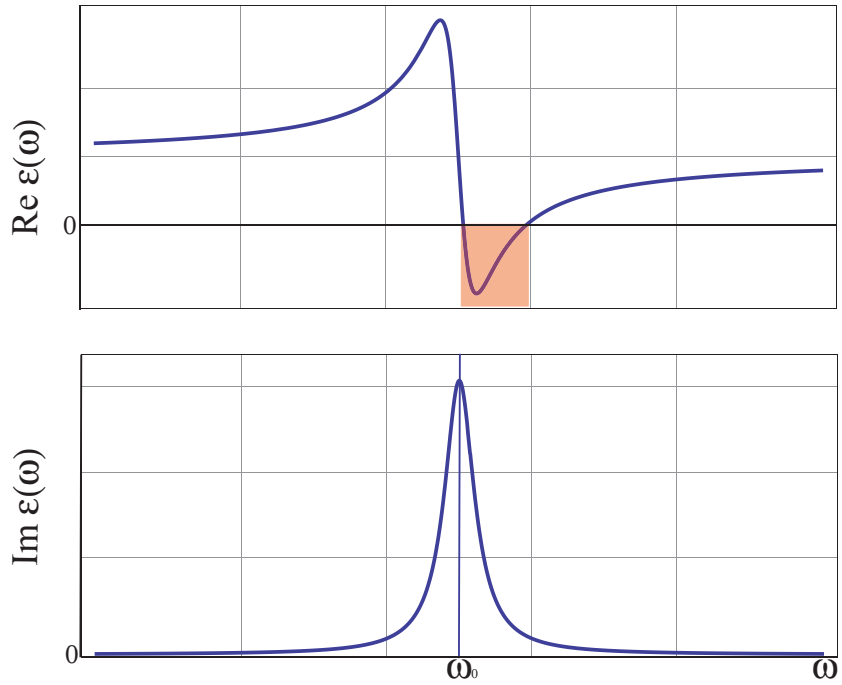

Figure 2.8: Typical real and imaginary part of dielectric function $\varepsilon(\omega)$ modeled by equation 2.2. The coloured rectangle underlines the negative region in the real part of permittivity.

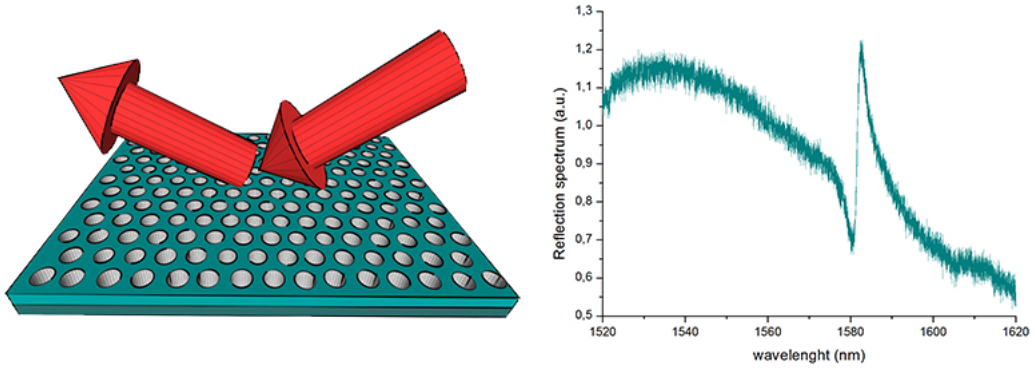

Figure 2.9: Sketch of the external radiation interacting with a photonic crystal slab. When the radiation couples with a photonic crystal mode, a spike in the reflection spectrum appears.

nal environment. Due to the extremely narrow shape of the resonances superposed on the background reflection, they can be used to design optical bandpass filters with elevated symmetrical response and low sidebands [46] or distributed feedback lasers (DFB) with high Q-factor [47]. Moreover the confinement of the optical field within the slab can be used to trap [48] single particle or to enhance the signal from fluorescent elements, making possible high-sensitivity sensors [49]. In addition such structures can be exploited as optical switches or very high quality optical filter [50], useful in advanced optical signal processing [51], taking advantages form the narrow width of the resonance.
In Chapter 4 reflection spectra collected from a negative refractive photonic crystal will be reported. In particular, by studying a hexagonal airhole lattice in silicon, we highlight that the out-of-plane incoming radiation is negatively refracted in the structure.In addition, we propose a new theoretical approach to the guided resonance phenomenon, based on the Fresnel formula, which completes the usually adopted phenomenological model in the context of the Fano resonance approach.

2.3.3 Bound states in continuum

In the last years field enhancement in dielectric structured media has attracted an increasing interest. In general when an incident beam impinges on a lattice the reflected beam can have anomalous variation of the reflected signal. Specifically, it has been demonstrated that perfect light confinement can be achieved because of a particular type of localized state, a **Bound state in the continuum**, first predicted in quantum systems by von Neumann and Wigner [52].

These resonant states, due to the interaction between trapped electromagnetic modes, are characterized by practically zero width and may have a variety of potential applications. The only possibility for these special Fano resonances to completely decouple from the continuum of free-space modes is by mismatching their symmetries. However, fabrication imperfections partially break this simmetry, due to the regularity of the lattice, allowing the coupling of the external incoming beam. When a bound state in the radiation continuum occurs, the electromagnetic field is trapped by the structure for infinite time and, experimentally, it involves very narrow coupled resonances with a high Q value in an open structure. Numerical simulations shown that photonic crystals in high refractive index media can support this phenomenon and can be promising candidate for metal free plasmonic materials. An high field enhancement as large as 700 times the amplitude of the incident wave (see Fig.2.10), can be obtained in a thin structured layer lattice with a refractive index $n = 2$, respect to the amplitude of the incident wave. The key mechanism is a careful control of the lattice structure and of the thickness, which allows

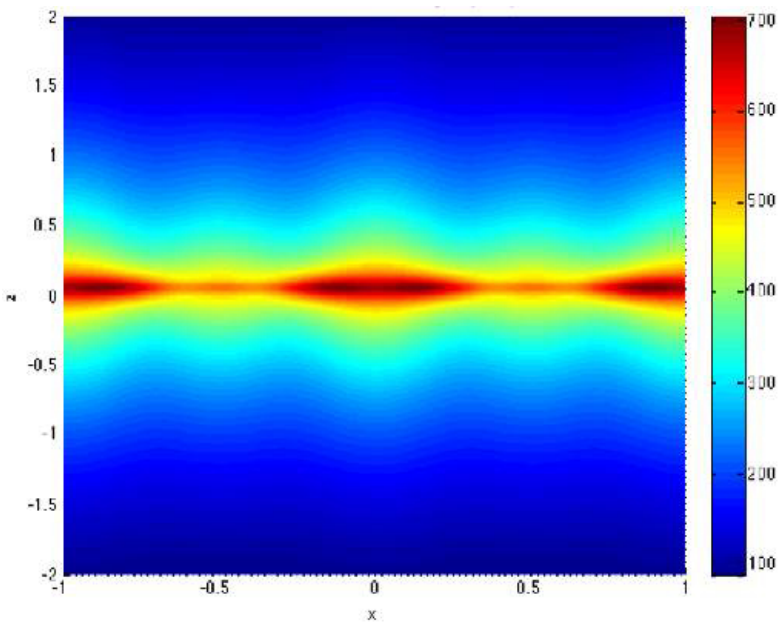

Figure 2.10: A vertical cut of the Electric Field amplitude in resonance condition calculated by using FDTD approach in the unit cell.

a stabilization of the coupling resonant mechanism and of the trapped mode. In Chapter 5 experimental details about the simulation, the fabrication and the characterization of photonic crystal membranes supporting bound states in continuum will be reported.

3

Plasmon-like surface states in negative refractive index photonic crystals

Galileo Galilei recognized the resonance effect in his study of musical strings as early as 1602. Subsequently it was found that resonances - such as mechanical, acoustic and electromagnetic ones - are a universal characteristic of many types of classical and quantum system.

Boris Luk'yanchuk et al.—The Fano resonance in plasmonic nanostructures and metamaterials, Nature Materials 9, 2010

3.1 Introduction

Surface plasmons were recognized for the first time in the pioneering work of Ritchie in the 1950 [53] and are essentially light waves that are trapped on the surface of a conductor, usually a metal, because of their interaction with the free electrons of the material. In this interaction, the free electrons respond collectively by oscillating in resonance with the light wave. The resonant interaction between the surface charge oscillations and the electromagnetic field of the light constitutes the Surface Plasmon and gives rise to its unique properties. Solving Maxwell's equations under the appropriate boundary conditions yields the Surface Plasmon dispersion relation, represented in figure 3.1:

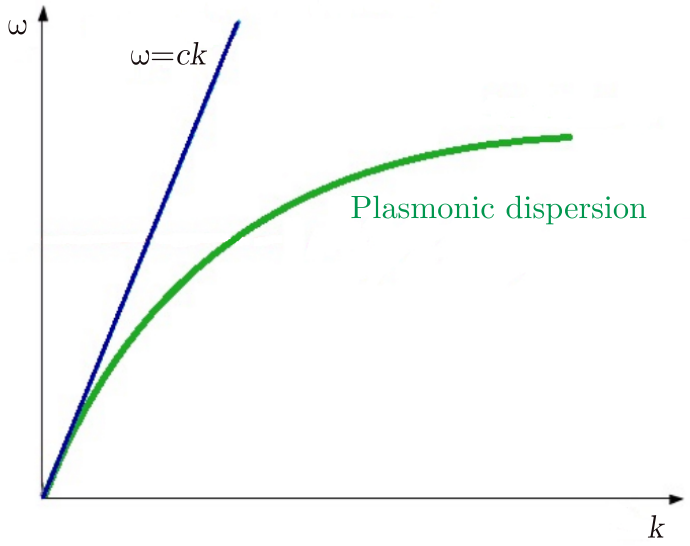

Figure 3.1: Typical shape of the plasmonic dispersion curve (green line) described by eq. 3.2. The blue line refers to the light line.

$$k_{SP} = k_0 \sqrt{\frac{\varepsilon_d \varepsilon_m}{\varepsilon_d + \varepsilon_m}} \tag{3.1}$$

where ε_m and ε_d are the permittivity of the metal and of the dielectric medium. Since a metal contains a large number of free electrons, its dielectric constant ε_m will be negative under a certain angular frequency, the so-called plasma frequency ω_p:

$$\varepsilon_m(\omega) = 1 - \frac{\omega_p^2}{\omega^2} \tag{3.2}$$

and generally this implies that for $\omega < \omega_p$ electromagnetic field cannot propagate in a metal. However, in this frequency range, a wave exists but propagates strictly along the interface between metal and dielectric medium, decaying exponentially into both sides. Concentrating light in this way at the surface leads to an electric field enhancement that can be used to manipulate light interactions and boost non-linear phenomena.

On the other side also a photonic crystal can be designed in order to have a negative permittivity in a certain frequency range (see 2.7) and this could entail the existence of surface states at the interface between a photonic crystal and a

dielectric medium with properties similar to the plasmonic ones. This is the starting idea for the detection of **Plasmon-like resonant states** in a negative photonic crystal.
In this chapter, theoretical and experimental evidences about the existence of surface waves propagating on the top surface of a 2D photonic crystal slab characterized by a negative effective permittivity are reported. In our case, the surface states are excited only at optical polarizations for which no band-gap is supported, being therefore conceptually different from the surface defect state (within the band-gap) due to the photonic crystal periodicity truncation [54]. The surface waves we observe are analogous to surface plasmons supported in metal-based structures and, as a matter of fact, the formalism describing them is close to the classical surface plasmon wave one, where a fundamental role is played by the negative permittivity of metal. Finally, it is worth noting that the proposed device represents a much simpler technological solution, with respect to the previous proposed 3D structures, to manage surface waves in photonic crystal metamaterials. In the following, the theoretical background is presented together with numerical results based on Finite-Difference Time-Domain (FDTD) method on a properly designed 2D photonic crystal slab, which allowed to obtain the spatial distribution of the discussed surface states. Furthermore, their detection by means of an evanescent-coupling method with a high refractive index prism is described, and the experimental reconstruction of their dispersion curve in (ω, k) is presented.

3.2 Materials and Method

3.2.1 Sample Fabrication

The photonic crystal sample is a slab composed of air cylindrical holes in silicon arranged in a hexagonal lattice and is fabricated in collaboration with the Molecular Foundry - Lawrence Berkeley National Laboratory in California. The photonic lattice is obtained using a high-precision nanofabrication process based on high-voltage electron beam lithography and a gas chopping inductively coupled plasma etching process, which alternates an etching step using SF_6 and Ar with a passivation step using CHF_3 and CH_4. Starting with a silicon-on-insulator (SOI) wafer (1.5 mm silicon layer on top of a 1 mm oxide layer), we spin on ZEP 520, a positive electron beam resist, at a thickness of 370 nm. This resist is a positive tone resist, which means that the exposed regions are the ones that will be removed after the electron-beam lithography process.
The resist is patterned using a Vistec VB300UHR EWF electron-beam lithogra-

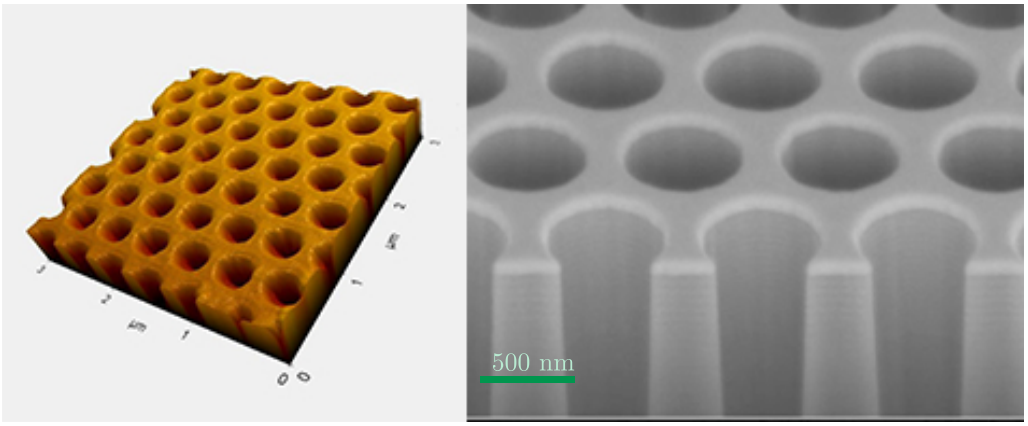

Figure 3.2: Atomic Force Macroscopy (AFM) and Scanning Electron Microscopy (SEM) of the air-cylindrical holes in a exagonal lattice.

phy system and is developed with n-amylacetate. The sought pattern to be written is first edited using the mask editor software L-Edit from Tanner Research. Since the ZEP-520a resist is a positive resist, the design consists of holes arranged in a hexagonal lattice. Thus, the electron beam-patterned resist is used as a mask to etch the underlying silicon layer, down to the SOI, in an Oxford Plasmalab 100 ICP-RIE with a resist mask. The SF_6 chemistry provides the free radicals for isotropic Si etching, while O_2 promotes the growth (at cryogenic temperatures) of a passivation film. This passivation film, with a generic temperature-sensitive formula of $Si_xF_yO_z$, protects the side walls of the etched structures and evaporates after the sample warms to room temperature, leaving behind a clean surface. The etching was performed at $-120°C$. The resulting pattern is formed of cylindrical air holes, and the device is characterized by a lattice constant $a = 472nm$, a hole radius $r = 0.385a$, a holes depht of 0.7 μm and an area of $1x1mm^2$. The ratio $r/a = 0.385$ guarantees the condition of a negative index medium in the region centered at the wavelenght $\lambda = 1.5\mu m$.

3.2.2 FDTD simulations

In order to know how the electromagnetic fields are propagating in space and time in the designed photonic crystal slab, the finite-difference time-domain (FDTD) modelling method is used. The key point of this technique is to discretise the time dependent Maxwell's equation using central-difference approximations to the space and time partial derivatives. In particular, the physical region over which

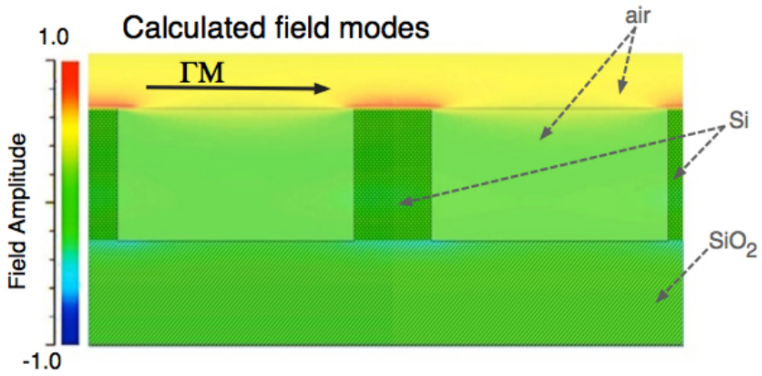

Figure 3.3: Two elementary cell of the 2D photonic crystal slab with the calculated field distribution in correspondence of a wavevector in M point of the Brillouin zone. This field is localized in proximity of the photonic crystal-air interfaces with an enhancement factor of about 80.

the simulation will be performed, i.e. *computational domain* is established. The structure is divided into a finite lattice of grid points, and the material of each cell within the computational domain must be specified. The finite-difference equations are solved at these grid points for a given instant in time and the computation is repeated for each time step.
By using this approach, the mode distribution of all through the structure are calculated. As shown in Fig. 3.3, the simulated electric field is localized close to the air-photonic crystal slab interface, confirming the assumption that a surface wave can exist also on the top of a negative photonic crystal. The device exhibits an effective negative refractive index around the normalized frequency $\omega_n = a/\lambda = 0.31$. The dispersion curve calculated along the ΓM direction (see the red curve in figure 3.6a) is similar to the Surface Plasmon wave dispersion reported in fig.3.1, with the crucial difference that the allowed values of the parallel wavevectors ($k_{//}$) are upper limited to π/a. In fact, the dispersion lines in a periodic structure are folded into the first Brillouin zone, taking into account the periodicity of the wave vector. Moreover, for the chosen experimental parameters (TM polarization), there is not a photonic bandgap that prevents wave propagation.

3.2.3 Experimental details

The surface states in the reflection spectra of the 2D photonic crystal slab have been detected by means of an evanescent-coupling method with a high refractive index prism. In particular we used the Kretschmann configuration, usually adopted to excite surface plasmons in metals in order to underline the similarity also into the coupling method. The experimental set-up is shown in Fig. 3.4. Monochromatic

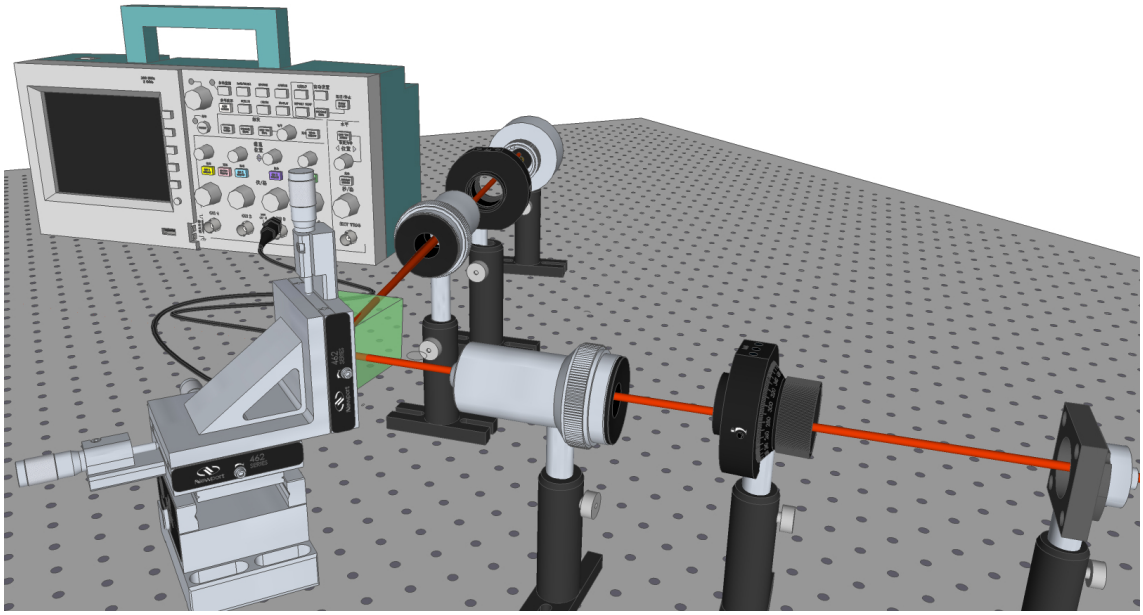

Figure 3.4: Sketch of the experimental set-up used to couple laser light (Tuneable diode laser 1520-1620 nm) into the photonic crystal by means of an evanescent-coupling method with a high refractive index prism. The input radiation is polarized and focused on the sample by an objective. The reflected signal is then collected by another objective and detected by a photodiode connected to an oscilloscope.

light from a tunable CW diode laser (Ando AQ4321D; λ=1520-1620 nm, P_{max}=5 mW) is polarized parallel to the incident plane and then focused by a long working distance 50x objective lens (Mitutoyo L03030105A) at the bottom face of a SFL11 prism (refractive index=1.74). The incidence angle θ is larger than the critical total internal reflection angle (θ_c= 35.1°) and varied in the range between 57-63° with a step of 1° to change the in-plane wavenumber $k_{//}$. The 2D photonic crystal is brought in contact with the bottom of the prism by means of a precision clamping-screw necessary to tune the thickness of the sub-micrometric air layer acting as a coupling zone between the prism and the photonic crystal slab. The wavelength λ of the laser radiation can be scanned in the range between 1520-1620 nm. By varying λ the evanescent wave can penetrate the bottom face of the prism and, whenever the proper value of $k_{//}$ is matched, couple the surface modes of the 2D photonic crystal with a consequent reduction of the intensity of the reflected light. The reflected light is collected by a second 50x objective lens and measured by a photodiode (Thorlabs high-speed InGaAs DET410) connected to an oscilloscope.

3.3 Results and discussion

When the coupling between the evanescent wave and the surface mode takes place, the intensity of the reflected light is reduced giving place to a typical resonance peak (see Fig. 3.5). The resonance is observed only for a TM polarization (i.e., electric field vector parallel to the incident plane), therefore in presence of negative effective permittivity [38, 55], but in absence of any band-gap. For this reason, this phenomenon is completely different from the surface states in a three-dimensional photonic crystal previously observed by Ishizaki and Noda [54] where the effect is due to the combination of photonic band-gap and index guiding.
The reflectance spectrum obtained at the angle of incidence θ=60° is shown in Fig. 3.5-(a). In order to determine the minimum reflectivity value in Fig. 3.5, we fitted all the data with a Fano line-shape [56, 57], taking into account the interference between direct and resonant scattering. In contrast to a Lorentzian resonance, the Fano resonance exhibits a distinctly asymmetric shape and arises from the constructive and destructive interference of a narrow discrete resonance with a broad spectral line or continuum. This resonance phenomenon occurs in light scattering from simple spherical particles, but also plasmonic nanostructure [57], such as metallic layer or nanoparticles, and photonic crystals [56] can exhibit sharp Fano resonances. Thus, the reflection spectrum is fitted with a Fano line-shape

Table 3.1: Fano fit parameter results

θ (deg)	ω (a/λ)	q	γ (a/λ)
± 1	$\pm 2{\cdot}10^{-5}$	± 0.004	± 0.5
57	0.31085	0.130	20.4
58	0.31084	0.128	20.5
59	0.31048	0.129	21.0
60	0.31058	0.130	19.9
61	0.30984	0.129	19.9
62	0.30941	0.127	20.0
63	0.30846	0.131	20.3

given by:

$$R(\omega) = R_d + R_g \frac{(q\gamma_F + \omega + \omega_0)^2}{(\omega - \omega_0)^2 + \gamma_F^2} \tag{3.3}$$

where R_d is the direct contribution, while the second term is the resonant contribution with amplitude R_g, frequency ω_0 and linewidth γ_F; q is the Fano factor which determines the asymmetrical shape. As clearly shown in Fig. 3.5-(a), the Fano line-shape well fits the experimental data. The obtained fit parameters are reported in Table 3.1. The slightly asymmetrical shape is due to the combination of two factors: a large and broad resonance due to the slab and a sharp resonance due to the surface wave coupling.
By collecting the reflection spectra for various incident angles and measuring the relative resonance peak frequencies, the dispersion characteristics of the surface states for various photonic crystal directions can be derived. In Fig. 3.6-(b) is reported the measured dispersion characteristic of the surface modes as function of the in-plane wavenumber $k_{//} = n_{prism} k_0 \sin\theta$, where $k_0 = 2\pi/\lambda_0$ is the wavenumber in the vacuum, and θ the incidence angle.

At low $k_{//}$ the surface modes approach the light line asymptotically, and at large $k_{//}$ the frequency of the mode reach a plateau value. The measured values agree with the simulated dispersion curve (red line in Fig. 3.6) obtained by using the 3D FDTD method. The agreement between the simulation and the measured data confirms the surface plasmon-like nature of the measured wave. More precisely, the combination of the evanescent-mode coupling technique with the experimental observation that the modes are confined below the light line (dashed line in Fig. 3.6) already implies that such modes are inherently evanescent in air.

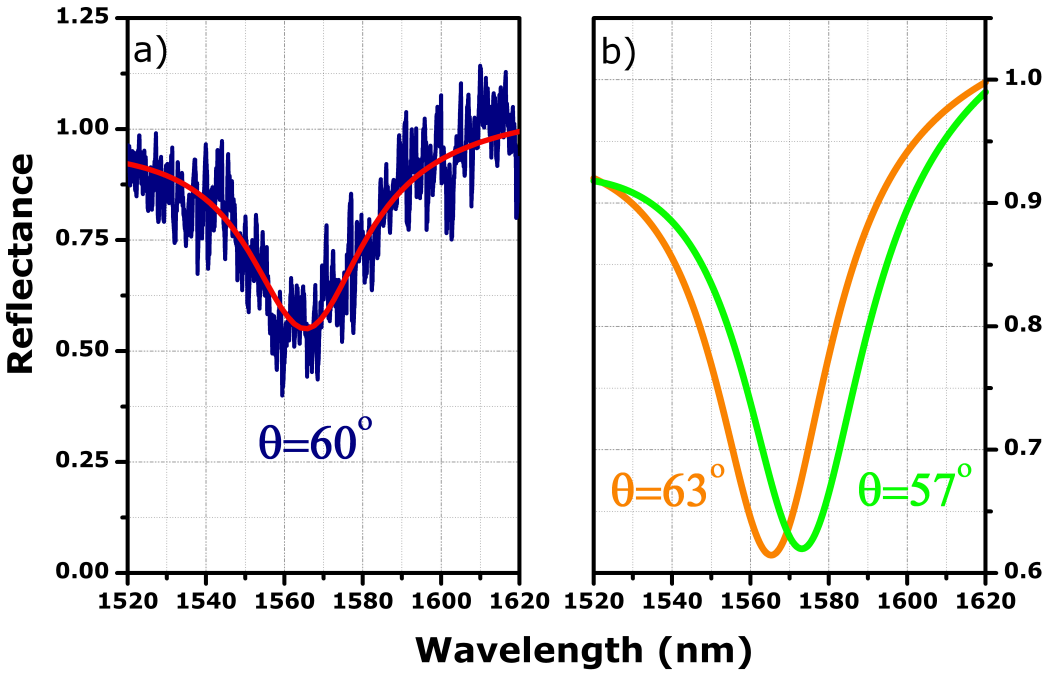

Figure 3.5: (a)Experimental reflectance spectrum at θ=60° (blue line) and best-fit by Fano line-shape (red line). (b) Fits relative to two different angles of incidence.

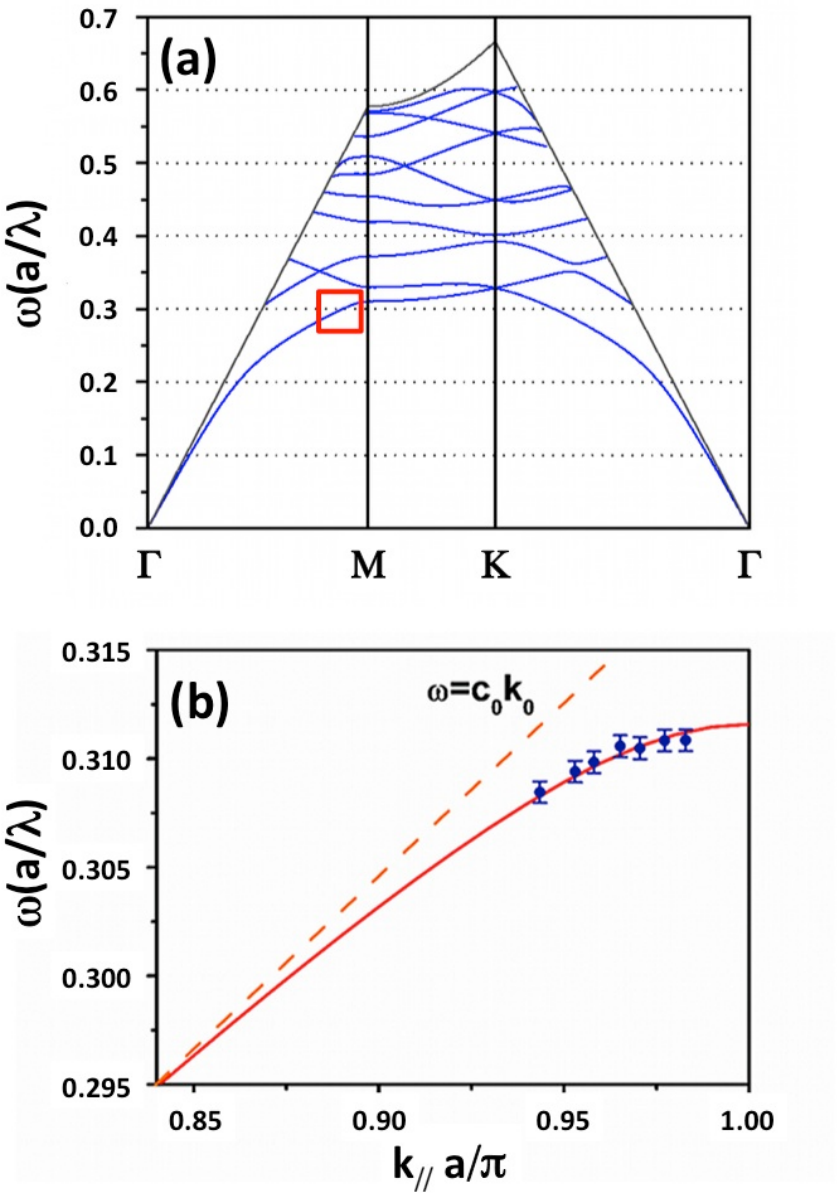

Figure 3.6: (a) Simulated dispersion of odd modes in photonic crystal slab. The red rectangle highlight the experimentally analysed region. (b) Measured (blue dots) and simulated (red line) dispersion characteristic of the 2D photonic crystal slab surface modes. The light line is also shown (dashed line).

3.4 Final considerations

In this first block of my experimental work I have demonstrated that, in a 2D photonic crystal slab, photons can be confined and propagate through surface states related to the metamaterial negative refractive index properties. In particular this waves localized at the surface can be excited in a negative permittivity photonic crystal and have features similar to the plasmonic ones in a metal. The experimental methods exploited to excite and detect such surface waves is also similar to those used in standard plasmonic structures, considering that the surface-plasmon-like wavevector cannot directly couple to the wavevector in air. These optical results, combined with contemporary micro- and nano-fabrication techniques, can find important applications for the control of the radiation field by 2D photonic crystal slabs. A remarkable implication of these surface modes is the analogy with Surface Plasmons and the efficient coupling of light from an external medium. Crucially, in our case the light manipulation is achieved in an absorption-free medium opening the way to important new sensing applications. In next chapter, I will report results about another resonance phenomenon, named *Guided Mode Resonances*, coupled in the same photonic crystal sample. In this case I show you the possibility to excite the modes allowed into a photonic crystal let the external radiation interact with the band structure.

4

Guided mode resonances in negative refractive index photonic crystals

It is a well-known fact that in the spectra formed by a diffraction-grating the light is unevenly distributed, that is the total light in any one spectrum will not recombine to form white light. I have been examining a most remarkable grating recently ruled on one of the Rowland dividing-engines in which this uneven distribution is carried to a degree almost incomprehensible.

R.W. Wood—On a remarkable case of uneven distribution of light in a diffraction grating spectrum, Philosophical Magazine Series 6, 1902.

4.1 Introduction

In the previous chapter, the possibility to excite resonance surface states at the interface between a negative photonic crystal and air has been discussed. However, resonance peaks in reflection or transmission spectra can be detected also when the external radiation coupled with the modes propagating into the photonic crystal. In particular, in this chapter novel insight into the reflectivity properties of a negative refracting photonic crystal slab are revealed. By studying an hexagonal

air holes lattice in silicon, we highlight that the radiation incoming out of plane is negatively refracted in the structure. If the in-plane properties of negative refraction in a photonic crystal slab has been studied in last years [58–64], for the first time negative refraction is here experimentally detected out-of-plane. Specifically, an imaging of the radiation coupled into a photonic crystal slab when the resonance occurs is reported. By using an infrared camera, we were able to visualize the interaction between the incident light and coupled radiation backward propagating. In addition, we propose a new theoretical approach of the **Guided Mode Resonance** phenomenon, based on Fresnel formula, which completes the usually adopted phenomenological model [65] and which shows a very good agreement with the experimental data.

4.2 Guided mode resonances in photonic crystal slabs

As discussed in Chaper 1, photonic crystal slabs are a particularly important class of photonic crystal structures consisting in a periodic arrangement with a finite height. This kind of structure can support in-plane guided modes that are completely confined by the slab without any coupling to external radiations. They cannot escape from the structure and are guided into the slab. Outside the slab, the wave vector of these modes becomes complex and shows an exponentially decaying intensity profile. However a photonic crystal slab can also interact with external radiation, via the coupling of a *guided mode resonance*. A guided mode resonance arises from resonant coupling between external radiation and modes of a photonic crystal slab and manifests itself as a spike in the reflectivity signal [43–45]. They are polarization and angle dependent and, due to their nature, they are very sensitive to the external environment and a variety of applications are allowed [46–51]. In chapter 2, the band structure of a photonic crystal slab has been shown. Radiation modes lie above the light line and they can be even or odd depending on the mirror simmetry of the slab. Furthermore the guided modes above the light line can now couple to radiation modes and possess a finite lifetime. These modes therefore become guided resonances.
The theoretical model widely used in literature for the analysis of the guided resonances in a photonic crystal slab is obtained using phenomenological considerations based on the line shape analysis of the resonances [65]. A guided resonance appears as a peak in a reflection or transmission spectrum and can be considered as an overlapping between a Lorentz resonance shape and a Fabry-Perot background. In fact, by examining the time dependence of the fields, it is possible to

distinguish two different steps in the time sequences, the initial pulse and a long decay. The presence of these two steps involved the presence of two paths in the reflection or transmission process. The first is the direct process, due to interaction between the radiation and the slab, while the second one is an indirect process due to the interaction of a portion of the radiation with the photonic crystal. This energy portion can excite the guided resonance and its power decays slowly out of the structure and produces the long decaying tail. The Fourier transform of the decaying tail is the typical symmetric Lorentzian line shape. Thus, the transmission or reflection spectrum is given by the interference between the two pathways. In particular, if r_d and t_d are the direct transmission coefficients, the transmitted amplitude and the reflected amplitude can be written as:

$$t = t_d + f\frac{\gamma}{i(\omega - \omega_0) + \gamma} \tag{4.1}$$

$$r = r_d \pm f\frac{\gamma}{i(\omega - \omega_0) + \gamma} \tag{4.2}$$

where ω_0 is the center frequency, γ is the width of the Lorentzian shape and f is the complex amplitude of the resonant mode. The plus and minus sign in Eq 4.2 refers to resonant modes that are even and odd, respectively, with respect to the mirror plane parallel to the slab. The complex amplitude can be determined by using the relation:

$$|t|^2 + |r|^2 = |t_d|^2 + |r_d|^2 = 1 \tag{4.3}$$

By combining them with the 4.1 and 4.2, we obtained the constraint:

$$f = -(t_d \pm r_d) \tag{4.4}$$

In conclusion, the model just reported is based on the analysis of the reflection or transmission spectrum. By using this method it is possible to fit with a good accuracy the spectrum of a photonic crystal slab taking into account the direct contribution do to interaction between the radiation and a uniform slab and the indirect contribution due to the presence of the resonance. Moreover it is possible to determine the resonance width γ and the complex amplitude f, which is indipendent of the resonance width. However, this kind of phenomenological approach cannot give information about the origin of the coupling process between the external radiation and the photonic crystal structure. In the next paragraph a new model based on physics considerations will be discussed.

4.3 Guided mode resonances in negative refracting photonic crystals

4.3.1 A new theoretical approach

As stated in chapter 1, one of the most important property of a photonic crystal is the possibility to design and fabricate it in order to have a negative refractive index in a certain frequency range. In previous chapter we reported that this feature makes the photonic crystal slab similar to a metal and that surface states are allowed [66]. In addition to this phenomenon, this periodic structure can support also other resonance states and it has been shown [67] that they can be analyzed by treating it as a *multilayer system*. This property has been experimentally demonstrated by performing ellipsometric measurements on the photonic crystal slab and acquiring the signals ratio:

$$\frac{r_p}{r_s} = \tan\psi e^{-i\Delta}$$

where r_p and r_s are the complex Fresnel coefficients for p and s polarization and ψ and Δ are, respectively, the acquired spectrum and the phase spectrum. Thus, the photonic cystal slab can be considered as made up of the substrate (e.g. Silicon Oxide), the patterned area, modeled as a generic Lorentz oscillator, and the environment (e.g. the air).

$$\varepsilon_1 = \varepsilon_{SiO_2}$$

$$\varepsilon_2 = \varepsilon(\omega) = \frac{\mathrm{f}\omega_0^2}{\omega_0^2 - \omega^2 + i\gamma\omega} + \varepsilon_\infty \tag{4.5}$$

$$\varepsilon_3 = \varepsilon_{air}$$

where ε is the dielectric constant, ω_0 the resonant frequency and γ the damping constant (in figure 4.1 the multilayer sample model is sketched).

In this way the resonator behavior is *inherent* in the structure and the photonic crystal is schematized as an homogenous material with $\epsilon(\omega)$ given by (4.5). In such a case we can use the usual Fresnel relations in order to study the resonances features in the reflectivity spectrum. For example, for a three-layer system *silicon oxide/photonic crystal/air* the reflectivity R for p-polarized light is given by [42]:

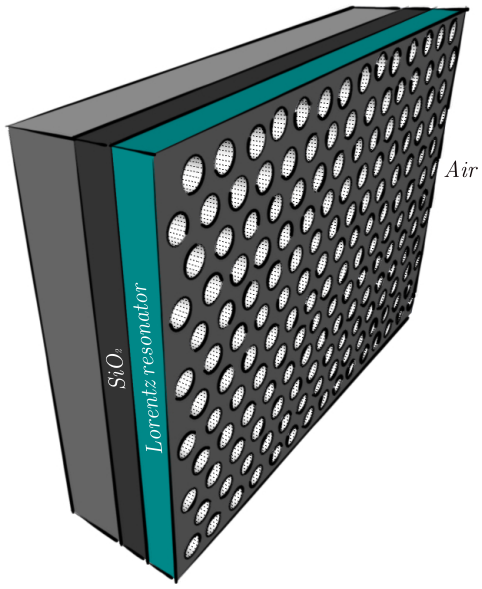

Figure 4.1: Sketch of the Oxide/PhC - Lorentz Resonator/air system.

$$R = |r_{123}|^2 = \left| \frac{r_{12} + r_{23} \exp(2ik_{z2}d)}{1 + r_{21}r_{23} \exp(2ik_{z2}d)} \right|^2 \tag{4.6}$$

with the reflection coefficients:

$$r_{ij} = \frac{\varepsilon_j k_{zi} - \varepsilon_i k_{zj}}{\varepsilon_j k_{zi} + \varepsilon_i k_{zj}} \tag{4.7}$$

and the wave vector components along z axis:

$$k_{zi} = \sqrt{\varepsilon_i \frac{\omega^2}{c^2} - \frac{\omega^2}{c^2} \sin^2\theta} \tag{4.8}$$

By using this approach, the reflection/transmission signals can be analyzed, taking into account also the presence of the resonance spikes overlapped to the spectra.

4.3.2 Experimental setup

The photonic crystal sample is a slab constituted by a 2D hexagonal lattice with a thickness of 0.7 μm, shown in Fig.4.2. Photonic lattice is obtained by a high-precision nanofabrication process with high-voltage electron beam lithography

and a gas chopping inductively coupled plasma etching process. The pattern is formed by cylindrical air holes and it is etched on a Silicon-on-Insulator (SOI) wafer. The device is characterized by a lattice constant a = 472 nm, a hole radius r=0.385a and an area of 1x1 mm. The ratio r/a=0.385 guarantees the condition of negative index medium $\overrightarrow{v}_g \cdot \overrightarrow{k} < 0$[59][68][61][58][62][60][64]. In this case, the photonic crystal behaves as a medium with an effective isotropic index $n_{eff} = -1$ for the wavelength of 1.55 μm. The fabrication is performend in collaboration with the Molecular Foundry - Lawrence Berkeley National Laboratory in California. Experimental reflectivity spectra from the photonic crystal sample are obtained using a tunable CW diode laser (Ando AQ4321D) which emits monochromatic light with a maximum variable power of 5 mW and a wavelength variable between 1520 nm and 1620 nm. Since the guided mode resonances are polarization dependent [43–45], the radiation is linearly polarized and is then focused at the top surface of the sample. The light reflected from the sample is polarized again and detected by a photodiode (Thorlabs high-speed InGaAs DET410). The incidence angle θ has been changed from 40° to 75°. The experimental set-up is schematized in Fig.4.2.

4.3.3 Results and discussion

As previously illustrated, a sharp peak appears into the reflection spectrum when the coupling between the incident radiation and a guided mode occurs. The resonance has been observed only for a p-polarization, i.e. with the electric field vector parallel to the incident plane. Although guided resonances have been studied since many years, there are no experimental evidences concerning the propagation of the coupled light through the photonic crystal and there is a gap in the study of the modes really excited inside the structure. Whenever the coupling occurs, we suppose that the radiation propagates through the photonic crystal and can be detected by the out-of-plane scattering from the surface. Fig. 4.4 shows the infrared (IR) images of the radiation coupled into the structure at the resonance condition (λ=1588 nm and θ=65°) taken in front of the slab and on its lateral side. Surprisingly, the radiation propagates for few millimeters into the photonic crystal. In correspondence of a guided resonance, the light passes through the whole photonic crystal (1x1mm^2), passes also through the adjacent SOI planar waveguide (about 1 mm length) and is then scattered at the end of the SOI region by the irregularities of the surface illuminating the whole perimeter of the right SOI region, Fig. 4.4a. Changing the wavelength slightly out of resonance (λ=1591 nm), the light does not couple with the structure and the SOI perimeter is no more illuminated Fig.4.4c.

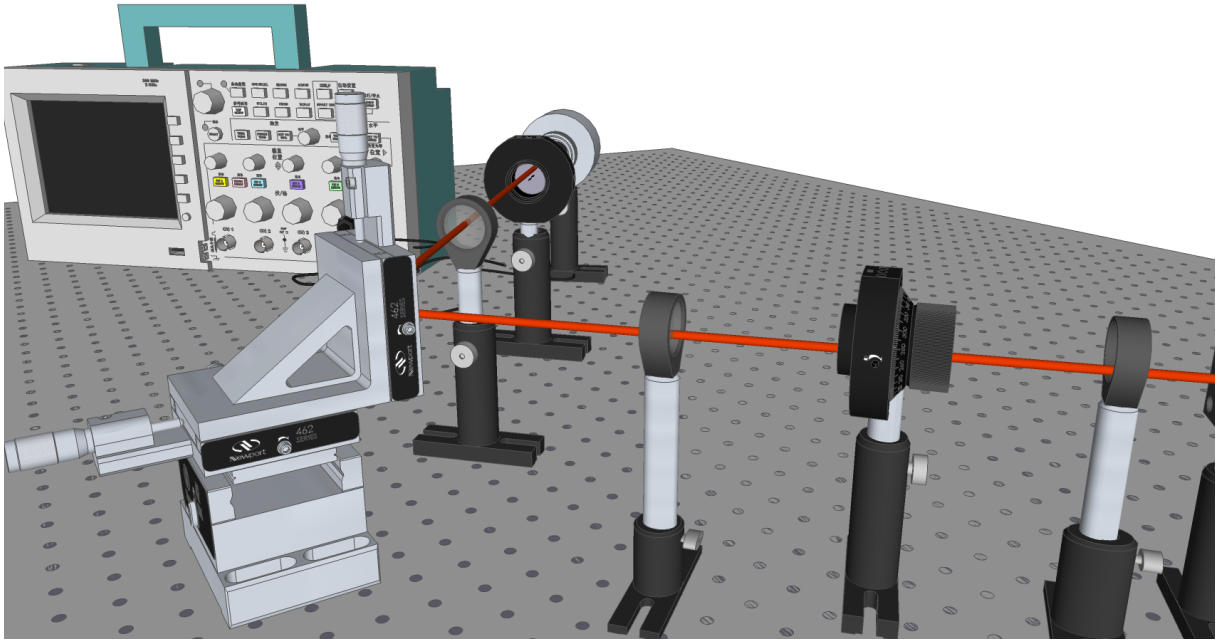

Figure 4.2: Schematic view of the experimental set-up used to couple laser light (Tunable diode laser 1520-1620 nm) into the photonic crystal. The input radiation is polarized and focused on the sample. The reflected signal is then polarized and detected by a photodiode connected to an oscilloscope.

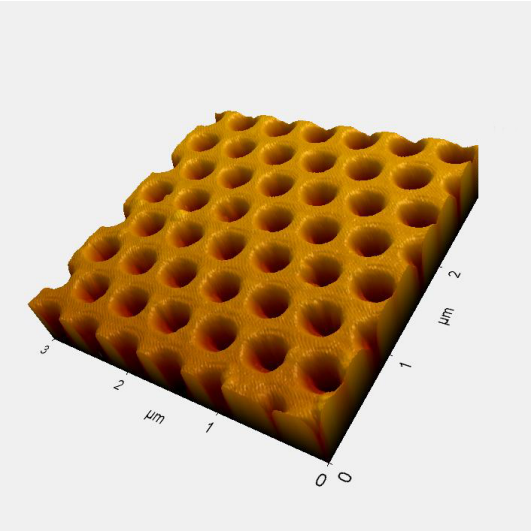

Figure 4.3: AFM.

More interesting result is the back-propagation of the coupled radiation and this can be connected with negative index behavior of the photonic crystal under consideration. This effect is confirmed by a Rigorous Coupled Wave Approach (RCWA) simulation, a semi-analytical method in computational electromagnetics where fields are represented as a sum of spatial harmonics in the Fourier-space. The calculated time average Poynting vector inverts direction crossing the photonic crystal interface in a few tens of nanometers, Fig. 4.6b.

Finally we validate our new theoretical approach fitting the experimental spectrum directly with Fresnel formula (4.6). The calculated fit curve shows an excellent agreement with the experimental spectrum, as reported in Fig. 4.5a. This confirms that negative index photonic crystal layer is strongly correlated with a resonant effective permittivity [69] that in this case can be modeled with a Lorentzian function (eq. 4.5) [67].

Moreover we estimated the experimental quality factor Q. The value obtained is in the order of 10^3 and is among the highest values experimentally determined for a 2D PhC slab. In addition, by varying the angle of incidence in the reflectivity spectrum, we calculated the band structure of the photonic crystal [43–45]. In Fig. 4.5b the measured dispersion characteristic of the surface modes as function of the in-plane wavenumber is reported. Once again the measured values (square dots) are in excellent agreement with the simulated dispersion curve (triangle dots) obtained by using RCWA. This corresponds to the sign of the calculated and measured group velocity of the mode along the parallel wavevector, k_p. Indeed from

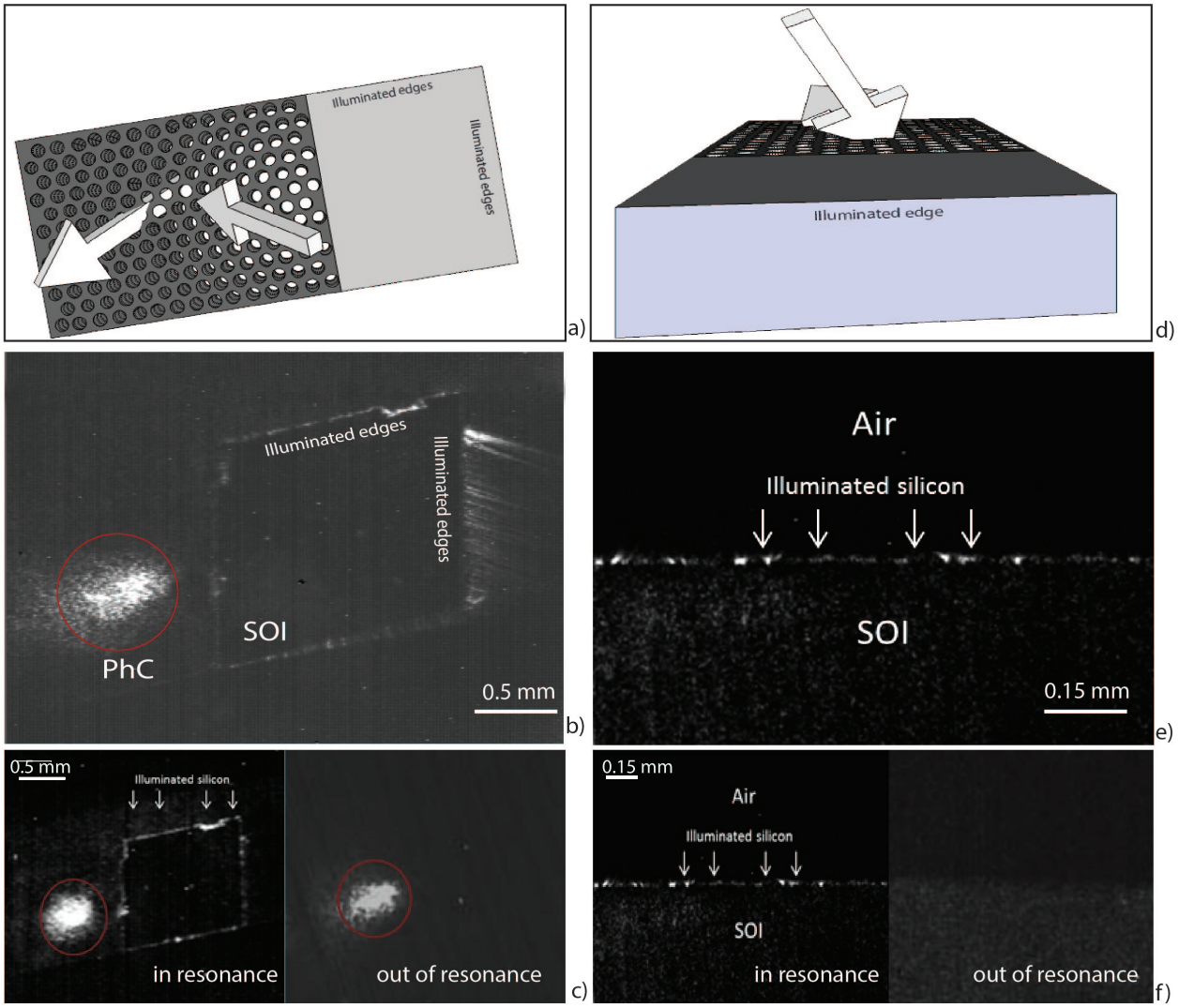

Figure 4.4: Infrared images of the illuminated SOI region when the resonance occurs (b,d), λ=1588 nm and out of the resonance condition (c,e), λ=1591 nm. The pictures are taken on the top of the sample (d-e) and on the lateral side of the slab (b-c). Figure 2a: picture of the IR camera positions).

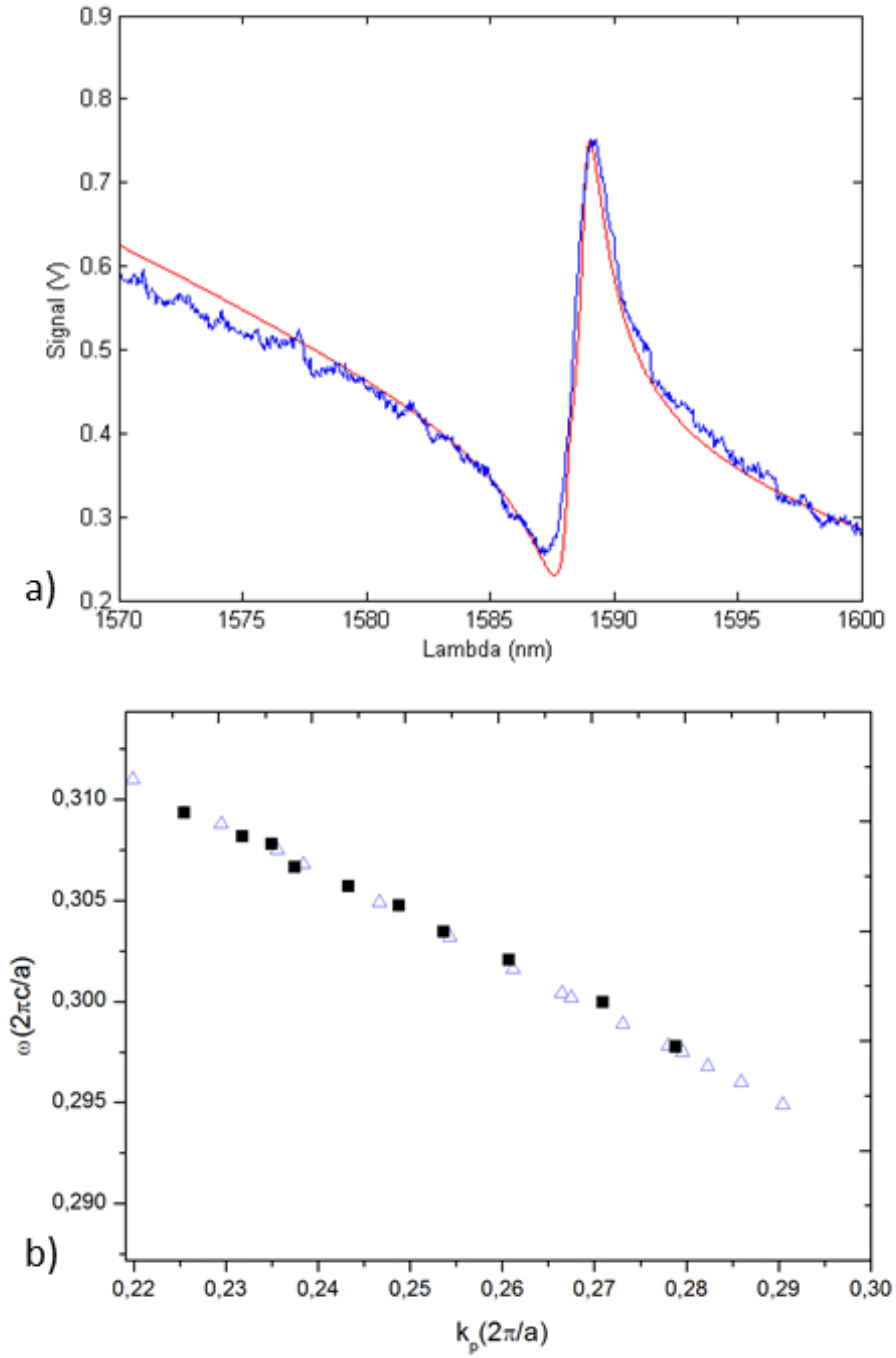

Figure 4.5: : a) Comparison between theoretical and experimental points. The fit curve(red line) shows a good agreement with the experimental spectrum (blue line) . b) Comparison between calculated (triangle dots) and determined (square dots) band structure.

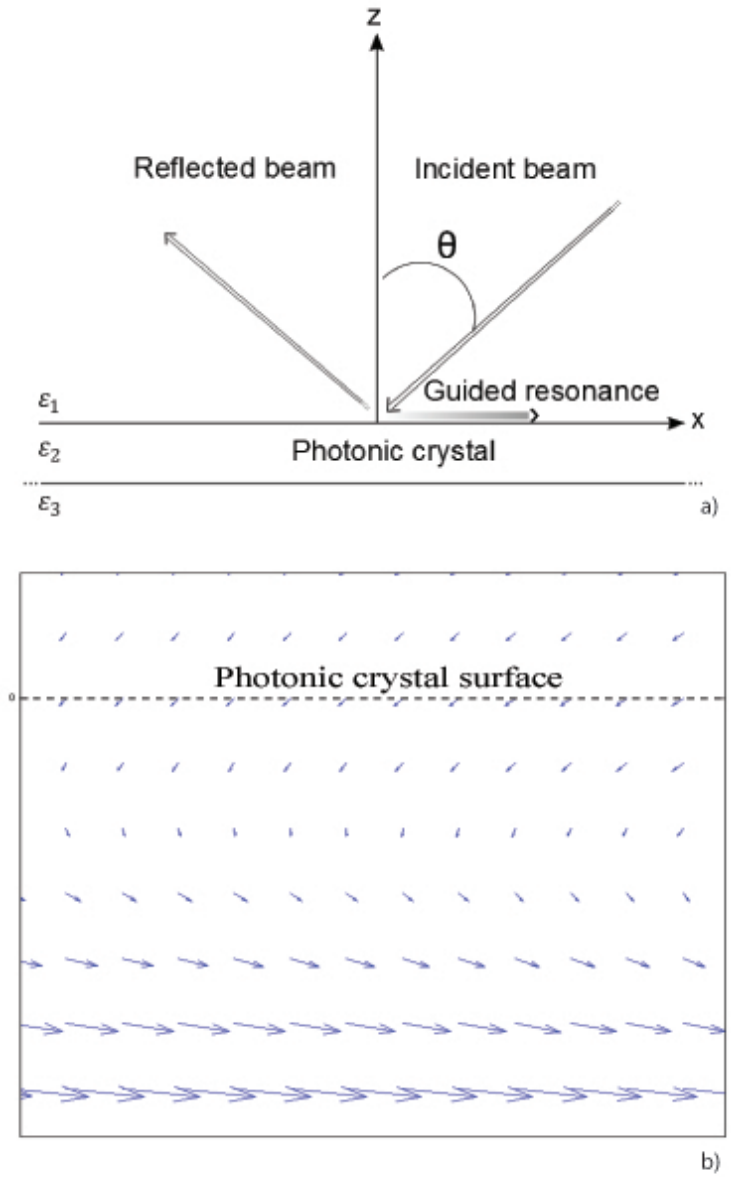

Figure 4.6: The sketch of the incident, reflected and guided beam (a). The calculated time average Poynting vector in a 60x60 nm^2 area in the xz plane, crossing the photonic crystal surface in the resonance condition (b).

Fig. 4.5b we get $\overrightarrow{v_g} = \frac{\partial \omega}{\partial k_p} < 0$, in agreement with the results obtained with the imaging analysis.

4.3.4 Final considerations

In this chapter we presented a new insight on guided resonances phenomenon in photonic crystal structure. In addition to the usual study of the reflection spectrum,imaging measurements proving the coupling of the external radiation with photonic crystal modes are reported. Furthermore we succeed in following the propagation of the guided radiation into the structure, showing that the light is back-propagating for few millimiters into the slab. We connected this effect to the negative behavior of the photonic crystal and we modeled its effective permittivity with a Lorentzian function. Using this model, we were able to fit the experimental spectrum with a simple Fresnel relation, improving the usual standard phenomenological line-shape analysis.

5

Bound states in continuum in photonic crystal membranes

A long time ago, von Neumann and Wigner showed that there are quantum systems which have bound states above the continuum threshold. Later, physical systems with this remarkable property were found. Finally, it was proved that bound states in the continuum can occur due to the direct and via-the-continuum interaction between quasistationary states and can be viewed as resonances with practically infinite lifetimes.

D. C. Marinica, A. G. Borisov and S.V. Shabanov—Bound States in Continuum in Photonics, PRL 100, 2008

Introduction

Local enhancement of the electric field in photonic structures is extremely appealing for a wide range of applications such as sensing, nonlinear phenomena, energy conversion [70–73]. In particular an electromagnetic wave of a specific frequency can be localized and trapped by structures such as photonic [34, 74, 75] and plasmonic [76] nanocavities, in which outgoing waves are completely forbidden. However, the field enhancement of structured dielectric surfaces is a relatively unexplored field, with an increasing interest in the last years [24–27].

Very recently [77] it has been demonstrated that perfect light confinement can be achieved in photonic crystal slabs because of a particular type of localized state: a **Bound State in the Continuum** (BIC). Historically, BICs first appeared in quantum systems thanks to von Neumann and Wigner [52] who interpreted the phenomenon as the interference of resonances in direct and via the continuum channels. Hereafter it was demonstrated that this effect affects not only the quantum systems but also many areas of physics, including photonics [78–81], aquatic, and acoustic waves [82], etc.
In this last chapter, the possibility to excite BICs in a photonic crystal membrane is shown. Specifically numerical simulations demonstrate that a suitably designed photonic crystal in a low contrast dielectric media can exhibit an extremely high field enhancement of a factor 10^6 in intensity larger then the incident beam. The membranes are fabricated by means two different fabrication techniques, the *Nanoimprint Lithography* and the *Electron beam lithography* , in two different media, Titania and Silicon Nitride. Finally, experimental evidences about the presence of BICs in this structured layers will be reported.

5.1 Simulations

Lattice resonances are an inherent property of the periodic structure that is independent from the external excitation. In particular, some modes with infinite lifetimes can exist at normal incidence, i.e. in the Γ point of the Brillouin zone, where symmetry protects such modes preventing the radiation coupling outside the photonic crystals [83, 84]. Some symmetry consideration can help in the modes analysis. In particular let now remind that in the Γ point of the Brillouin zone a square lattice photonic crystal slab, as in Fig. 5.1a, has a C_{4v} point group symmetry inside the lattice plane and a C_{1h} symmetry in direction normal to the lattice plane, corresponding to even/odd symmetry respect to such mirror plane. The symmetry condition matching allows only doubly degenerates modes to couple with a normal incident wave and for such a reason the guided mode resonances are always doubly degenerate [85].

The numerical study of the excited modes in the structure had been performed by using a full tri-dimensional Rigorous Coupled Wave Approach (RCWA) based on a Fourier modal expansion [86]. The designed structure consists of a square lattice of holes in a material with refractive index equal to 2. Fig.5.1b shows the calculated band. At a first analysis, the principal band around the normalized frequency 0.96 is identified. However, by zooming the region around the incident angle $\theta = 0°$ (see Fig.5.1c) extremely narrow bands appear around the frequency

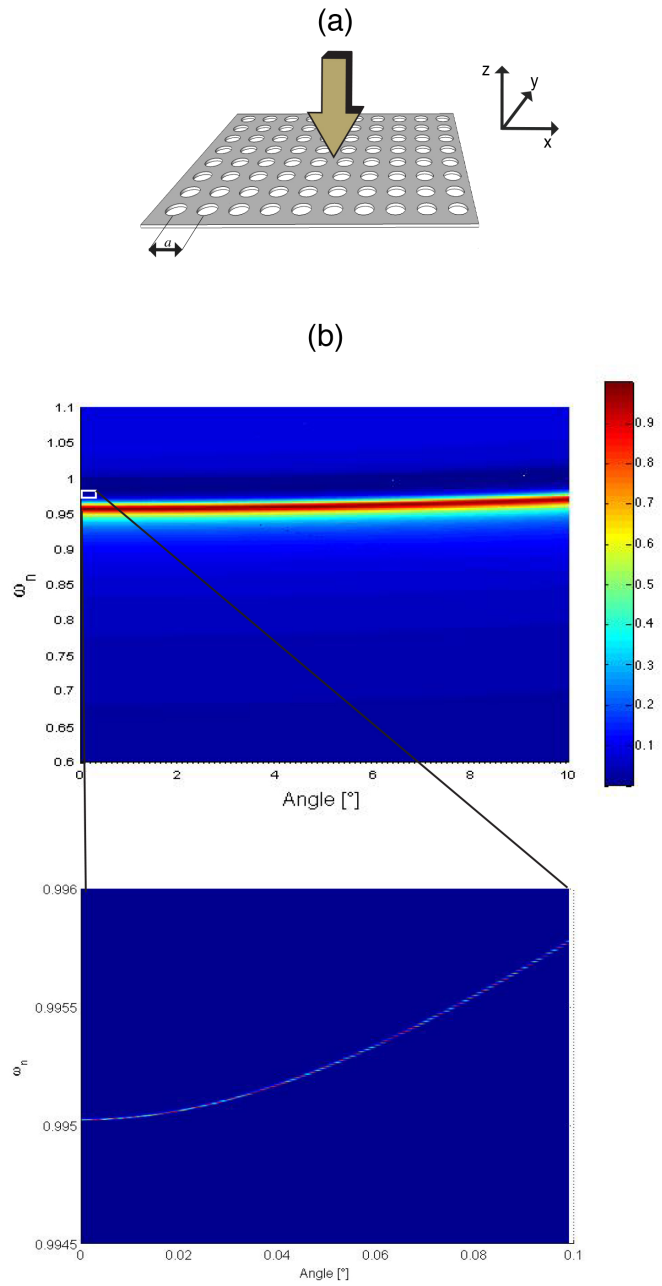

Figure 5.1: a) Sketch of the photonic crystal consisting of a square lattice of holes in a material with refractive index equal to 2. The sample is designed in order to have resonance modes at normal incident direction. b) Calculated modes by means RCWA: in addition to the principal modes, a band with a very sharp profile appear close to normal incidence (see the zoom).

0.995. In order to highlight them high resolution numerical calculation of around 10^{-5} in terms of normalized frequency is required.
Moreover, we studied the reflectivity as a function of the normalised slab thickness for normal incident beam, i.e. directed along the z-axis and considering the incident electric field as directed along the x-axis (see 5.2). Also in this case different bands are visible, the principal modes at $\omega = 0.95$ and the modes with an extremely narrow profile (fig.5.2c). In particular, the reflectivity evaluated at normal incidence for a normalised thickness $0.12a$ has a very narrow peak with a quality factor as high as $Q = 2 \cdot 10^5$ (see fig.5.2b).

Let now analyze the electric field distribution within the PhC slab in correspondence of the two bands of Fig.5.2a. In general, all eigenstates in a slab contain a mixture between TM and TE modes so that it is not possible rigorously define a TE or TM polarization. However, it is still possible to distinguish between TM-like or TE-like in modes according to the dominant component of the excited electric fields (see Chapter 1). Although at normal incidence purely 2D TE and TM modes are degenerate, in a 2D slab modes split because of the different effective index of the slab for the two polarizations, in agreement with previous analysis [83]. In correspondence of $\omega_n = 0.96$ in the middle of the larger band in Fig.5.2, the electric field is almost completely directed along the x direction, i.e. parallel to the incident beam. This is illustrated in Figure 5.3a-c where the intensity of the electric field along the different direction is shown. The maximum field intensity in the x-direction is about 85 times the intensity of the incident beam, which can be useful for some application but it is not enough to enhance weak effect such as the Raman signal emission. Figure 5.3d shows the 3D picture of the electric field vector in the median plane of the slab. The electric field is directed along the x-direction and, residing in the (x,y) plane of the lattice, this resonances can be classified as TE-like.
In Figure 5.4 is shown the electric field of the very narrow resonance in correspondence of the $\omega = 0.995$. As illustrated in Figures 5.4a-c, the field is strongly enhanced not only in the (x,y) plane where the incident field lies, but also along z-direction i.e. longitudinally to the incident beam direction. In particular, along the z-direction the field intensity is about two orders of magnitude higher than the intensity along the x direction and is six orders of magnitude larger than the incident beam, which is therefore particularly appealing for amplifying most of the nonlinear phenomena. In this case, the electric field is essentially directed along the z-direction, as showed in Fig.5.4d. Modes residing on the narrow band of figure 5.1 and figure 5.2 are then TM-like modes. We underline that in case of normal incidence the resonant electric field is parallel to the incident wave vector. The resonant frequency is just under the excitation of high-order in the lattice which

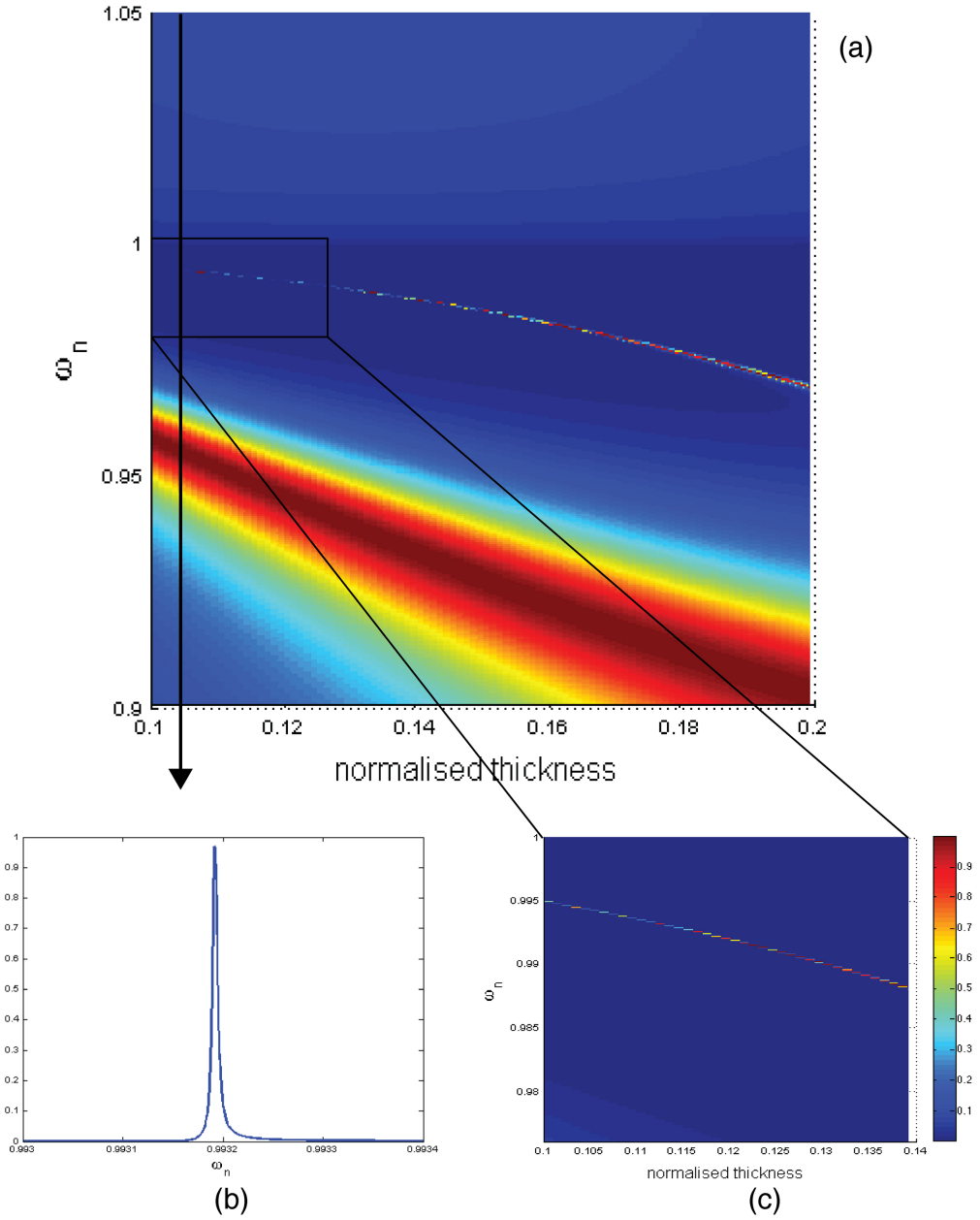

Figure 5.2: a) Calculated reflectivity as function of normalised photonic crystal thickness and c) a zoom of the bound states modes region. b) Resonance peak corresponding to the thickness of 0.12a.

corresponds to $\omega = 1$ for a normal incidence in a square lattice. Due to the conservation of the tangential component of the wave vector and electric field, zero in both cases, the mode cannot couple with radiative modes outside of the PhC slab where longitudinal modes are not permitted. It is therefore a real bound state within the continuum of radiation [79, 87]

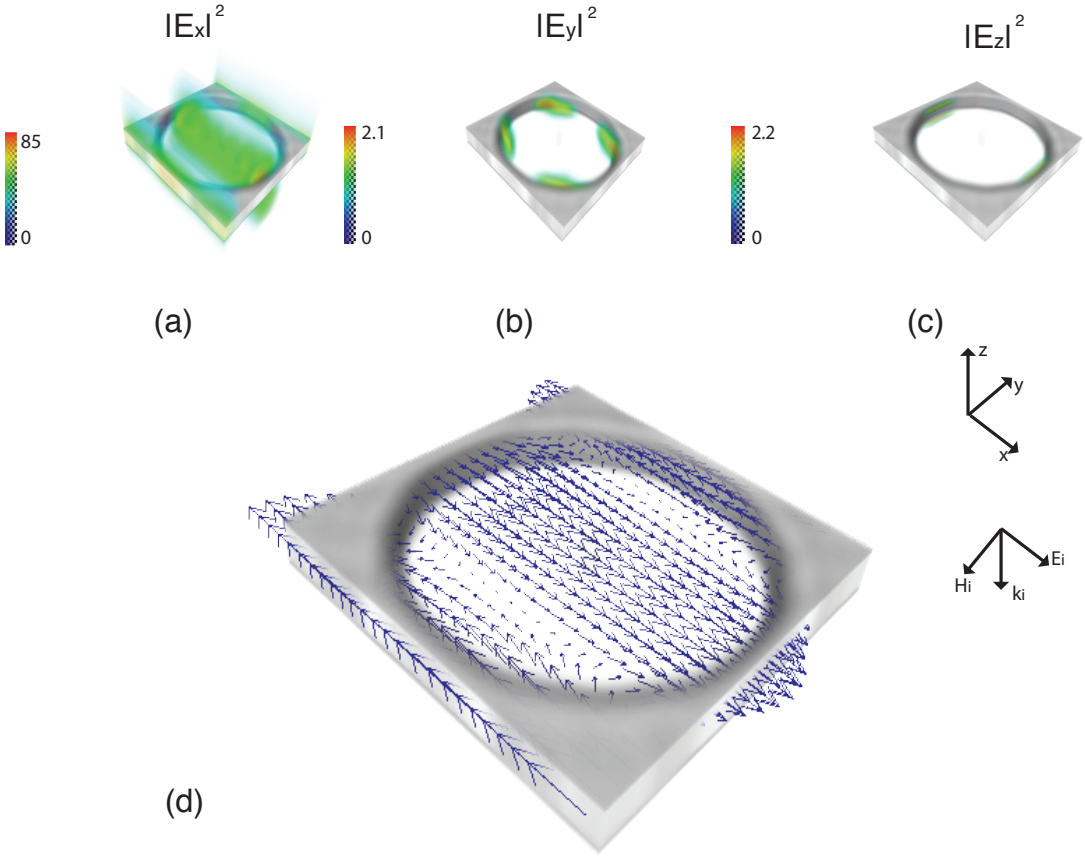

Figure 5.3: The electric field for a normal incident beam in correspondence of $\omega_n = 0.96$. The electric field intensity along x, y and z-directions (a)-(c). The electric field vector in the slab median plane (d).

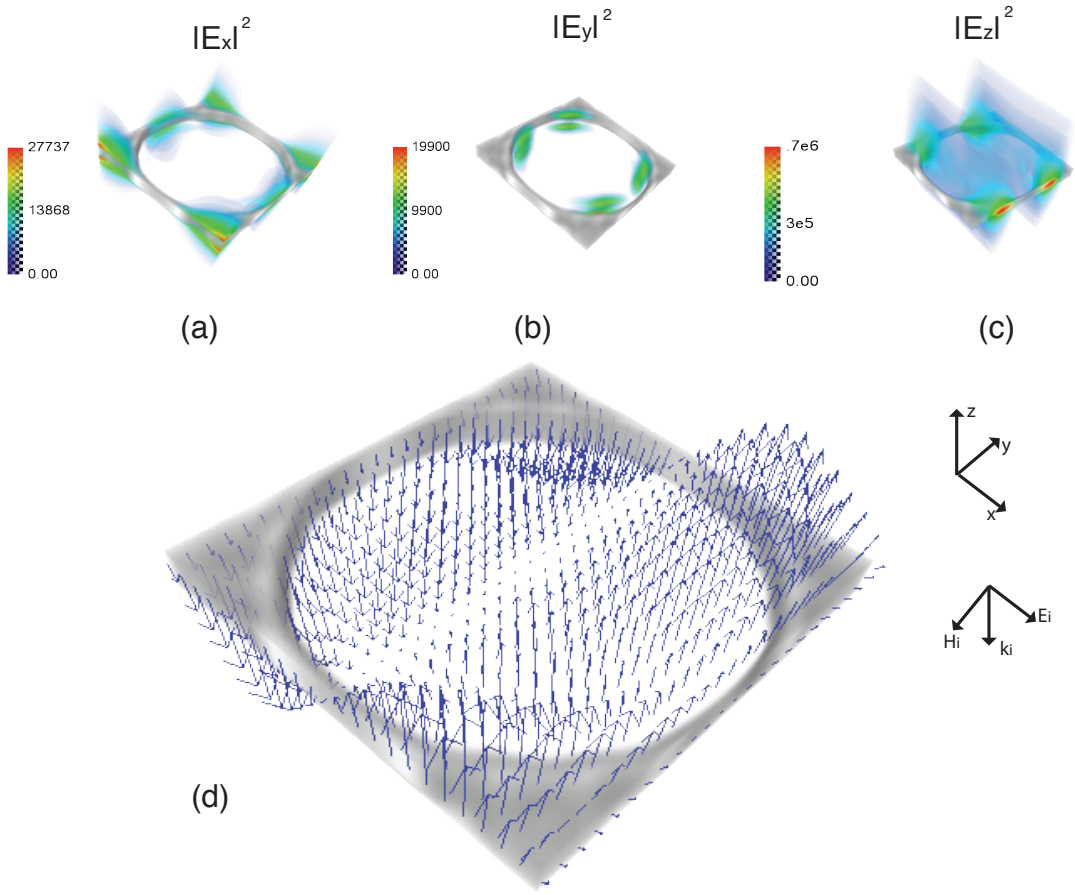

Figure 5.4: The electric field for a normal incident beam in correspondence of $\omega_n = 0.995$. The electric field intensity along x, y and z-directions (a)-(c). The electric field vector in the slab median plane (d).

5.2 Samples fabrication and characterization

In order to realize high-quality factor resonances in photonic crystal membranes, we compared two different fabrication techniques, the Nanoimprint Lithography and the Electron Beam Lithography. The first one is a very interesting technique which permits to obtain nanostructured sample reducing the production cost while the second one is the classical method which guarantees the realization of very high quality photonic crystal structures. The square lattice is patterned on two different material, Titania (TiO_2) and Silicon Nitride (Si_3N_4) layers.

5.2.1 Titania membranes on glass

Sample Fabrication:Nanoimprint Lithography

Nanoimprint Lithography is a smart technology for patterning surfaces at the nanometer scale over large areas at low cost [18, 19]. The nanoimprint process basically consists of printing deformable surfaces with a nanostructured mold. It is possible to have several copies of the same template or to pattern a large areas by printing in series the mold. In particular the fabrication technique consists of three principal steps (Figure 5.6): the template fabrication, the imprint of the mold on the suitable material and the final demolding with the transfer of the pattern on the material.
In this work I will present a new fabrication process based on Nanoimprint lithography, used to pattern **photonic crystal membranes on TiO_2 films** and completely performed in the Molecular Foundry Clean Room of the Lawrence Berkeley National Laboratory in California. This process is slightly different from the classical one and it is the result of a long series of tempts. For the sake of shortness, I will present directly the successful process. In fig. 5.5 the principal steps are resumed.

Figure 5.5: Scheme of Nanoimprint lithography: 1) Template fabrication, 2)Imprint on a suitable layer, 3) Transfer of the pattern on the material

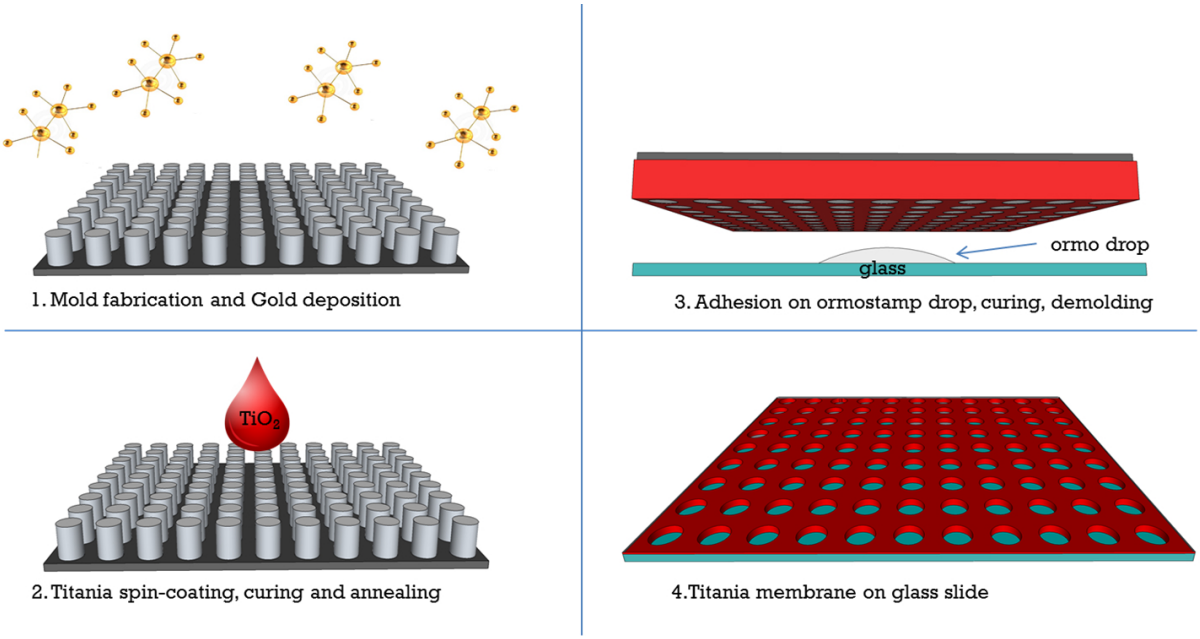

Figure 5.6: Sketch of the main fabrication steps: 1) once the mold is fabricated, a thin layer of gold is deposited on the whole surface; 2) the template is covered of Titania; 3) the template with the cured Titania inside is pressed on a glass substrate and sticked with an ormostamp drop; 4) after the demolding the pattern is transfered on the titania.

Table 5.1: Fabrication parameter for photonic crystal membranes. λ wavelenght, a lattice constant, r holes radius, d holes depth.

λ (nm)	a (nm)	r (nm)	d (nm)
532	355	89	54
780	521	130	78

The first step is the mold fabrication. In particular, the square lattice of holes is patterned by means electron beam lithography and subsequent coupled plasma etching process. The fabrication parameters are optimized in order to have resonant peaks for two different wavelenghts, 532 nm and 780 nm (see table 5.1). The result is a template of pillars in Silicon (see fig. 5.8). A thin gold layer of 10 nm is then deposited on the whole mold surface by means of a Semicore SC600 thermal evaporator. This film will act as an anti-sticking layer that will ease the demolding of the photonic crystal membrane from the template.

The second step is the deposition of titania (TiO_2) film on the mold. We use hybrid TiO_2-based resin synthesized by mixing titanium ethoxide precursor with 3-butenoic acid, a photoinitiator and an organic crosslinker dissolved in propylene glycol methyl ether acetate (PGMEA) solvent [88, 89]. Films are spin-coated at 2000 -3000 rpm and soft baked at 100°C for 1 min to create uniform solvent-free films; the film thickness can be varied from 20 nm up to 1 μm depending on the concentration of the titania precursor. Films are then cured under 100 W cm^{-2} UV-light exposure for 10 min. The result is shown in figure 5.9.
The imprinted patterns is finally annealed on a hot plate in air. Infact the refractive index of this hybrid TiO_2-based resin can be tuned with the temperature. In particular the refractive index reachs the value of around 2 if annealed at 400°C for 1 hour (see fig. 5.7). In addition, the extinction coefficient k goes down to zero (below the detection level) for annealing temperatures higher than around 300^0C and thus the annealing treatment guarantees the transparency of the inorganic films for visible light .
At this point, the membrane is ready to be demolded from the template. In order to do this, the surface has to be stuck to the substrate, a glass slide. We chose an Inorganic-organic Hybrid Polymer, the Ormostamp, as glue. It is highly transparent for UV and visible light and mechanically and thermally stable. So an ormostamp drop is put on the glass slide and the mold covered with the cured titania is pressed against the glass. The so composed system is exposed to UV-light for 1 min in order to cross-link the Ormostamp material and then the membrane is

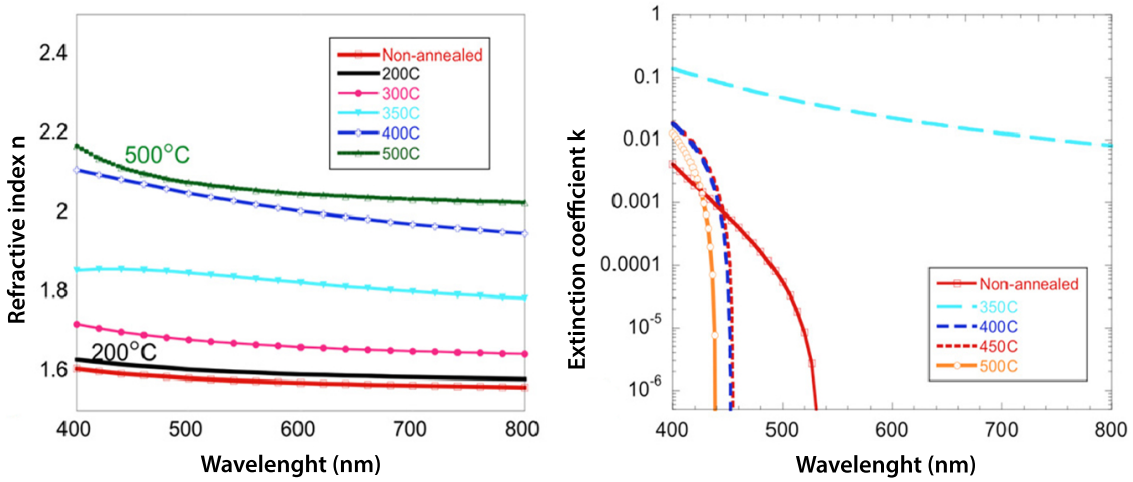

Figure 5.7: Ellipsometry characterization of TiO_2 films for various annealing temperatures: (a) refractive index; (b) extinction coefficient as a function of the wavelength for an annealing time of 1 h. *From ref. [89]*

taken off from the template. In figure 5.10 the result is shown. The lattice and the holes are regular and the only defects are the replication of the mold irregularities. Despite of the good quality of the photonic crystal, the surface presents a roughness that appears to be of crucial importance for the optimization of the resonances Q-factor. As a result, the resonances in the transmission spectra are broadened. However, we are improving the fabrication technique by trying different anti-sticking layers and different glues.

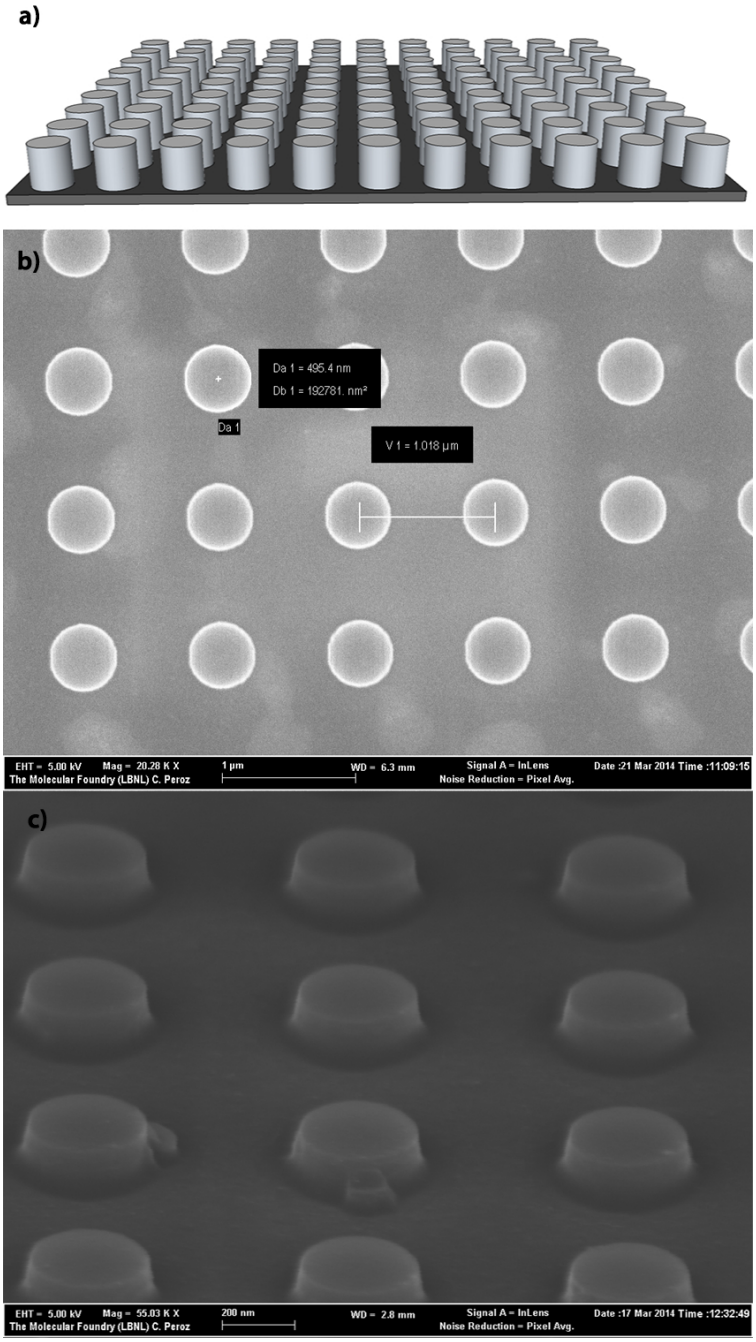

Figure 5.8: From the top: a) Sketch of the mold in Silicon; b) SEM image of the patterned are before etching; c) SEM image of the pillars in silicon after the etching process.

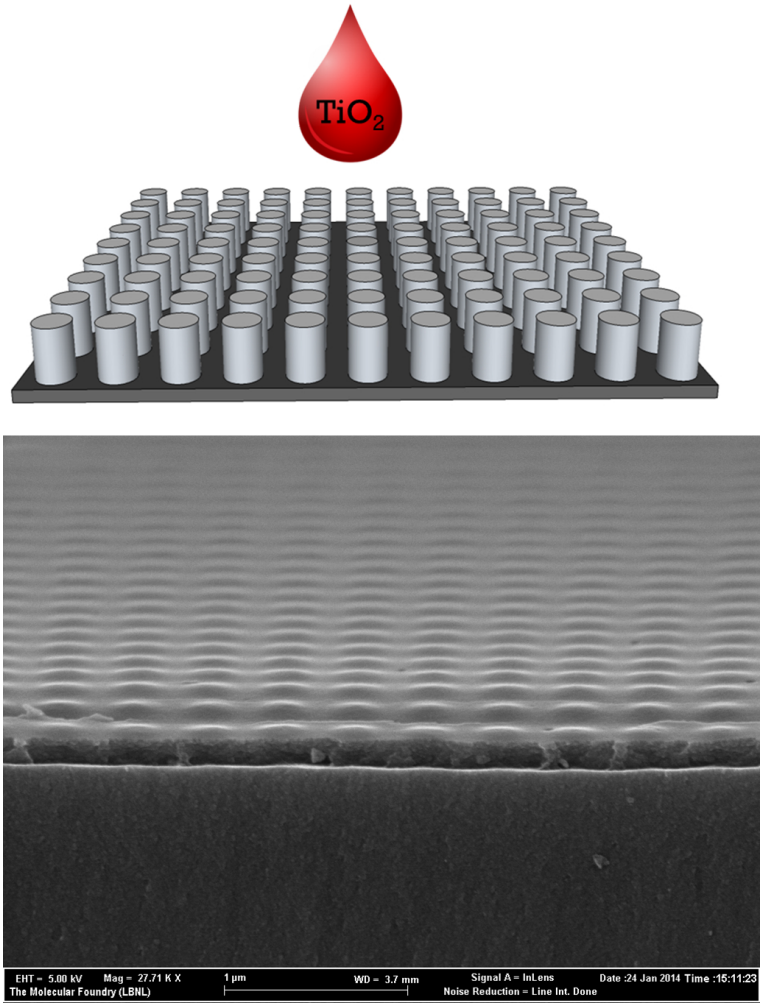

Figure 5.9: Second fabrication step: the titania solution is deposited by means a spin-coating process. The result is a uniform film of TiO_2 filling the space between the pillars (SEM image).

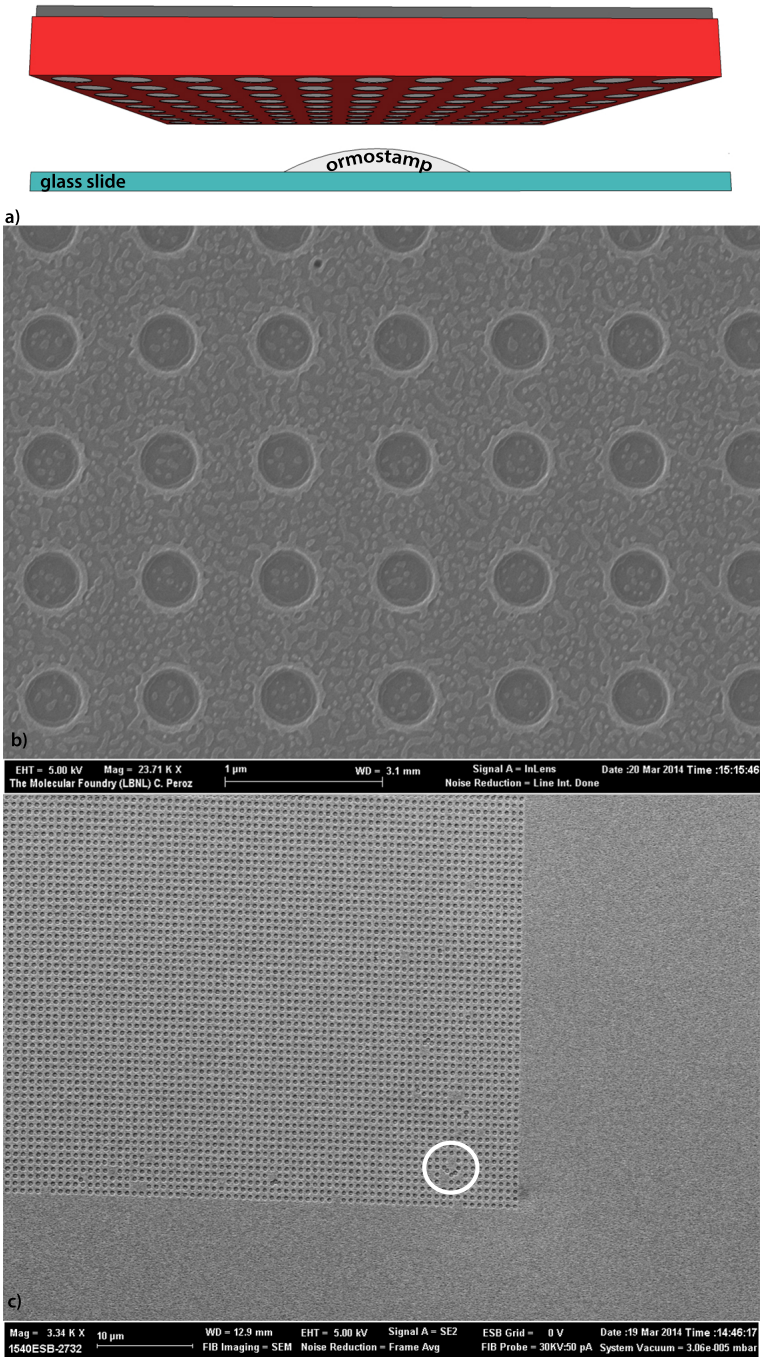

Figure 5.10: a) Sketch of the third fabrication step: the titania membrane with the mold is stuck on a glass slide by means an ormostamp drop. b) and c) SEM images of the final result: the holes are regular, and the defects (into the white circle) are mold irregularities. The gold, visible as some grains on the surface, can be easily removed.

5.2.2 Silicon Nitride membranes on quartz

Sample Fabrication: Electron Beam Lithography

Silicon Nitride membranes are realized by using the Electron Beam Lithography, the traditional fabrication technique that allows to obtain photonic crystals with an high quality. Silicon Nitride is deposited on a quartz substrate by Plasma-Enhanced Chemical Vapor Deposition (PECVD) by using $1\%\ SiH_4/Ar = 100sccm$ (Standard Cubic Centimeters per Minute) and $N_2 = 50sccm$. Silicon nitride refractive index n is measured by Horiba Jobin Yvon Uvisel Spectroscopy Ellipsometer. For the visible range, the refractive index is about 2, so we use the same fabrication parameters of titania membranes (see table 5.1). The patterned silicon nitride is then etched by means coupled plasma etching process using CHF_3 and O_2. Fig. 5.12 shows the final result.

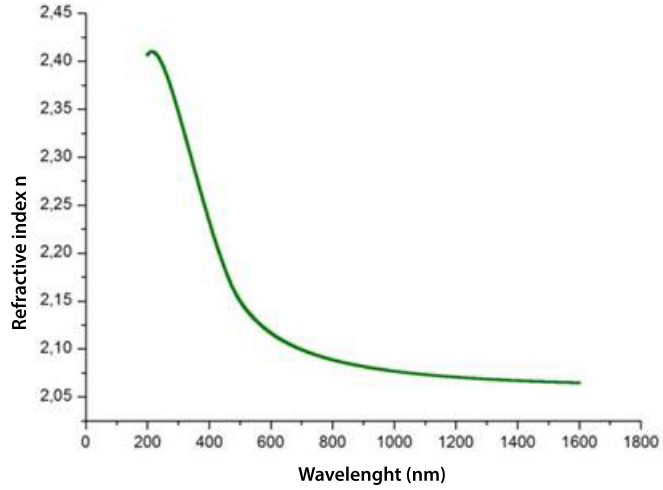

Figure 5.11: Ellipsometric measurements of silicon nitride refractive index.

Experimental details

In order to excite and collect the resonance peaks into the trasmission spectrum, a suitable experimental setup has been refined (Figure 5.13). A super continuum source (Super K Extreme - NKT Photonics) emits light covering the entire 400-2400 nm wavelength range. The light is collimated and polarized, then travel through the photonic crystal mounted on a xyz stage. The sample can be rotated by means an automatic rotational stage allowing rotational steps of 0.01°. The

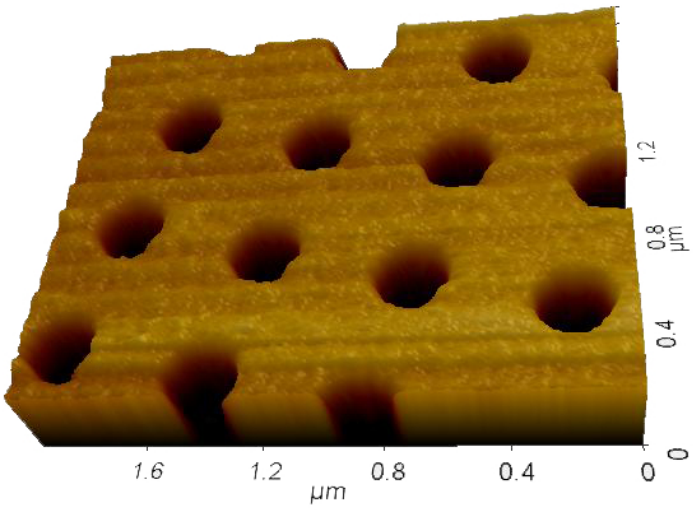

Figure 5.12: Atomic Force Microscopy (AFM) image of silicon nitride photonic crystals consisting of air-cylindrical holes in a square lattice.

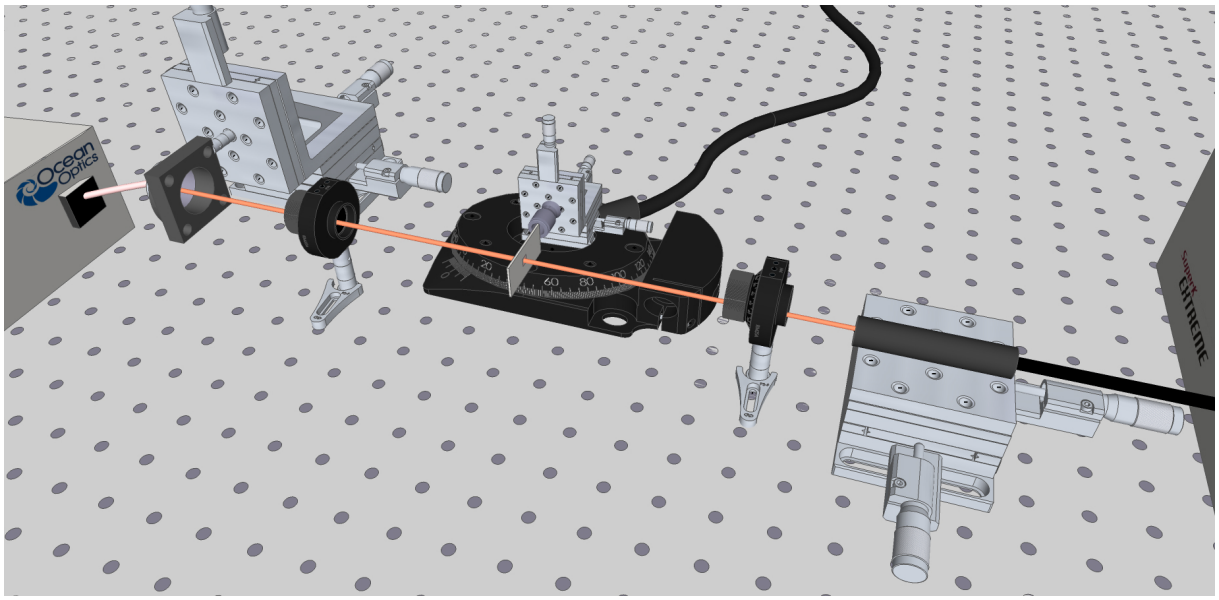

Figure 5.13: Sketch of the experimental setup. A supercontinuum source (Super K Extreme - NKT Photonics) emits collimated light from 400 to 2400 nm. Once polarized, the radiation passes through the sample mounted on an automatic rotational stage. The beam is thus polarized again and collected and analyzed by a compact spectrometer (Ocean Optics HR 4000)

transmitted spectra are polarized again and collected by using a compact spectrometer (Ocean Optics HR 4000) with a resolution of 0.25 nm and a range of 350nm-800nm.
The trasmission spectra are collected by using two different configurations, cross polarization and no cross polarization. In particular when the incident wave is polarized at $\phi = 0°$ or $\phi = 90°$ the transmitted wave has the same polarization. So, the cross-polarized collection filters the continuum contribution and only the resonances are seen, as these have non-zero x and y components. The results are compared with the non-filtered spectra in no cross polarization configuration.

Results and discussion

The analyzed samples are designed in order to have the resonance peaks at 532 nm and 780 nm at normal incident direction. For both samples, transmission spectra are collected at different incident angles around $\theta = 0°$. By plotting the resonance peaks intensity in the (frequency, angle) plane, the band diagrams are reconstructed.

Resonances at 780 nm The transmitted signal is collected in cross polarization configuration and in no cross configuration. All the spectra are normalized to the transmission signal of the unpatterned quartz.
Figure 5.15 (top) shows the spectrum collected at normal incident direction for the no cross configuration ss, i.e. s-polarized input, s-polarized output (electric field vector perpendicular to the incident plane): three resonance are collected. By comparing the data with the simulation results, it is possible to distinguish that the two bigger ones belong to the principal photonic crystal modes. The third one is a more narrow peak and corresponds to the bound state. When the incident angle $\theta \neq 0°$, the bound states band splits in more curves. Figure 5.15 down shows the result for $\theta = 0.9°$: three resonances appear into the transmission spectrum. Specifically the Full Width at Half Maximum (FWHM) of the narrowest one is about 0.31 nm. Since the spectrometer has a resolution of about 0.25 nm, this value is close to the limiting one.
By changing the incident angle, it is possible to reconstruct the dispersion band of the photonic crystal. In fig. 5.16 the experimental p-modes band are reported. The upper bands are the principal photonic crystal modes. Under the normalized frequency 0.7, bands with a very sharp profile appear, the bound states. The same phenomena can be observed also in cross polarization configuration (see 5.16 down). In this case the degeneracy of bound state modes is more evident.
By using the RCWA analysis, the theoretical bands predicted for the silicon ni-

tride membrane are determined. In figure 5.14 the dispersion band referring to p-polarized modes is reported. The agreement with the experimental dispersion diagrams shape (fig. 5.16) is excellent.

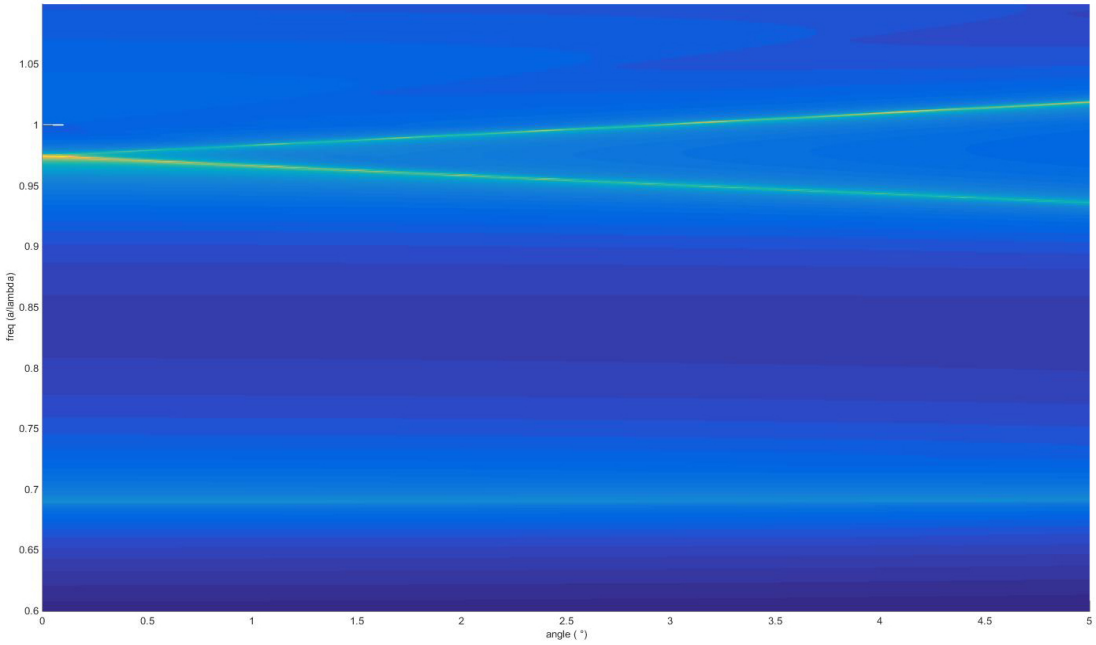

Figure 5.14: Calculated band for p-modes simulated by means RCWA approach. The upper bands are the principal photonic crystal modes, the lower one is the bound states band.

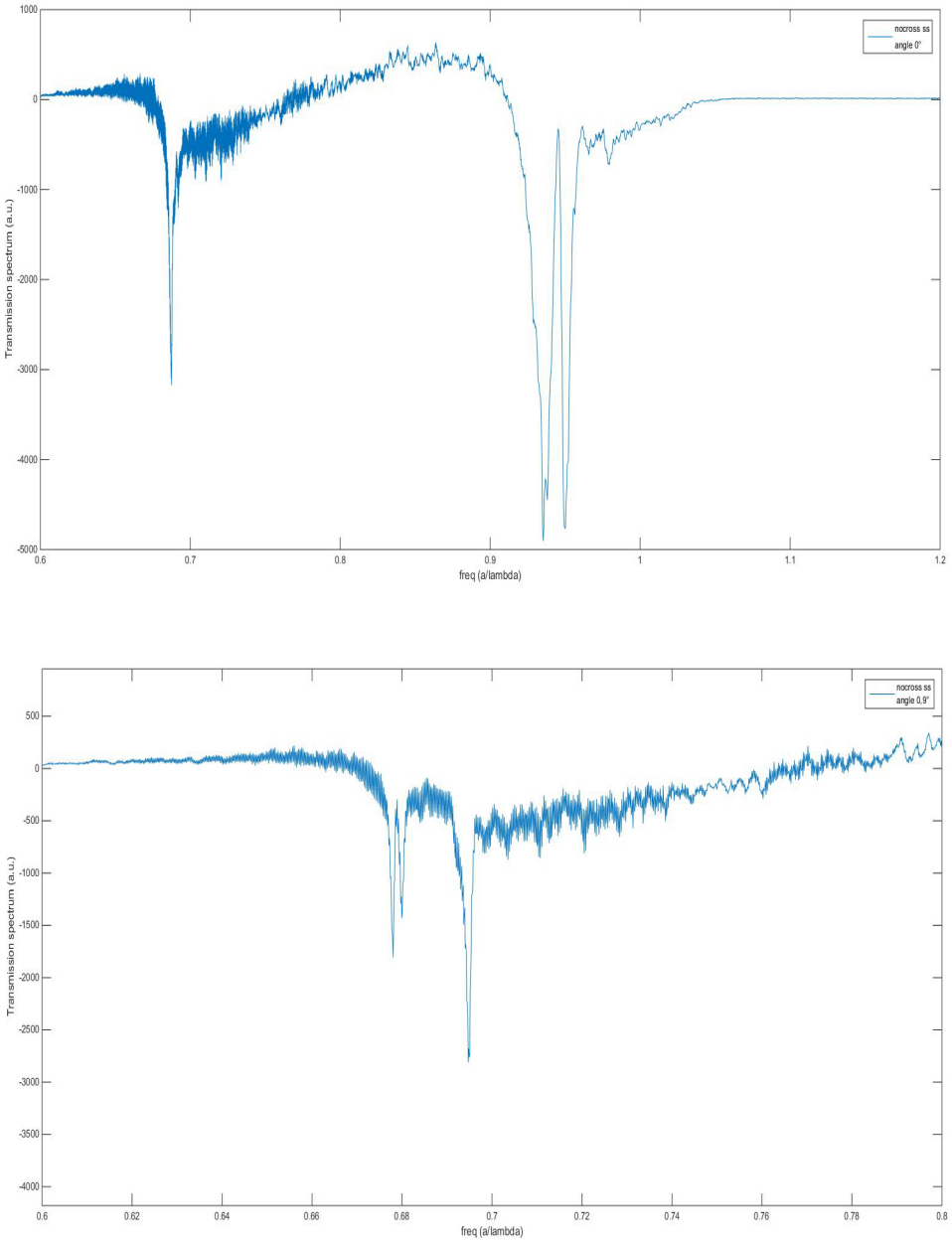

Figure 5.15: Transmission spectrum collected from the sample (780 nm). No cross polarization configuration, incident angle $\theta = 0°$ (top) and incident angle $\theta = 0.9°$ (down).

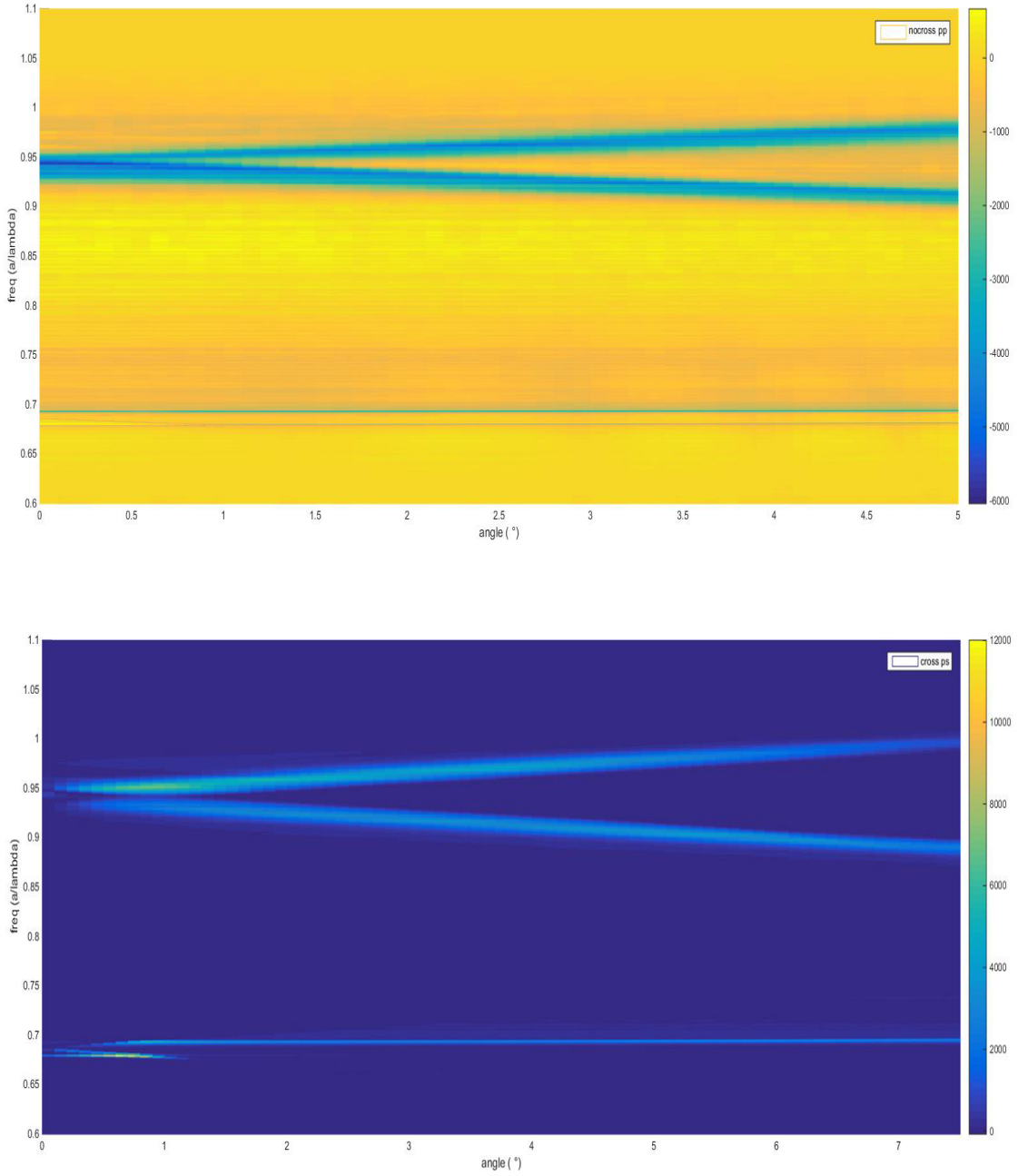

Figure 5.16: Experimental reconstructed band collected in pp no cross polarization and in ps cross polarization. The upper bands are the principal photonic crystal modes, the lower one is the bound states band.

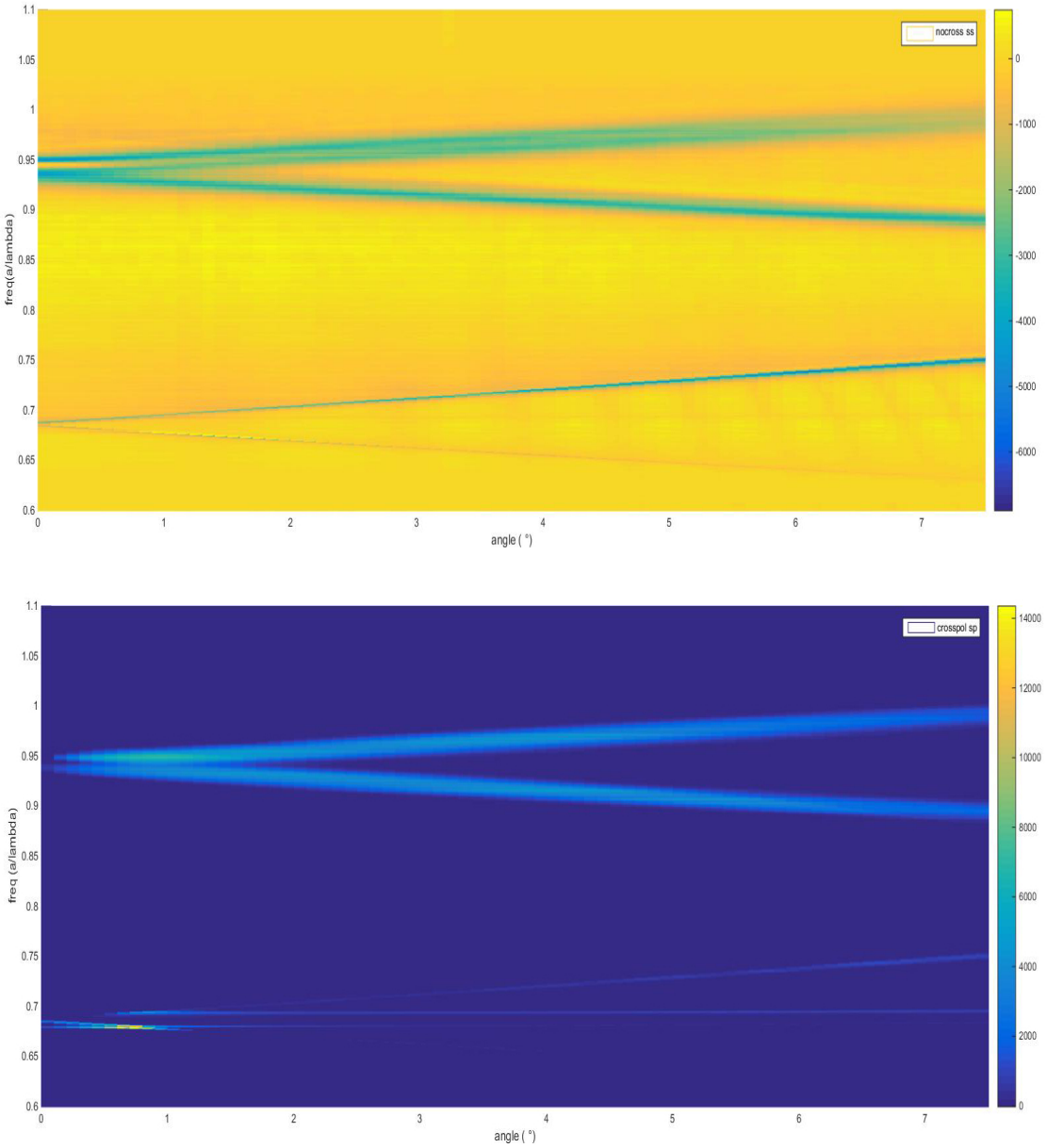

Figure 5.17: Experimental reconstructed band collected in ss no cross polarization and in sp cross polarization. The upper bands are the principal photonic crystal modes, the lower one is the bound states band.

Resonances at 530 nm The same measurements are performed also on the sample designed in order to have the resonance peak at 530 nm. Two of the collected transmission spectra are reported in fig. 5.18 and in fig.5.19. In fig. 5.18 the incident angle is only 0.048° far from the normal incident direction. In this case the FWHM is 0.26 nm and it is comparable with the spectrometer resolution (0.25 nm). Thus this parameter prevent us to detect more narrow peaks. Fig. 5.19 shows the three peak appearing for the incident angle $\theta = 1.6°$.
By performing an angular scan from 0° to 4° the experimental dispersion bands are determined. In this case the principal modes of the photonic crystals are out of the spectrometer range, so they are not visible in the experimental spectra (see fig.5.20 and fig.5.21). Also in this set of samples, the degeneracy of bound states is evident.

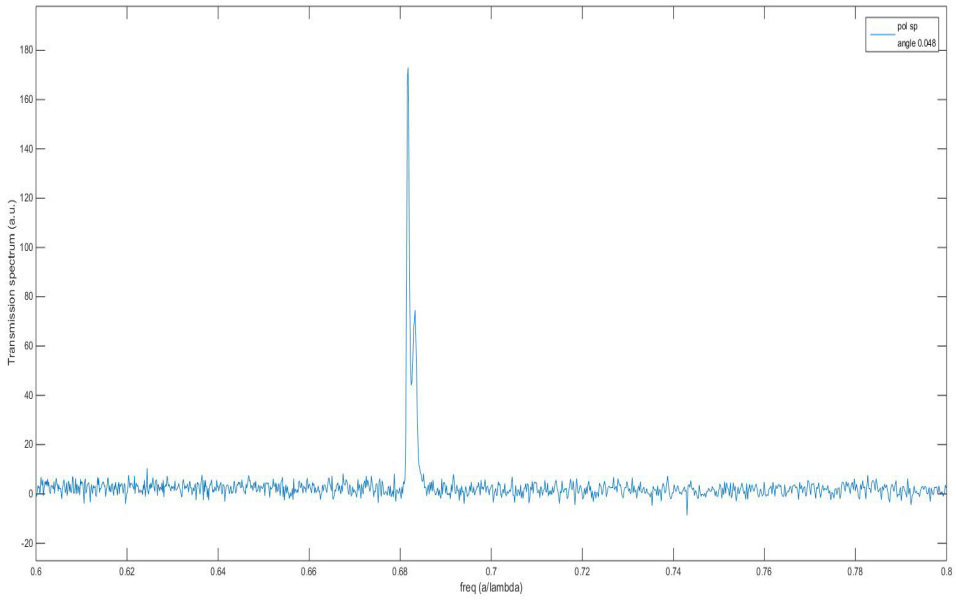

Figure 5.18: Transmission spectrum collected from the sample (530 nm). Cross polarization configuration s-input, p-output, incident angle $\theta = 0.048°$.

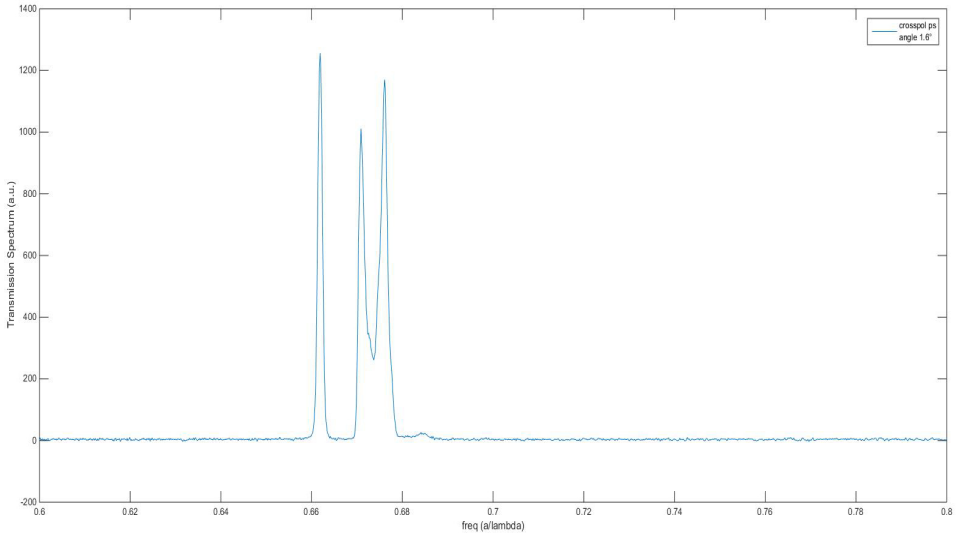

Figure 5.19: Transmission spectrum collected from the sample (530 nm). Cross polarization configuration p-input, s-output, incident angle $\theta = 1.6°$.

5.3 Final considerations

In this chapter important preliminary results about the high quality resonances coupling have been reported. Two different kinds of samples are fabricated and analyzed, titania membranes on silicon oxide and silicon nitride on quartz. TiO_2 photonic crystals are realized by using a new fabrication process based on nanoimprint lithography. Although the final photonic crystals looked good, the roughness of the surface prevented us to detect the calculated resonances. We are improving the fabrication features because this technique can turn out to be an appealing method to fabricate high quality photonic crystals in large numbers with low costs. On the other hand, Si_3N_4 photonic crystals fabricated by means electron beam lithography reveal the calculated resonances in the transmission spectrum. In particular, resonances with a FWHM comparable with the spectrometer resolution have been detected. This samples are ready to be tested for photonic applications, such as enhancement of Raman spectroscopy signal, Fluorescence emission, nonlinear phenomena or as sensor.

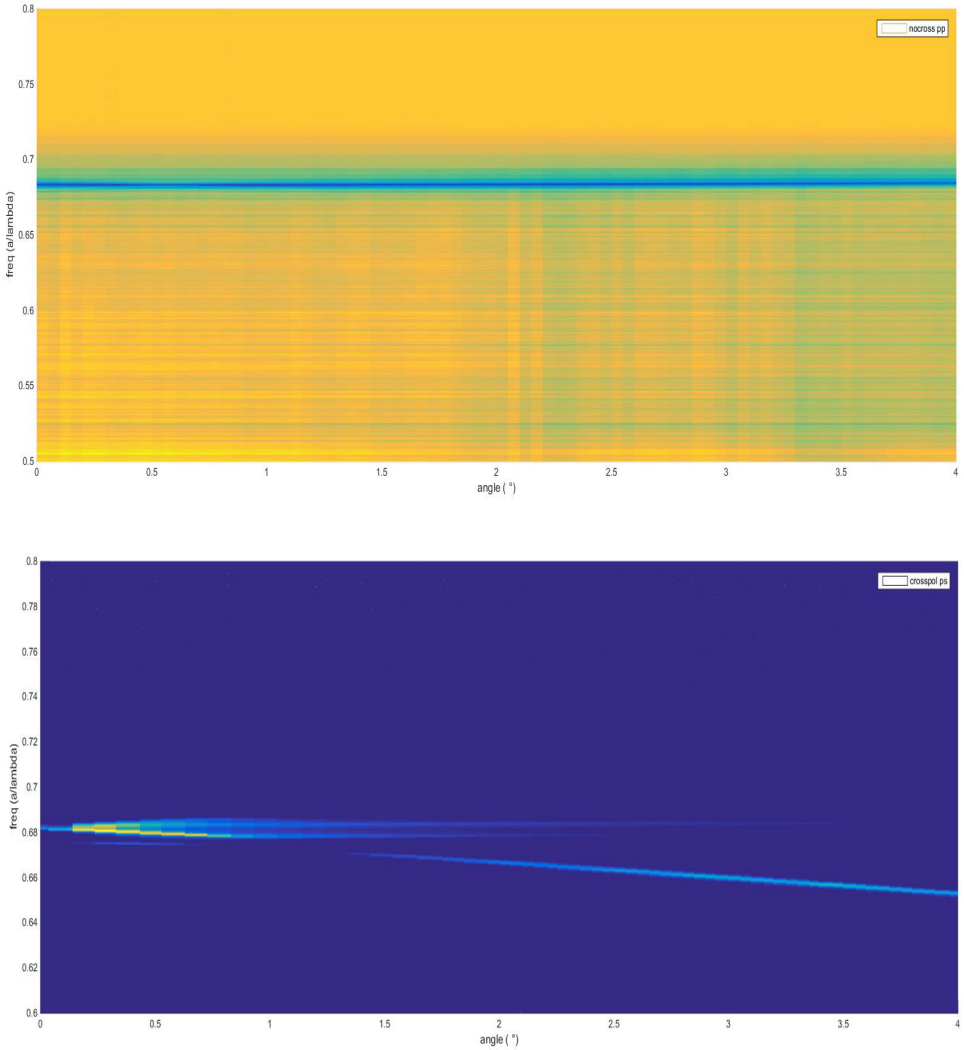

Figure 5.20: Experimental reconstructed band collected in pp no cross polarization and in ps cross polarization.

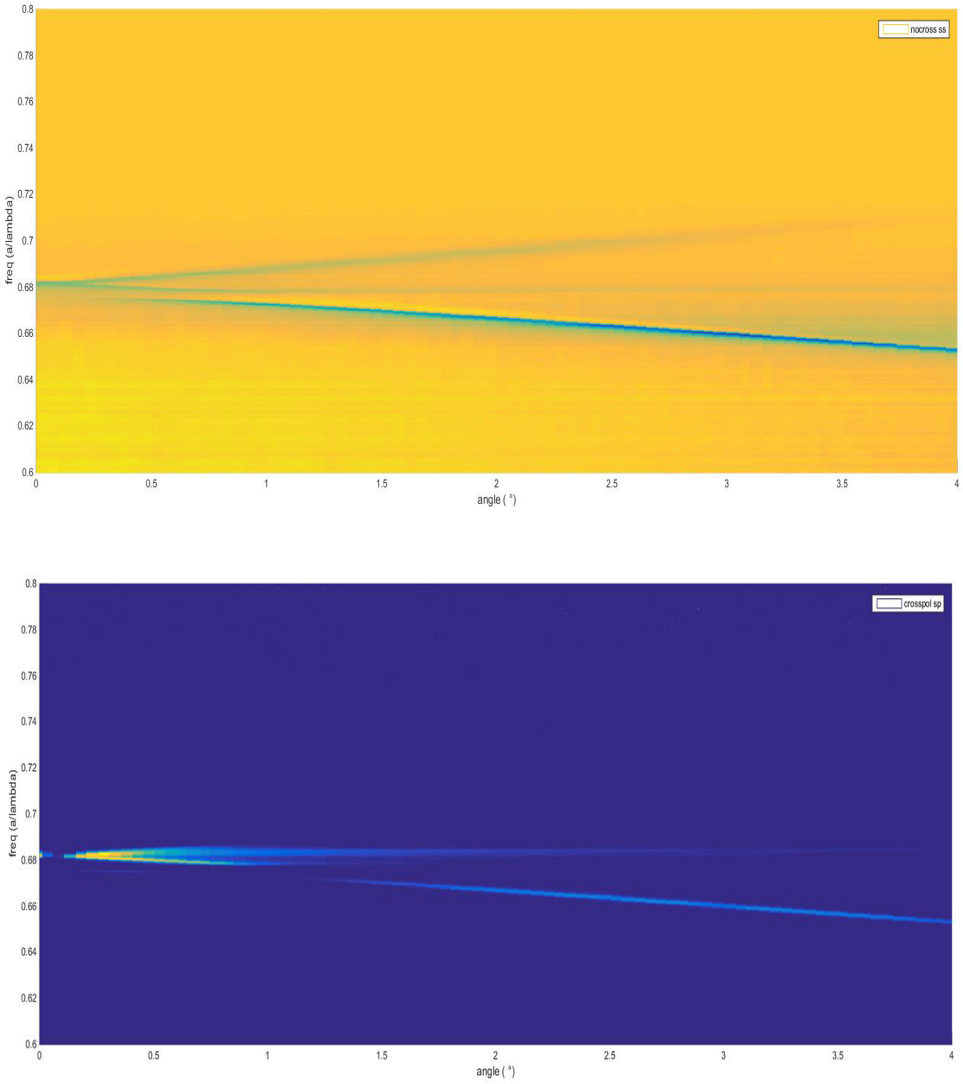

Figure 5.21: Experimental reconstructed band collected in ss no cross polarization and in sp cross polarization.

Conclusions

In this PhD thesis a theoretical and experimental study on resonant states in photonic crystals has been presented. In particular, three new different phenomena have been deeply analyzed: *Plasmon-like states*, *Guided Mode resonances* and *Bound states in continuum*.
Plasmon-like states are peaks appearing in the reflection spectrum of a negative refracting photonic crystal in silicon. These modes exhibit features analogous to the plasmon states in metallic structures: the field is confined at photonic crystal/air interface and the dispersion band, which is below the light line, has the typical plasmonic shape. The coupled resonances have a low Q-factor, of about 10, and are excited in the infrared region.
Guided mode resonances have the electromagnetic power strongly confined within the photonic crystal slab and can couple to external infrared radiation. The strongly connection with the negative refractive behaviour has been experimentally underlined in a silicon photonic crystal structure. In addition a new theoretical approach has been employed by considering the resonant behaviour inherent into the photonic crystal structure and thus by modeling its effective permittivity with a Lorentzian function. The Q-factor, determined by fitting the experimental curves, is about 10^2 and therefore, guided resonances can be employed as efficient sensors to monitor the refractive index variations of the external environment.
Finally, new structures have been designed, fabricated and characterized in order to excite *Bound States in Continuum* in photonic crystal membranes. These resonances have a predicted infinite life-time connected with a huge filed enhancement. In particular, numerical simulations shown that the enhancement factor is about 10^6 distributed over all the structure. The planned lattice has been patterned on two materials, Titania and Silicon Nitride, high-index dielectric media with an high transparency at visibile wavelenghts. Two fabrication methods have been used: Nanoimprinting Lithography and Electron Beam Lithography. The transmission spectra of the fabricated samples shows very narrow resonances comparable with the spectral resolution of the experimental setup. The experimental Q-factor is about 10^3 but, considering losses from both material absorption and

scattering due to fabrication imperfections , it can reach values of about 10^6.
These results can find interesting applications in the control of the radiation field in absorption-free media, avoiding the typical limitation of metallic plasmonic structure. In addition, in this case the field enhancement is distributed in a large area despite what happen in other nanostructures with high-field enhancement, such as nanoantennas or nanocavities. A remarkable application of these very narrow resonant modes can be the development of high refractive index sensors based on optical resonance shift. Furthermore the high field enhancement connected to the resonances can be applied to boost fluorescence signal or nonlinear phenomena of material implanted inside the photonic crystal. Finally, the resonant photonic crystals can be employed as enhancing substrates for Raman spectroscopy.

Ringraziamenti

Ringrazio innanzitutto il mio tutor Vito Mocella che, in questi 3 anni, ha sempre mostrato grande rispetto per le mie idee e la mia indipendenza, cercando di trasmettermi la sua creatività e sopportando la mia testardaggine e la mia irriverenza.
Ringrazio Ivo Rendina per la fiducia che ha da sempre riposto in me e tutti i ricercatori, gli amministrativi e i ragazzi dell'IMM con i quali ho condiviso tanti momenti di divertimento e di crescita.
Un ringraziamento a parte va fatto a coloro che hanno reso unica questa mia esperienza. Anna Chiara, guida e amica, esempio di ciò che significa amare la scienza e credere nella ricerca in Italia. Edoardo, compagno di grasse risate, di momenti esilaranti e di tante discussioni. Stefano, l'amico di una vita. Senza di loro sarebbe stato tutto più noioso.
I ringraziamenti alle persone care e amate non li scrivo qui, per loro non servono parole.

List of Figures

Bibliography

[1] Elin M. Larsson, Joan Alegret, Mikael Kll, and Duncan S. Sutherland. Sensing characteristics of NIR localized surface plasmon resonances in gold nanorings for application as ultrasensitive biosensors. *Nano Letters*, 7:1256–1263, 2007.

[2] Jonas Beermann, Sergey M Novikov, Kristjan Leosson, and Sergey I Bozhevolnyi. Surface enhanced Raman imaging: periodic arrays and individual metal nanoparticles. *Optics express*, 17(15):12698–12705, 2009.

[3] a E Krasnok, I S Maksymov, a I Denisyuk, P a Belov, a E Miroshnichenko, C R Simovski, and Yu S Kivshar. Optical nanoantennas. *Physics-Uspekhi*, 56:539–564, 2013.

[4] Adam D. McFarland and Richard P. Van Duyne. Single silver nanoparticles as real-time optical sensors with zeptomole sensitivity. *Nano Letters*, 3:1057–1062, 2003.

[5] Prashant K. Jain, Kyeong Seok Lee, Ivan H. El-Sayed, and Mostafa a. El-Sayed. Calculated absorption and scattering properties of gold nanoparticles of different size, shape, and composition: Applications in biological imaging and biomedicine. *Journal of Physical Chemistry B*, 110:7238–7248, 2006.

[6] C E Talley, J B Jackson, C Oubre, N K Grady, C W Hollars, S M Lane, T R Huser, P Nordlander, and N J Halas. Surface-enhanced Raman scattering from individual Au nanoparticles and nanoparticle dimer substrates RID A-4896-2011 RID A-2560-2008 RID D-2935-2011. *Nano Letters*, 5:1569–1574, 2005.

[7] Zhongyong Wang, Peng Tao, Yang Liu, Hao Xu, Qinxian Ye, Hang Hu, Chengyi Song, Zhaoping Chen, Wen Shang, and Tao Deng. Rapid Charging of Thermal Energy Storage Materials through Plasmonic Heating. *Scientific Reports*, 4:6246, 2014.

[8] Xiaowei Guo. Surface plasmon resonance based biosensor technique: A review. *Journal of Biophotonics*, 5(7):483–501, 2012.

[9] Pei-Yu Chung, Tzung-Hua Lin, Gregory Schultz, Christopher Batich, and Peng Jiang. Nanopyramid surface plasmon resonance sensors. *Applied physics letters*, 96(26):261108, June 2010.

[10] Ting-Yu Liu, Kun-Tong Tsai, Huai-Hsien Wang, Yu Chen, Yu-Hsuan Chen, Yuan-Chun Chao, Hsuan-Hao Chang, Chi-Hung Lin, Juen-Kai Wang, and Yuh-Lin Wang. Functionalized arrays of Raman-enhancing nanoparticles for capture and culture-free analysis of bacteria in human blood. *Nature Communications*, 2:538, 2011.

[11] Xiaobo Yin and Lambertus Hesselink. Goos-Hanchen shift surface plasmon resonance sensor. *Applied Physics Letters*, 89:2004–2007, 2006.

[12] Radan Slavík and Jií Homola. Ultrahigh resolution long range surface plasmon-based sensor. *Sensors and Actuators, B: Chemical*, 123:10–12, 2007.

[13] Martin Nirschl, Florian Reuter, and Janos Vörös. Review of transducer principles for label-free biomolecular interaction analysis. *Biosensors*, 1:70–92, 2011.

[14] Mikael Svedendahl, Si Chen, Alexandre Dmitriev, and Mikael Käll. Refractometric sensing using propagating versus localized surface plasmons: A direct comparison. *Nano Letters*, 9:4428–4433, 2009.

[15] Thomas J. Constant, Tim S. Taphouse, Helen J. Rance, Stephen C. Kitson, Alastair P. Hibbins, and J. Roy Sambles. Surface plasmons on zig-zag gratings. *Optics Express*, 20(21):23921, 2012.

[16] Xinping Zhang, Hongmei Liu, Jinrong Tian, Yanrong Song, and Li Wang. Band-selective optical polarizer based on gold-nanowire plasmonic diffraction gratings. *Nano Letters*, 8:2653–2658, 2008.

[17] Janina Kneipp, Harald Kneipp, and Katrin Kneipp. SERS—a single-molecule and nanoscale tool for bioanalytics. *Chemical Society reviews*, 37:1052–1060, 2008.

[18] Janina Kneipp, Harald Kneipp, Margaret McLaughlin, Dennis Brown, and Katrin Kneipp. In vivo molecular probing of cellular compartments with gold nanoparticles and nanoaggregates. *Nano Letters*, 6:2225–2231, 2006.

[19] Giulia Rusciano, A C De Luca, Giuseppe Pesce, Antonio Sasso, Giorgia Oliviero, Jussara Amato, Nicola Borbone, Stafano D'Errico, Vincenzo Piccialli, Gennaro Piccialli, and Luciano Mayol. *Anal. Chem.*, 83:6849–6855, 2011.

[20] Liangcheng Zhou, Qiaoqiang Gan, Filbert J Bartoli, and Volkmar Dierolf. Direct near-field optical imaging of UV bowtie nanoantennas. *Optics express*, 17(22):20301–20306, 2009.

[21] Matthias D Wissert, Carola Moosmann, Konstantin S Ilin, Michael Siegel, Uli Lemmer, and Hans-Jürgen Eisler. Gold nanoantenna resonance diagnostics via transversal particle plasmon luminescence. *Optics express*, 19(4):3686–3693, 2011.

[22] R Cush, JM Cronin, WJ Stewart, CH Maule, J Molloy, and NJ Goddard. *Biosens Bioelectron*, 8(7):347–354, 1993.

[23] Mathieu L Juan, Maurizio Righini, and Romain Quidant. Plasmon nano-optical tweezers. *Nature Photonics*, 5(May):349–356, 2011.

[24] Logan K. Ausman and George C. Schatz. Whispering-gallery mode resonators: Surface enhanced Raman scattering without plasmons. *Journal of Chemical Physics*, 129(2008):0–10, 2008.

[25] Chang-ling Zou, Jin-ming Cui, Fang-wen Sun, Xiao Xiong, Xu-bo Zou, Zheng-fu Han, and Guang-can Guo. Photonic Bound State in the Continuum for Strong Light-matter Interaction. (1):1–5, 2013.

[26] Silvia Romano, Stefano Cabrini, Ivo Rendina, and Vito Mocella. Guided resonance in negative index photonic crystals: a new approach. *Light: Science & Applications*, 3(August 2013):e120, 2014.

[27] Gilliard N Malheiros-Silveira, Gustavo S Wiederhecker, and Hugo E Hernández-Figueroa. Dielectric resonator antenna for applications in nanophotonics. *Optics express*, 21(1):1234–9, 2013.

[28] Dominic Lepage, Alvaro Jiménez, Jacques Beauvais, and Jan J Dubowski. Conic hyperspectral dispersion mapping applied to semiconductor plasmonics. *Light: Science & Applications*, 1(June):e28, 2012.

[29] E. Yablonovitch. Inhibited Spontaneous Emission in Solid-State Physics amd Electronics.pdf. *Physical Review Letters*, 58(20):2060–2062, 1987.

[30] Sajeev John. Strong localization of photons in certain disordered dielectric superlattices. *Physical Review Letters*, 58(23):2486–2489, 1987.

[31] R. D. Meade J. Joannopoulos, S. G. Johnson, J. N. Winn. *Photonic Crystals, Molding the Flow of light*. second edi edition, 2007.

[32] M Notomi. Theory of light propagation in strongly modulated photonic crystals : Refractionlike behavior in the vicinity of the photonic band gap. 62(16):696–705, 2000.

[33] V. Mocella, S. Cabrini, a. Chang, P. Dardano, L. Moretti, I. Rendina, D. Olynick, B. Harteneck, and S. Dhuey. Self-Collimation of Light over Millimeter-Scale Distance in a Quasi-Zero-Average-Index Metamaterial. *Physical Review Letters*, 102(13):133902, April 2009.

[34] Yoshihiro Akahane, Takashi Asano, Bong-shik Song, and Susumu Noda. High- Q photonic nanocavity in a two-dimensional photonic crystal. *Nature*, 425(October):944–947, 2003.

[35] Marko Loncar, Tomoyuki Yoshie, Axel Scherer, Pawan Gogna, and Yueming Qiu. Low-threshold photonic crystal laser. *Applied Physics Letters*, 81(15):2680, 2002.

[36] S M Maier. *Plasmonics: Fundamentals and Applications*, volume 223. Springer-Verlag, 2007.

[37] H Raether. *Surface Plasmons on smooth and rough surfaces and on gratings*. Springer-Verlag: Berlin, 1986.

[38] P Dardano, M Gagliardi, I Rendina, S Cabrini, and V Mocella. *Ligth: Science & Applications*, 1:e42, 2012.

[39] R W Wood. XLII. On a remarkable case of uneven distribution of light in a diffraction grating spectrum. *Philosophical Magazine Series 6*, 4(21):396–402, September 1902.

[40] L Rayleigh. On the Dynamical Theory of Gratings . In *Proceedings of the Royal Society of London Series A*, pages 399–416, 1907.

[41] A Hessel and A A Oliner. A new theory of Wood's anomalies on optical gratings. *Applied optics*, 4(10):1275–1297, 1965.

[42] Heinz Raether. Surface plasmons on smooth and rough surfaces and on gratings. Springer Verlag, 1988.

[43] V N Astratov, D M Whittaker, I S Culshaw, R M Stevenson, M S Skolnick, T F Krauss, and R M De La Rue. Photonic band-structure effects in the reflectivity of periodically patterned waveguides. *Physical Review B*, 60(24):16255–16258, 1999.

[44] V N Astratov, I S Culshaw, R M Stevenson, D M Whittaker, M S Skolnick, T F Krauss, and R M Rue. Resonant coupling of near-infrared radiation to photonic band structure waveguides. *Journal of lightwave technology*, 17(11):2050, 1999.

[45] V N Astratov, R M Stevenson, I S Culshaw, D M Whittaker, M S Skolnick, T F Krauss, and R M De La Rue. Heavy photon dispersions in photonic crystal waveguides. *Applied Physics Letters*, 77(2):178–180, 2000.

[46] R Magnusson and S S Wang. Transmission bandpass guided-mode resonance filters. *Applied optics*, 34(35):8106–8109, 1995.

[47] Shyh Wang. Two-dimensional distributed-feedback lasers and their applications. *Applied Physics Letters*, 22(9):460–462, 1973.

[48] Jing Ma, Luis Martínez, and Michelle L Povinell. A Slot-Suzuki-Phase Photonic Crystal for Optical Trapping via Guided Resonance Modes. *Optics Express*, 20(6):6816–6824, 2012.

[49] C Kappel, A Selle, M A Bader, and G Marowsky. Double grating waveguide structures: 350-fold enhancement of two-photon fluorescence applying ultrashort pulses. *Sensors and Actuators B: Chemical*, 107(1):135–139, May 2005.

[50] R Magnusson and S S Wang. New principle for optical filters. *Applied Physics Letters*, 61(9):1022–1024, 1992.

[51] Wonjoo Suh and Shanhui Fan. All-pass transmission or flattop reflection filters using a single photonic crystal slab. *Applied Physics Letters*, 84(24):4905–4907, 2004.

[52] J von Neumann and Eugene P. Wigner. Über merkwürdige diskrete Eigenwerte. *Physikalische Zeitschrift*, 30:465–467, 1929.

[53] R. H. Ritchie. Plasma Losses by Fast Electrons in Thin Films. *Physical Review*, 106(5):874, 1957.

[54] Kenji Ishizaki and Susumu Noda. *Nature*, 460(7253):367–371, 2009.

[55] V Mocella, S Cabrini, A S P Chang, P Dardano, L Moretti, I Rendina, D Olynick, B Harteneck, and S Dhuey. *Phys Rev Lett*, 102:133902, 2009.

[56] M. V. Rybin, a. B. Khanikaev, M. Inoue, K. B. Samusev, M. J. Steel, G. Yushin, and M. F. Limonov. Fano Resonance between Mie and Bragg Scattering in Photonic Crystals. *Physical Review Letters*, 103(July):1–4, 2009.

[57] U. Fano. The Theory of Anomalous Diffraction Gratings and of Quasi-Stationary Waves on Metallic Surfaces (Sommerfelds Waves). *Journal of the Optical Society of America*, 31(1935):213, 1941.

[58] M Notomi. Theory of light propagation in strongly modulated photonic crystals: Refractionlike behavior in the vicinity of the photonic band gap. *Physical Review B*, 62:10696–10705, 2000.

[59] V Mocella, S Cabrini, A Chang, P Dardano, L Moretti, I Rendina, D Olynick, B Harteneck, and S Dhuey. Self-Collimation of Light over Millimeter-Scale Distance in a Quasi-Zero-Average-Index Metamaterial. *Physical Review Letters*, 102(13):133902, April 2009.

[60] Masaya Notomi. Negative refraction in photonic crystals. *Optical and Quantum Electronics*, 34(1/3):133–143, 2002.

[61] Giuseppe Di Caprio, Principia Dardano, Giuseppe Coppola, Stefano Cabrini, and Vito Mocella. Digital holographic microscopy characterization of superdirective beam by metamaterial. *Optics letters*, 37(7):1142, 2012.

[62] Vito Mocella, Principia Dardano, Luigi Moretti, and Ivo Rendina. Influence of surface termination on negative reflection by photonic crystals. *Optics Express*, 15(11):6605–6611, 2007.

[63] S Kocaman, R Chatterjee, N C Panoiu, and J F McMillan. Observation of zeroth-order band gaps in negative-refraction photonic crystal superlattices at near-infrared frequencies. *Phys. Rev. Lett.*, 102:203905, 2009.

[64] Vito Mocella, Principia Dardano, Ivo Rendina, and Stefano Cabrini. An extraordinary directive radiation based on optical antimatter at near infrared. *Optics Express*, 18(24):25068–25074, 2010.

[65] Shanhui Fan and J Joannopoulos. Analysis of guided resonances in photonic crystal slabs. *Physical Review B*, 65(23):235112–8, June 2002.

[66] Edoardo De Tommasi, Anna Chiara De Luca, Stefano Cabrini, Ivo Rendina, Silvia Romano, and Vito Mocella. Plasmon-like surface states in negative refractive index photonic crystals. *Applied Physics Letters*, 102(8):081113, 2013.

[67] Principia Dardano, Massimo Gagliardi, Ivo Rendina, Stefano Cabrini, and Vito Mocella. Ellipsometric determination of permittivity in a negative index photonic crystal metamaterial. *Light: Science & Applications*, 1(12):e42–, December 2012.

[68] R Chatterjee, N C Panoiu, K Liu, Z Dios, and M B Yu. Achieving subdiffraction imaging through bound surface states in negative refraction photonic crystals in the near-infrared range. *Phys. Rev. Lett.*, 100:187401, 2008.

[69] K. Vynck, D. Felbacq, E. Centeno, A. I. Căbuz, D. Cassagne, and B. Guizal. All-dielectric rod-type metamaterials at optical frequencies. *Phys. Rev. Lett.*, 102:133901, Mar 2009.

[70] D. Rosenblatt, a. Sharon, and a.a. Friesem. Resonant grating waveguide structures. *IEEE Journal of Quantum Electronics*, 33(11):2038–2059, 1997.

[71] Patrice Genevet, Jean Philippe Tetienne, Evangelos Gatzogiannis, Romain Blanchard, Mikhail a. Kats, Marlan O. Scully, and Federico Capasso. Large enhancement of nonlinear optical phenomena by plasmonic nanocavity gratings. *Nano Letters*, 10:4880–4883, 2010.

[72] Jacob B Khurgin and Greg Sun. Plasmonic enhancement of the third order nonlinear optical phenomena: figures of merit. *Optics express*, 21(22):27460–80, 2013.

[73] Nikhil Ganesh, Wei Zhang, Patrick C Mathias, Edmond Chow, J a N T Soares, Viktor Malyarchuk, Adam D Smith, and Brian T Cunningham. Enhanced fluorescence emission from quantum dots on a photonic crystal surface. *Nature nanotechnology*, 2(8):515–20, August 2007.

[74] S Noda, a Chutinan, and M Imada. Trapping and emission of photons by a single defect in a photonic bandgap structure. *Nature*, 407(October):608–10, 2000.

[75] Kazuyoshi Hirose, Yong Liang, Yoshitaka Kurosaka, Akiyoshi Watanabe, Takahiro Sugiyama, and Susumu Noda. Watt-class high-power, high-beam-quality photonic-crystal lasers. *Nature Photonics*, 8(May):406–411, 2014.

[76] Bumki Min, Eric Ostby, Volker Sorger, Erick Ulin-Avila, Lan Yang, Xiang Zhang, and Kerry Vahala. High-Q surface-plasmon-polariton whispering-gallery microcavity. *Nature*, 457(7228):455–458, 2009.

[77] Jeongwon Lee, Bo Zhen, Song-Liang Chua, Wenjun Qiu, John Joannopoulos, Marin Soljačić, and Ofer Shapira. Observation and Differentiation of Unique High-Q Optical Resonances Near Zero Wave Vector in Macroscopic Photonic Crystal Slabs. *Physical Review Letters*, 109(6):067401, August 2012.

[78] Yonatan Plotnik, Or Peleg, Felix Dreisow, Matthias Heinrich, Stefan Nolte, Alexander Szameit, and Mordechai Segev. Experimental Observation of Optical Bound States in the Continuum. *Physical Review Letters*, 107(18):183901, October 2011.

[79] D. Marinica, a. Borisov, and S. Shabanov. Bound States in the Continuum in Photonics. *Physical Review Letters*, 100(18):183902, May 2008.

[80] Mario I. Molina, Andrey E. Miroshnichenko, and Yuri S. Kivshar. Surface bound states in the continuum. *Physical Review Letters*, 108(February):1–4, 2012.

[81] Evgeny N. Bulgakov and Almas F. Sadreev. Bound states in the continuum in photonic waveguides inspired by defects. *Physical Review B - Condensed Matter and Materials Physics*, 78(August):1–8, 2008.

[82] Richard Porter and D. V. Evans. Embedded Rayleigh-Bloch surface waves along periodic rectangular arrays. *Wave Motion*, 43:29–50, 2005.

[83] P. Paddon and Jeff Young. Two-dimensional vector-coupled-mode theory for textured planar waveguides. *Physical Review B*, 61(3):2090–2101, 2000.

[84] T. Ochiai and K. Sakoda. Dispersion relation and optical transmittance of a hexagonal photonic crystal slab. *Physical Review B*, 63:1–7, 2001.

[85] K. Sakoda. *Optical Properties of Photonic Crystals*. Optical Sciences, 2005.

[86] Nicolas Chateau and Jean-Paul Hugonin. Algorithm for the rigorous coupled-wave analysis of grating diffraction. *Journal of the Optical Society of America A*, 11(4):1321, 1994.

[87] J. M. Foley, S. M. Young, and J. D. Phillips. Symmetry-protected mode coupling near normal incidence for narrow-band transmission filtering in a dielectric grating. *Physical Review B - Condensed Matter and Materials Physics*, 89:1–9, 2014.

[88] Ramakrishnan Ganesan, Jarrett Dumond, Mohammad S M Saifullah, Su Hui Lim, Hazrat Hussain, and Hong Yee Low. Direct patterning of TiO 2 using step-and-flash imprint lithography. *ACS Nano*, 6(2):1494–1502, 2012.

[89] Carlos Pina-Hernandez, Valeria Lacatena, Giuseppe Calafiore, Scott Dhuey, Konstantin Kravtsov, Alexander Goltsov, Deirdre Olynick, Vladimir Yankov, Stefano Cabrini, and Christophe Peroz. A route for fabricating printable photonic devices with sub-10 nm resolution. *Nanotechnology*, 24:065301, 2013.